

**ISTANBUL TECHNICAL UNIVERSITY ★ ENERGY INSTITUTE**

**EFFECT OF HEAT LEAKAGE ON THE OPTIMAL PERFORMANCE OF  
A TWIN-SPOOL TURBOFAN ENGINE**

**M.Sc. THESIS**

**Mert ÇOLAKOĞLU**

**Energy Science and Technology Division**

**Energy Science and Technology Programme**

**DECEMBER 2015**



**ISTANBUL TECHNICAL UNIVERSITY ★ ENERGY INSTITUTE**

**EFFECT OF HEAT LEAKAGE ON THE OPTIMAL PERFORMANCE OF  
A TWIN-SPOOL TURBOFAN ENGINE**

**M.Sc. THESIS**

**Mert ÇOLAKOĞLU  
(301131017)**

**Energy Science and Technology Division**

**Energy Science and Technology Programme**

**Thesis Advisor: Prof. Dr. Ahmet DURMAYAZ**

**DECEMBER 2015**



**İSTANBUL TEKNİK ÜNİVERSİTESİ ★ ENERJİ ENSTİTÜSÜ**

**BİR EŞ MERKEZLİ ÇİFT MİLLİ TURBOFAN MOTORUNUN OPTİMAL  
PERFORMANSINA ISI KAYBININ ETKİSİ**

**YÜKSEK LİSANS TEZİ**

**Mert ÇOLAKOĞLU  
(301131017)**

**Enerji Bilim ve Teknoloji Anabilim Dalı**

**Enerji Bilim ve Teknoloji Programı**

**Tez Danışmanı: Prof. Dr. Ahmet DURMAYAZ**

**ARALIK 2015**



Mert ÇOLAKOĞLU, a M.Sc. student of ITU Energy Institute student ID 301131017 successfully defended the thesis entitled “EFFECT OF HEAT LEAKAGE ON THE OPTIMAL PERFORMANCE OF A TWIN-SPOOL TURBOFAN ENGINE”, which he prepared after fulfilling the requirements specified in the associated legislations, in the presence of the jury whose signatures are below.

**Thesis Advisor :**      **Prof. Dr. Ahmet DURMAYAZ**      .....

İstanbul Technical University

**Jury Members :**      **Prof. Dr. Filiz BAYTAŞ**      .....

İstanbul Technical University

**Prof. Dr. Mustafa ÖZDEMİR**      .....

İstanbul Technical University

**Date of Submission : 27 November 2015**

**Date of Defense : 21 December 2015**





*To my parents and fiancée,*



## **FOREWORD**

This thesis focuses on effect of heat leakage on the optimal performance of a twin-spool turbofan engine by utilizing thermodynamic cycle analysis. Optimal design parameters and selected performance indicators have been inspected considering heat leakage effect on them.

First and foremost, I would like to gratefully thank to my advisor Prof. Dr. Ahmet Durmayaz who has supported me during all the phases of my M.Sc. study. He has shown me great patience, wisdom and guidance with his praiseworthy experience and charity, and helped me generously carrying my study onward with his deep and mature knowledge. He has also provided me with support of attending to an international symposium so that I have gained valuable experience in the way of being a future scientist. I would like to present my respect and gratitude to him for all of his efforts.

Some parts of the thesis has been presented in the 7<sup>th</sup> International Ege Energy Symposium & Exhibition, Uşak, Turkey, in June 18-20 2014, and published in the Proceedings of the Conference. Besides, the Best Paper Award, among approximately 140 papers presented in the conference, has been presented to Colakoglu, M., Tanbay, T., Durmayaz, A. and Sogut, O.S. for this paper. Moreover, the presented paper has been selected and accepted for publication in the International Journal of Exergy.

Hence, I also would like to thank to Ph.D. student Tayfun Tanbay from Institute of Energy and Prof. Dr. Oğuz Salim Söğüt from Department of Naval Architecture and Ocean Engineering for their valuable contribution to the study.

Lastly, I would like to thank to my parents and to my fiancée due to their full support and encouragement on my M.Sc. study with all my gratitude.

December 2015

Mert ÇOLAKOĞLU  
(Industrial Engineer)



## TABLE OF CONTENTS

	<u>Page</u>
<b>FOREWORD</b> .....	<b>ix</b>
<b>TABLE OF CONTENTS</b> .....	<b>xi</b>
<b>ABBREVIATIONS</b> .....	<b>xv</b>
<b>LIST OF SYMBOLS</b> .....	<b>xvii</b>
<b>LIST OF TABLES</b> .....	<b>xxi</b>
<b>LIST OF FIGURES</b> .....	<b>xxiii</b>
<b>SUMMARY</b> .....	<b>xxv</b>
<b>ÖZET</b> .....	<b>xxix</b>
<b>1. INTRODUCTION</b> .....	<b>1</b>
1.1 Purpose of the Thesis .....	2
1.2 Literature Review .....	3
<b>2. SELECTED FUNDAMENTAL CONCEPTS OF THERMODYNAMICS UTILIZED IN THE THESIS</b> .....	<b>9</b>
2.1 Enthalpy .....	9
2.2 Stagnation (Total) Properties .....	10
2.3 Speed of Sound and Mach Number.....	11
2.4 Chocking at the Nozzle Exit.....	12
2.5 Entropy .....	12
2.6 Exergy .....	14
2.7 Brayton Cycle.....	16
<b>3. A REVIEW OF PERFORMANCE INDICATORS USED IN THE THERMODYNAMIC ANALYSIS OF TURBOJET AND TURBOFAN CYCLES</b> .....	<b>19</b>
3.1 Turbojet Cycle and Turbojet Engine .....	19
3.2 Turbofan Cycle and Single-Spool Turbofan Engine.....	21
3.3 Performance Indicators Utilized in the Thermodynamic Analysis of Turbojet and Turbofan Engines .....	22
3.3.1 Thrust specific fuel consumption ( <i>TSFC</i> ) .....	24
3.3.2 Specific thrust ( $F_s$ ) .....	25
3.3.3 Propulsive efficiency ( $\eta_P$ ) .....	25
3.3.4 Thermal efficiency ( $\eta_{th}$ ).....	26
3.3.5 Overall efficiency ( $\eta_o$ ).....	27
3.3.6 Exergetic efficiency ( $\eta_{ex}$ ).....	28
3.3.7 Coefficient of ecological performance ( <i>CEP</i> ) .....	29
3.3.8 Exergy destruction factor ( $f_{exd}$ ) .....	29
3.3.9 Waste exergy ratio ( $r_{wex}$ ) .....	30
3.3.10 Environmental effect (impact) factor ( $f_{eef}$ ) .....	30
3.3.11 Exergetic sustainability index ( $\theta_{exs}$ ).....	30
3.3.12 Improvement potential ( $I\dot{P}$ ) .....	31
3.3.13 Relative irreversibility ( $\chi_i$ ) .....	31

3.3.14 Fuel depletion ratio ( $\delta_i$ ) .....	32
<b>4. THEORETICAL MODEL FOR THE THERMODYNAMIC ANALYSIS ABOUT THE EFFECT OF HEAT LEAKAGE ON THE OPTIMAL PERFORMANCE OF A TWIN-SPOOL TURBOFAN ENGINE.....</b>	<b>33</b>
4.1 Processes and Assumptions .....	35
4.2 Mass Flow Rates and Ratios.....	37
4.3 Heat Leakage Rates and Ratios .....	39
4.4 Power Consumption and Production Balances.....	46
4.4.1 Power consumed by fan.....	47
4.4.2 Power consumed by LPC .....	47
4.4.3 Power consumed by HPC.....	47
4.4.4 Power produced by HPT .....	48
4.4.5 Power produced by LPT .....	50
4.4.6 Thrust and propulsive power .....	51
4.4.6.1 Thrust .....	51
4.4.6.2 Propulsive power.....	53
4.4.7 Thrust specific fuel consumption, specific thrust and overall efficiency .....	54
4.4.7.1 Thrust specific fuel consumption ( $TSFC$ ) .....	54
4.4.7.2 Specific thrust ( $F_s$ ) .....	54
4.4.7.3 Overall efficiency ( $\eta_o$ ).....	55
4.4.8 Thermodynamic property relations .....	55
4.4.8.1 Operating conditions, design parameters and performance parameters utilized in the thesis.....	55
4.4.8.2 Diffuser.....	57
4.4.8.3 Fan.....	62
4.4.8.4 LPC and HPC .....	68
4.4.8.5 Combustion chamber.....	70
4.4.8.6 HPT and LPT .....	73
4.4.8.7 Core nozzle.....	78
4.4.8.8 Fan nozzle .....	83
4.4.9 Coefficient of ecological performance, entropy generation rate and exergy destruction factor .....	87
<b>5. RESULTS AND DISCUSSIONS .....</b>	<b>95</b>
5.1 Optimal Values of Coupled Design Parameters with 3-D Figures.....	96
5.1.1 Determination of optimum values of performance indicators with respect to $r_{C,Total}$ and $\beta$ .....	96
5.1.2 Determination of optimum values of performance indicators with respect to $r_{C,Total}$ and $r_F$ .....	99
5.1.3 Determination of optimum values of performance indicators with respect to $r_{C,Total}$ and $T_{max}$ .....	100
5.1.4 Determination of optimum values of performance indicators with respect to $r_F$ and $\beta$ .....	101
5.1.5 Determination of optimum values of performance indicators with respect to $r_F$ and $T_{max}$ .....	101
5.1.6 Determination of optimum values of performance indicators with respect to $\beta$ and $T_{max}$ .....	102
5.2 Effect of Heat Leakage on the Optimal Design Parameters and Performance Indicators .....	103
5.2.1 Comparison of the results of two types of heat leakages $\epsilon_{LK1}$ and $\epsilon_{LK2}$ .....	103

5.2.2 Variations of performance indicators with respect to design parameters and $\varepsilon_{LK1}$ .....	105
5.2.2.1 Variation with respect to $r_{C,Total}$ .....	106
5.2.2.2 Variation with respect to $r_F$ .....	109
5.2.2.3 Variation with respect to $\beta$ .....	111
5.2.2.4 Variation with respect to $T_{max}$ .....	114
5.2.3 Optimum values of performance indicators with respect to design parameters .....	117
5.2.4 Relative change of performance indicators at different levels of design parameters with respect to change in $\varepsilon_{LK1}$ .....	117
5.2.4.1 Relative % change of performance indicators at small, optimum and large $r_{C,Total}$ values .....	119
5.2.4.2 Relative % change of performance indicators at small, optimum and large $r_F$ values .....	121
5.2.4.3 Relative % change of performance indicators at small, optimum and large $\beta$ values .....	124
5.2.4.4 Relative % change of performance indicators at small, optimum and large $T_{max}$ values .....	126
<b>6. CONCLUSIONS AND RECOMMENDATIONS</b> .....	<b>131</b>
6.1 Conclusions of the Thesis .....	131
6.2 Recommendations for Future Studies .....	133
<b>REFERENCES</b> .....	<b>135</b>
<b>APPENDICES</b> .....	<b>141</b>
<b>CURRICULUM VITAE</b> .....	<b>147</b>





## ABBREVIATIONS

<b>amu</b>	: Atomic mass unit
<b>CC</b>	: Combustion chamber
<b>CEP</b>	: Coefficient of ecological performance
<b>FN</b>	: Fan nozzle
<b>HPC</b>	: High-pressure compressor
<b>HPT</b>	: High-pressure turbine
<b>IP</b>	: Improvement potential
<b>kg</b>	: Kilogram
<b>kJ</b>	: Kilojoule
<b>kN</b>	: Kilonewton
<b>kPa</b>	: Kilopascal
<b>kW</b>	: Kilowatt
<b>LPC</b>	: Low-pressure compressor
<b>LPT</b>	: Low-pressure turbine
<b>Ma</b>	: Mach
<b>MJ</b>	: Megajoule
<b>MW</b>	: Megawatt
<b>TSFC</b>	: Thrust specific fuel consumption
<b>2-D</b>	: Two-dimensional
<b>3-D</b>	: Three-dimensional



## LIST OF SYMBOLS

<i>A</i>	: Area ( $\text{m}^2$ )
<i>c</i>	: Specific heat ( $\text{kJ kg}^{-1} \text{K}^{-1}$ )
<i>C</i>	: Carbon mass fraction in fuel; Compressor
<i>d</i>	: Differential
<i>e</i>	: Differential-pressure-change based irreversibility correction factor for adiabatic compression (or expansion) process
<i>ex</i>	: Exergy ( $\text{kJ kg}^{-1}$ )
$\dot{E}x$	: Exergy flow rate (kW)
<i>f</i>	: Factor
<i>F</i>	: Thrust (kN); Fan
<i>g</i>	: Gravitational acceleration ( $\text{m s}^{-2}$ )
<i>h</i>	: Specific enthalpy ( $\text{kJ kg}^{-1}$ )
<i>H</i>	: Enthalpy (kJ); Hydrogen mass fraction in fuel
<i>k</i>	: Specific heat ratio
$\dot{m}$	: Mass flow rate ( $\text{kg s}^{-1}$ )
<i>M</i>	: Mach number
<i>N</i>	: Nozzle; Nitrogen mass fraction in fuel
<i>O</i>	: Oxygen mass fraction in fuel
<i>P</i>	: Pressure (kPa)
$\underline{Q}$	: Heat (kJ)
$\dot{Q}$	: Heat transfer rate (kW)
<i>r</i>	: Pressure ratio; Ratio
<i>R</i>	: Ideal gas constant ( $\text{kJ kg}^{-1} \text{K}^{-1}$ )
$\bar{R}$	: Universal gas constant ( $\text{kJ mol}^{-1} \text{K}^{-1}$ )
<i>s</i>	: Specific entropy ( $\text{kJ kg}^{-1} \text{K}^{-1}$ )
<i>S</i>	: Entropy ( $\text{kJ K}^{-1}$ ); Sulphur mass fraction in fuel
$\dot{S}$	: Entropy generation rate ( $\text{kW K}^{-1}$ )
<i>t</i>	: Time (s)
<i>T</i>	: Temperature (K); Turbine
<i>u</i>	: Specific internal energy ( $\text{kJ kg}^{-1}$ )
<i>U</i>	: Internal energy (kJ)
<i>v</i>	: Velocity ( $\text{m s}^{-1}$ )
<i>v</i>	: Specific volume ( $\text{m}^3 \text{kg}^{-1}$ )
<i>V</i>	: Volume ( $\text{m}^3$ )
$\dot{W}$	: Power (kW)
<i>x</i>	: Mole fraction
<i>X</i>	: Exergy (kJ)
<i>z</i>	: Elevation (m)

## Greek Letters

$\alpha$	: Fuel-to-air mass flow ratio in CC
----------	-------------------------------------

$\beta$	: By-pass ratio
$\gamma$	: Bleed air ratio
$\delta$	: Differential; Fuel depletion ratio
$\Delta$	: Difference
$\varepsilon$	: Heat leakage ratio; Heat exchanger efficiency
$\eta$	: Efficiency
$\theta$	: Cooling air ratio
$\Theta$	: Index
$\rho$	: Density ( $\text{kg m}^{-3}$ )
$\varphi$	: Ratio of specific chemical exergy to lower heating value
$\phi$	: Specific nonflow exergy ( $\text{kJ kg}^{-1}$ )
$\chi$	: Relative irreversibility
$\psi$	: Specific stream exergy ( $\text{kJ kg}^{-1}$ )

### Subscripts

$0$	: Stagnation condition
<i>aux</i>	: Auxiliary
<i>avg</i>	: Average
<i>act</i>	: Active constraint
<i>b</i>	: Bleed air
<i>c</i>	: Core
<i>C</i>	: Compressor
<i>CC</i>	: Combustion chamber
<i>chem</i>	: Chemical
<i>cool</i>	: Cooling air
<i>cr</i>	: Critical
<i>CV</i>	: Control volume
<i>D</i>	: Diffuser
<i>dest</i>	: Destruction
<i>e</i>	: Exit
<i>eef</i>	: Environmental effect
<i>ex</i>	: Exergy
<i>exd</i>	: Exergy destruction
<i>exs</i>	: Exergetic sustainability
<i>f</i>	: Fuel; Friction
<i>F</i>	: Fan
<i>FN</i>	: Fan nozzle
<i>gen</i>	: Generation
<i>H</i>	: Heat exchanger
<i>HP</i>	: High pressure
<i>HPC</i>	: High-pressure compressor
<i>HPT</i>	: High-pressure turbine
<i>i</i>	: Inlet; $i^{\text{th}}$ component
<i>in</i>	: Input
<i>int rev</i>	: Internally reversible
<i>j</i>	: $j^{\text{th}}$ stage
<i>k</i>	: Heat transfer location
<i>LPC</i>	: Low-pressure compressor
<i>LHV</i>	: Lower heating value

<b><i>LK1</i></b>	: Leaked from CC
<b><i>LK2</i></b>	: Leaked to ambient
<b><i>LPT</i></b>	: Low-pressure turbine
<b><i>M1</i></b>	: Mechanical for the first turbine
<b><i>M2</i></b>	: Mechanical for the second turbine
<b><i>max</i></b>	: Maximum
<b><i>min</i></b>	: Minimum
<b><i>N</i></b>	: Nozzle
<b><i>o</i></b>	: Overall
<b><i>opt</i></b>	: Optimum
<b><i>out</i></b>	: Output
<b><i>p</i></b>	: Pressure
<b><i>P</i></b>	: Propulsive
<b><i>recv</i></b>	: Recovered
<b><i>s</i></b>	: Specific; Isentropic; Shock waves; Stage
<b><i>supp</i></b>	: Supplied
<b><i>th</i></b>	: Thermal
<b><i>v</i></b>	: Volume
<b><i>wex</i></b>	: Waste exergy



## LIST OF TABLES

	<u>Page</u>
<b>Table 4.1</b> : Mass flow rates. ....	<b>38</b>
<b>Table 4.2</b> : Operating conditions, design and performance parameters. ....	<b>56</b>
<b>Table 5.1</b> : Comparisons of the variations of performance indicators with $\varepsilon_{LK1}$ when $\varepsilon_{LK2} = 2\%$ and those with $\varepsilon_{LK2}$ when $\varepsilon_{LK1} = 2\%$ for small (1) and large (7) values of $\beta$ . ....	<b>104</b>
<b>Table 5.2</b> : The optimum values of design parameters and corresponding maximum values of $CEP$ , $\eta_o$ and $F_s$ and minimum values of $f_{exd}$ , $TSFC$ and $\dot{S}_{gen}$ at $\varepsilon_{LK1} = 0\%$ , $2\%$ and $4\%$ when $\varepsilon_{LK2} = 2\%$ . ....	<b>118</b>





## LIST OF FIGURES

	<u>Page</u>
<b>Figure 2.1</b> : An open-cycle gas-turbine engine (Çengel and Boles, 2005). ....	17
<b>Figure 2.2</b> : A closed-cycle gas-turbine engine (Çengel and Boles, 2005).....	17
<b>Figure 2.3</b> : T-s diagram for the ideal Brayton Cycle (Çengel and Boles, 2005). ....	18
<b>Figure 3.1</b> : T-s diagram for an open ideal jet propulsion cycle. ....	20
<b>Figure 3.2</b> : A turbojet engine with its components (Çengel and Boles, 2005). ....	21
<b>Figure 3.3</b> : A turbofan engine (Tanbay et al, 2015). ....	23
<b>Figure 3.4</b> : Cross section of a turbofan engine (Rolls Royce, 1996). ....	23
<b>Figure 3.5</b> : T-s diagram of a turbofan engine. ....	24
<b>Figure 4.1</b> : The turbofan engine configuration and station numbering utilized in the thesis. ....	34
<b>Figure 4.2</b> : T-s diagram of the turbofan engine cycle and corresponding station numbering utilized in the thesis. ....	34
<b>Figure 4.3</b> : A diffuser (Çengel and Boles, 2005). ....	57
<b>Figure 4.4</b> : A turbofan (Langston, 2011). ....	63
<b>Figure 4.5</b> : A twin-spool axial compressor (Rolls Royce, 1996). ....	69
<b>Figure 4.6</b> : An annular combustion chamber (Rolls Royce, 1996). ....	71
<b>Figure 4.7</b> : A twin-turbine (Rolls Royce, 1996). ....	74
<b>Figure 4.8</b> : A nozzle or exhaust (inner red arrows show core nozzle) (Rolls Royce, 1996). ....	78
<b>Figure 4.9</b> : A nozzle or exhaust (outer blue arrows show fan nozzle) (Rolls Royce, 1996). ....	84
<b>Figure 5.1</b> : Relative change of performance indicators with respect to $r_{c,Total}$ and $\beta$ simultaneously. ....	97
<b>Figure 5.2</b> : Relative change of performance indicators of $CEP$ and $\eta_o$ with respect to $r_{c,Total}$ and $r_F$ simultaneously. ....	99
<b>Figure 5.3</b> : Relative change of performance indicators of $CEP$ and $\eta_o$ with respect to $r_{c,Total}$ and $T_{max}$ simultaneously. ....	100
<b>Figure 5.4</b> : Relative change of performance indicators of $CEP$ and $\eta_o$ with respect to $r_F$ and $\beta$ simultaneously. ....	101
<b>Figure 5.5</b> : Relative change of performance indicators of $CEP$ and $\eta_o$ with respect to $r_F$ and $T_{max}$ simultaneously. ....	102
<b>Figure 5.6</b> : Relative change of performance indicators of $CEP$ and $\eta_o$ with respect to $\beta$ and $T_{max}$ simultaneously. ....	103
<b>Figure 5.7</b> : Relative change of performance indicators with respect to $r_{c,Total}$ at three values of $\varepsilon_{LK1}$ . ....	106
<b>Figure 5.8</b> : Relative change of performance indicators with respect to $r_F$ at three values of $\varepsilon_{LK1}$ . ....	109
<b>Figure 5.9</b> : Relative change of performance indicators with respect to $\beta$ at three values of $\varepsilon_{LK1}$ . ....	112

<b>Figure 5.10</b> : Relative change of performance indicators with respect to $T_{max}$ at three values of $\varepsilon_{LK1}$ .....	<b>114</b>
<b>Figure 5.11</b> : Relative % change of performance indicators at small, optimum and large levels of $r_{C,Total}$ .....	<b>119</b>
<b>Figure 5.12</b> : Relative % change of performance indicators at small, optimum and large levels of $r_F$ .....	<b>122</b>
<b>Figure 5.13</b> : Relative % change of performance indicators at small, optimum and large levels of $\beta$ .....	<b>124</b>
<b>Figure 5.14</b> : Relative % change of performance indicators at small, optimum and large levels of $T_{max}$ .....	<b>127</b>

## EFFECT OF HEAT LEAKAGE ON THE OPTIMAL PERFORMANCE OF A TWIN-SPOOL TURBOFAN ENGINE

### SUMMARY

Transportation is one of the main areas where energy is utilized and it plays a crucial role in human life. Besides ground and marine transportation, aviation has also an important share in energy utilization, which utilizes thermal systems (aircraft engines) for producing power.

Recently, sustainability and efficiency studies on thermal systems have increased due to increasing concerns on effects of thermal systems on environment and life on the Earth. Many researchers have focused on more efficient and more sustainable technologies in terms of both thermal systems and other alternative systems. Most of the studies have been performed on optimization of thermal systems, and some of the researches have focused on heat losses on ground-type thermal systems. In literature, there has been observed a lack of a study investigating the effect of heat losses on aircraft engines in terms of energy and exergy performance, hence environmental performance.

In this regard, this thesis focuses on the effect of heat leakage on the optimal performance of a twin-spool turbofan engine, which type of engines are widely utilized by commercial aircrafts in aviation and under further development. Thermodynamic cycle analysis have been utilized in order to perform this investigation both for energy (the First Law of Thermodynamics); and exergy together with entropy (the Second Law of Thermodynamics) points of view.

Selected twin-spool engine configuration consists of a diffuser, fan, low-pressure compressor, high-pressure compressor, combustion chamber, high-pressure turbine, low-pressure turbine, and nozzle. After diffuser and fan, air stream is separated into two inside the engine, one stream continues through compressors, combustion chamber and turbines before being exhausted in nozzle; while the other stream (by-pass air stream) does not pass through the compressor – combustion chamber – turbine path; instead, it goes to nozzle after fan. Both streams are exhausted through nozzle but they do not mix, so the configuration of the twin-spool turbofan engine is unmixed.

Main design parameters selected to be varied in order to observe respective changes in the performance of the engine are total compressor pressure ratio  $r_{C,Total}$ , fan pressure ratio  $r_F$ , by-pass air ratio  $\beta$  and maximum turbine inlet temperature  $T_{max}$ . Moreover, bleed air, cooling air for turbines, power extraction for auxiliary equipment and polytropic efficiencies of turbomachinery have been taken into account in this thesis.

There have been selected six performance indicators of aircraft engine among the many others present in literature in order to be able to calculate and compare changes in the performance of the aircraft engine. These six performance indicators are the

coefficient of ecological performance  $CEP$ , the overall efficiency  $\eta_o$ , the exergy destruction factor  $f_{exd}$ , the thrust specific fuel consumption  $TSFC$ , the specific thrust  $F_s$ , and the entropy generation rate  $\dot{S}_{gen}$ . Three of the above performance indicators, namely the overall efficiency  $\eta_o$ , the thrust specific fuel consumption  $TSFC$ , and the specific thrust  $F_s$  are derived mainly by the First Law of Thermodynamics. On the other hand, the other three performance indicators namely coefficient of ecological performance  $CEP$ , the exergy destruction factor  $f_{exd}$ , and the entropy generation rate  $\dot{S}_{gen}$  are derived mainly by the Second Law of Thermodynamics.

Two types of heat leakages have been considered in the thesis. First one is heat leakage from the combustion process taking place at very high temperatures to the surrounding by-pass air (passing outside of the combustion chamber) through the combustion chamber wall. And the second heat leakage has been considered as the heat leakage from by-pass air to the ambient air which is very cold.

Variations of performance indicators with respect to changing design parameters have been calculated and interpreted. Also, the analysis have been done for different heat leakage levels. Relative importance of heat leakages have been compared in terms of their effect on performance indicators. Moreover, optimum values of design parameters and corresponding maximum or minimum values of performance indicators have been calculated at different heat leakage levels. Additionally, relative variations of performance indicators at different levels of design parameters for changing heat leakage have been investigated and interpreted.

It has been concluded in the thesis that very small values of  $r_{C,Total}$ ,  $r_F$  and  $T_{max}$  are not suitable areas in terms of  $CEP$  and  $\eta_o$  due sharp decreases. Also it has been observed that effect of design parameters on performance indicators depend on the values of other design parameters.

One of the major conclusions of this thesis has been that effect of heat leakage two is insignificant when compared to the effect of heat leakage one. Therefore, effect of heat leakage one have been taken under investigation, and focus has been on heat leakage one in the thesis.

It has been concluded that effect of heat leakage one is significant on  $CEP$ ,  $f_{exd}$  and  $\dot{S}_{gen}$  at all levels of design parameters including optimum levels, but the same conclusion is not valid for  $\eta_o$ ,  $TSFC$  and  $F_s$ . At small and optimum values of  $r_{C,Total}$ ,  $r_F$  and  $\beta$ ; and large and optimum values of  $T_{max}$ , effect of heat leakage one on  $\eta_o$ ,  $TSFC$  and  $F_s$  is not significant. However, it becomes more significant at large values of  $r_{C,Total}$ ,  $r_F$  and  $\beta$ ; and at small values of  $T_{max}$ .

Another main conclusion of the thesis is that performance indicators that are derived by the 2<sup>nd</sup> Law of Thermodynamics ( $CEP$ ,  $f_{exd}$  and  $\dot{S}_{gen}$ ) have been affected by heat leakage one more significantly than the other performance indicators which are derived by the 1<sup>st</sup> Law of Thermodynamics ( $\eta_o$ ,  $TSFC$  and  $F_s$ ). Reason of this difference is that heat loss from the combustion chamber is realized between two media having large temperature difference, so the heat loss process is highly irreversible and entropy generation rate is very high. Therefore, the 2<sup>nd</sup>-law-derived performance indicators are affected more significantly than the 1<sup>st</sup>-law-derived performance indicators.

It has also been concluded that optimum values of design parameters change with respect to the amount of heat leakage. As heat leakage ratio changes, optimum values of design parameters and corresponding values of performance indicators change.

And lastly, it has been observed that effect of heat leakage on the performance indicators are not linear.



## **BİR EŞ MERKEZLİ ÇİFT MİLLİ TURBOFAN MOTORUNUN OPTİMAL PERFORMANSINA ISI KAYBININ ETKİSİ**

### **ÖZET**

İnsan hayatının önemli ve kritik bir parçası olan ulaşım ve taşımacılık, enerji tüketiminde büyük bir paya sahiptir. Kara ulaşımı ve taşımacılığı ile deniz ulaşımı ve taşımacılığının yanı sıra hava ulaşımı ve taşımacılığında kullanılan araçlar da ısı sistemler (uçak motorları) yoluyla güç üretmektedir, bu sebeple de önemli bir enerji tüketim payına sahiptir. Dolayısıyla, fosil yakıt tüketimi konusunda havacılık sektörü de önem arz etmektedir.

Fosil yakıtlarla çalışan ısı sistemler enerji üretimi, aydınlatma, ısıtma, soğutma, taşımacılık ve ulaşım gibi pek çok alanda uzunca bir süredir yaygın bir şekilde kullanılmaktadır. Bu kullanımın aşırıya kaçması neticesinde çevreye verebileceği zararlar üzerine bilimsel araştırmalar son yıllarda artan bir biçimde literatürde yer almaktadır. Küresel ısınma, Dünya üzerindeki canlı türlerinin ve ekosistemlerin mevcudiyetini tehdit etmesi sebebiyle, ısı sistemlerin daha verimli ve daha sürdürülebilir şekilde tasarlanması ve kullanılması konusundaki çalışmaların yoğunlaştırılmasına sebep olmuştur. Diğer taraftan, alternatif güç üretim teknolojileri üzerinde çalışmalar da sürdürülmektedir.

Literatürde yer alan çalışmalar incelendiğinde pek çok farklı türdeki ısı sistemlerin verimliliği, optimizasyonu ve performansının artırılması konularında çalışıldığı ve bu çalışmaların oldukça geniş bir yelpazede bulunduğu görülmektedir. Diğer bir taraftan, ısı sistemlerin ısı kayıplarının etkisini inceleyen çalışmalar da literatürde mevcuttur. Ancak bu çalışmalar genellikle güç üretimi için kullanılan durağan ısı sistemler veya havacılık haricindeki motorlu taşıtların güç üretim sistemleri üzerinde yoğunlaşmıştır.

Literatür araştırmasının sonuçları değerlendirildiğinde, hava taşımacılığı yapan uçak motorlarının performansı üzerine ısı kayıplarının etkisini inceleyen bir çalışmanın literatürde mevcut olmadığı görülmüştür. Böyle bir çalışmanın, hem enerji hem de ekserji bakımından uçak motorunun performansına ısı kayıplarının etkisini irdelemesinin ve dolayısıyla ısı kayıplarının uçak motorunun ekolojik performansına olan etkisini ortaya koymasının literatüre yapacağı katkı önemli bulunmuştur.

Bu kapsamda, bu tez çalışmasında bir eş merkezli çift milli (twin-spool) turbofan uçak motorunun optimal performansına ısı kayıplarının etkisi hususuna odaklanılmıştır. Eş merkezli çift milli uçak motorları havacılıkta oldukça yaygın kullanılan bir motor türüdür. Ayrıca, gelişen teknoloji ile birlikte sürekli yeni nesilleri geliştirilmekte ve bu motorlar üzerinde ileri düzeyde araştırmalar devam etmektedir.

Gaz türbini sistemlerinin termodinamik analizleri, hal değişimleri ideal varsayıldığında, sabit entropide sıkıştırma, sabit basınçta ısı alma, sabit entropide genişleme ve sabit basınçta ısı atma proseslerinden oluşan Brayton çevrimi ile

yapılmaktadır. Brayton çevrimi, gaz türbini sistemleri için ideal bir çevrimdir ve bu çevrimde hava standardı kabulleri (air standard assumptions) geçerlidir. Tüm prosesler içten tersinir olarak varsayılır ve çevrimdeki akışkan tüm çevrim boyunca hava olarak varsayılır. Bu kapsamda gerçek çevrimlerdeki yanma prosesi ideal durum olan Brayton çevriminde ısı alma prosesi ile, egzoz prosesi ise ısı atma prosesi ile yer değiştirmiştir. Brayton çevriminden net mil gücü üretilmesi amaçlanırken, hava ulaşım araçları için geliştirilmiş olan turbojet ve turbofan çevrimlerinde ise türbin ile aslen kompresörün ihtiyacı olan gücün karşılanması amaçlanmaktadır. Turbofan motorları, Brayton çevriminden farklı olarak kompresör girişinde bir difüzör, difüzörün hemen ardında bir fan ve türbin çıkışında bir lüleyle sahip turbofan çevrimi ile çalışmaktadır. Fan çıkışında motorun içerisindeki hava akışı iki ayrı akışa ayrılır. Birincisi merkezi (ana) akış (core air flow), diğeri ise merkezi akışa paralel tali (ikinci) akıştır (by-pass air flow).

Merkezi akıştaki hava fanın ardından alçak basınç kompresörü, yüksek basınç kompresörü, yanma odası yolunu takip ederek yanma odasında yakıt ile yanma tepkimesine girer ve oluşan yüksek basınç ve sıcaklıktaki yanma ürünleri daha sonra yüksek basınç türbini ve alçak basınç türbini yolunu izleyerek, uçak hareketinin tersi yönde lüleden dışarı, uçak dışındaki durağan farz edilebilecek havanın üzerine doğru çok yüksek hızla püskürtülerek, dış ortamdaki havanın tepkisiyle uçağın ileri yönlü hareketini sağlayan itme kuvveti oluşturulur.

Tali akımdaki hava ise fandan sonra kompresör, yanma odası ve türbin grubunun dışından onlara paralel akarak herhangi bir yanma tepkimesine girmeden doğrudan lüleyle ulaşır ve yüksek hızla dışarı çıkarak itme kuvveti oluşturmaya katkı sağlar. Ana akım ile tali akım birbirine karışmadan motordan çıktıkları için bu tip motorlara akışları karışmayan (unmixed) motorlar denir.

Bu türden akışları karışmayan motor konfigürasyonunda fan ve düşük basınç kompresörünün ihtiyaç duyduğu gücü alçak basınç türbini üretirken, yüksek basınç kompresörünün ihtiyaç duyduğu gücü ise yüksek basınç türbini üretmektedir. Türbinler sadece kompresörlerin ve uçaktaki diğer yardımcı ekipmanların ihtiyaç duyduğu kadar güç üretir, dolayısıyla motorun içinden geçen akımın geriye kalan enerjisi motor çıkışında lüleyle kadar korunur, kalan bu büyük miktardaki enerjiyle uçağın hareketini sağlayan çok büyük itme kuvvetleri elde edilir.

Motorun çalışma koşulları, uçağın normal seyir irtifasında uçuşu fazındaki (cruise phase) sabit çevre koşullarında varsayılmış, dolayısıyla uçak içerisindeki birimlerde gerçekleşen prosesler sürekli-akışlı (daimi rejimde) (steady-state) prosesler olarak varsayılmıştır.

Genel itibariyle bakıldığında, bu tez kapsamında yapılan çalışma, bir termodinamik çevrim analizidir. Bu analizde amaç, Termodinamiğin 1. Yasası (dolayısıyla enerji) ve Termodinamiğin 2. Yasası (dolayısıyla entropi) analizi vasıtasıyla uçak motorunun performansının değerlendirilmesi ve seçilmiş bazı tasarım parametreleri ile ısı kayıplarının uçak motorunun performansına etkisinin incelenmesidir.

Dört farklı tasarım parametresi, turbofan uçak motorunun performansına olan etkilerinin gözlemlenebilmesi amacıyla çalışmada incelenmek üzere seçilmiştir. Bunlar toplam kompresör basınç oranı  $r_{c,Total}$ , fan (çıkış basıncı/giriş basıncı) basınç oranı  $r_F$ , tali hava akışında kütleli debi oranı  $\beta$  ve maksimum türbin giriş sıcaklığı  $T_{max}$ 'dir. Tez çalışmasında bu tasarım parametrelerinin farklı değerlerinin uçak motorunun performansı üzerine etkisi irdelenmiştir.



Tasarım parametrelerinin yansira çeşitli sistemlerde kullanılmak üzere kompresörden yapılan hava tahliyesi (bleed air), türbin giriş sıcaklığının kontrol altında tutulabilmesi için kompresörden çekilip türbine aktarılan soğutma havası (cooling air), uçaktaki yardımcı ekipmanları çalıştırmak için türbinden çekilen güç ve turbomakinaların politropik verimliliği de göz önünde bulundurularak hesaplara dahil edilmiştir.

Değişken parametrelerin motorun performansına olan etkisinin incelenebilmesi ve sayısal olarak değerlendirilebilmesi için literatürde mevcut olanlar arasından altı adet performans göstergesi (amaç fonksiyonu) belirlenmiştir. Bunlar ekolojik performans katsayısı  $CEP$ , turbofan motorunun toplam verimi  $\eta_o$ , ekserji yıkım faktörü  $f_{exd}$ , özgül yakıt tüketimi  $TSFC$ , özgül itme kuvveti  $F_s$ , ve toplam entropi üretim hızı  $\dot{S}_{gen}$  olarak sıralanabilir. Bunlar arasından turbofan motorunun toplam verimi, özgül yakıt tüketimi ve özgül itme kuvveti, Termodinamiğin 1. Yasası temelli performans göstergeleri, ekolojik performans katsayısı, ekserji yıkım faktörü ve entropi üretim hızı ise Termodinamiğin 2. Yasası temelli performans göstergeleridir.

Bu tez çalışmasında uçak motorunun yukarıda belirtilen 6 performans göstergesinin ve 4 tasarım parametresinin optimum değerlerine olan etkilerinin incelenmesi için iki farklı ısı kaybı dikkate alınmıştır. Birinci ısı kaybı, yanma odası içerisinde yüksek sıcaklıkta gerçekleşen yanma tepkimesi esnasında yanma odasından dışarıdan geçen tali hava akımına olan ısı kaybıdır. Bu kayıp, yanma odası duvarı üzerinden tali hava akımına ısı transferi şeklinde varsayılmıştır. İkinci ısı kaybı ise, tali hava akımından motorun dışındaki (çevredeki) çok soğuk atmosferik havaya olan ısı kaybıdır. İkinci ısı kaybının motorun iç ve dış yüzeyi arasında gerçekleştiği varsayılmıştır.

Literatürdeki bilgilerden faydalanılarak, ticari bir uçağın normal seyir irtifasındaki çevre koşulları yaklaşık olarak elde edilmiş, kompresör basınç oranı, fan basınç oranı, tali akış oranı, maksimum türbin sıcaklığı gibi tasarım parametrelerinin hangi aralıklarda olabileceği incelenmiştir. Ayrıca, soğutma havası akışı ile ana hava akışı arasındaki kütleli debi oranı, hava tahliye oranı, turbomakinaların politropik verim oranları, millerin mekanik verimleri gibi parametreler de literatürdeki çalışmalar incelenerek belirlenmiştir.

Havanın uçak turbofan motoruna giriş koşullarından, en son kısımda yanma ürünlerinin lüle çıkış koşullarına kadar tüm prosesler denklemlerle birbirine irtibatlandırılmış, ve giriş şartları ile tasarım parametrelerinin değerlerine göre bazı çalışma senaryoları için yanma ürünlerinin çıkış koşulları ve performans göstergelerinin optimal değerleri hesaplatılmıştır. Bu hesaplamalarda ısı kaybı oranının farklı değerleri de dikkate alınmış ve bu sayede hem tasarım parametrelerinin hem de ısı kaybı oranının farklı değerlerinin performans göstergeleri üzerindeki etkileri hesaplanabilmiştir.

Yapılan bu hesaplamalarla birlikte, tasarım parametreleri ikili gruplar halinde seçilerek bu parametrelerin  $CEP$  ve  $\eta_o$  üzerindeki eş zamanlı etkileri 3 boyutlu şekiller vasıtasıyla incelenmiş ve iki tasarım parametresi birden değişken olduğunda performans göstergesinin karakterinin nasıl değiştiği gözlemlenebilmiştir.

Buna göre  $CEP$  ve  $\eta_o$  performans göstergeleri bakımından  $r_{C,Total}$ ,  $r_F$  ve  $T_{max}$ 'ın çok küçük değerlerine sahip bölgeleri tasarım açısından uygun olmayan bölgelerdir; çünkü bu bölgelerde  $CEP$  ve  $\eta_o$ 'da ani düşüşler gözlemlenmiştir. Ayrıca, bir tasarım parametresinin değerindeki değişimin performans göstergesinin aldığı değere olan etkisinin, diğer tasarım parametrelerinin değerlerine doğrudan bağlı olduğu ve bu

durumun performans göstergesinin eğrisinin şeklini doğrudan etkilediği de gözlemlenmiştir.

Daha sonra, aynı koşullar altında iki farklı ısı kaybının değerindeki değişimin performans göstergelerinin değerlerine yaptığı etki gözlemlenmiş ve birbirlerine göre göreceli (bağıl) olarak karşılaştırması yapılmıştır.

Buna göre, yanma odasından tali akış havasına olan ısı kaybı (birinci ısı kaybı) etkisinin, tali akış havasından dış ortama olan ısı kaybı (ikinci ısı kaybı) etkisine göre çok daha önemli olduğu, ikinci ısı kaybı etkisinin birinci ısı kaybı etkisiyle karşılaştırıldığında nispeten küçük olduğu gözlemlenmiştir. Bu sebeple, bu tezde birinci ısı kaybının etkileri üzerine yoğunlaşmıştır.

Daha sonra, performans göstergelerinin değişen tasarım parametreleri değerleri karşısında hangi değerleri aldığı, tasarım parametreleri için hangi değerlerin optimum değerler olduğu ve karşılık gelen optimal (minimum ya da maksimum) performans göstergesi değerlerinin ne olduğu belirlenmiştir. Ayrıca ısı kaybının, performans göstergesinin aldığı değerlere ve tasarım parametrelerinin optimum değerlerine olan etkisi de incelenmiş ve hesaplanmıştır.

Bu hesaplama sonunda, birinci ısı kaybının  $CEP$ ,  $f_{exd}$  ve  $\dot{S}_{gen}$  performans göstergeleri üzerinde tasarım parametrelerinin tüm değerlerinde (optimum değerleri de dahil olmak üzere) oldukça etkili olduğu gözlemlenmiştir.

Ayrıca, diğer üç performans göstergesi ( $\eta_o$ ,  $TSFC$  ve  $F_s$ ) üzerindeki etkisi ile karşılaştırıldığında, birinci ısı kaybının  $CEP$ ,  $f_{exd}$  ve  $\dot{S}_{gen}$  üzerindeki etkisi  $r_{c,Total}$ ,  $r_F$  ve  $\beta$ 'nin küçük ve optimum değerlerinde ve  $T_{max}$ 'ın optimum ve büyük değerlerinde çok daha önemlidir. Diğer taraftan, birinci ısı kaybının  $\eta_o$ ,  $TSFC$  ve  $F_s$  üzerinde etkili olduğu bölge ise  $r_{c,Total}$ ,  $r_F$  ve  $\beta$ 'nin büyük değerleri ile  $T_{max}$ 'ın küçük değerleridir.

Isı kaybının  $CEP$ ,  $f_{exd}$  ve  $\dot{S}_{gen}$  üzerindeki etkisinin karakteristiği ile  $\eta_o$ ,  $TSFC$  ve  $F_s$  üzerindeki etkisinin karakteristiğinin farklı olduğu, sunulan sonuç grafikleri ve tabloları üzerinde yapılan gözlemlerin ve varılan sonuçların en önemlileridir. Bu farklılığın sebebi, yanma olayının çok yüksek bir sıcaklıkta gerçekleşmesi, dolayısıyla yanma odasından gerçekleşen ısı kaybının çok yüksek sıcaklık farkları arasında olmasıdır. Bu durum, ısı kaybının oldukça tersinmez bir proses olmasına ve bu proseste entropi üretim hızının oldukça yüksek olmasına sebebiyet vermektedir. Bu sebeple, Termodinamiğin 2. Yasası temelli olan  $CEP$ ,  $f_{exd}$  ve  $\dot{S}_{gen}$  performans göstergeleri, Termodinamiğin 1. Yasası temelli olan  $\eta_o$ ,  $TSFC$  ve  $F_s$  performans göstergelerine kıyasla ısı kaybı oranının artışından oldukça fazla oranlarda etkilenmektedir.

Ayrıca, ısı kaybı oranındaki değişimin, tasarım parametrelerinin optimum değerlerini de etkilediği, ısı kaybı oranındaki artış veya azalışa göre tasarım parametrelerinin optimum değerlerinde kaymalar olduğu yani tasarım parametrelerinin ısı kaybı etkisiyle farklı optimum değerlere sahip olduğu gözlemlenmiştir. Elbette ki bu durum, performans göstergelerinin değerlerini de değiştirmektedir.

Son olarak, tasarım parametrelerinin küçük, optimum ve büyük değerleri için performans göstergelerinin ısı kaybı artışlarıyla nispi değişimleri gözlemlenmiş ve buna göre ısı kaybı oranındaki lineer artışın performans göstergeleri değerleri üzerindeki değişime olan etkisinin lineer olmadığı gözlemlenmiştir.

## **1. INTRODUCTION**

From past to present, energy has been playing a crucial role in human life. Many technologies have been developed to utilize energy in all areas such as lighting, transportation, heating, cooling etc. One of the major areas that energy utilization constitutes an important point is transportation. In addition to ground and water transportation, aviation has also a key role in transportation and energy consumption.

In the last decades, sustainability concept has drawn attention all over the world, since human recognized the fact that conventional sources have been depleting and fossil fuels that have been utilized for many decades have major negative effects on environment. With this regard, studies on sustainability, ecofriendly products and efficiency have been increased significantly.

In order to investigate performance of thermal systems, energy and exergy concepts have been utilized as useful tools. In this point, thermodynamics is the related science branch analyzing the thermal systems. The First Law of Thermodynamics is utilized to analyze the conservation of quantity of energy, and The Second Law of Thermodynamics gives an opportunity to analyze the decrease in quality of energy, which corresponds to the exergy analysis concept.

By utilizing the thermodynamics tool, performance analyses of thermal systems have been conducted and effects of performance of thermal systems on environment have been investigated. With this motivation, many performance indicators for efficiency, ecology and sustainability have been developed by scientists in order to be able to make quantitative analyses.

As mentioned above, aviation is one of the major energy consuming sectors due to increasing demand, long distances and large carrying capacities. Aircrafts utilize specialized engines to operate and fly, which basically consumes fossil fuel and have effects on environment with their irreversibility, losses and emissions. Performance analyses of such large energy consumers and emission sources are crucial for

sustainable environment and development, and essential method to do this is using thermodynamic analysis.

## **1.1 Purpose of the Thesis**

Thermodynamic analysis is one of the most crucial stages for designing and developing the thermal systems. For sustainable future, negative environmental effects of thermal systems need to be reduced and performance of these systems need to be improved or optimized.

Many thermal systems have been analyzed in terms of energy and exergy efficiency, irreversibility, environmental effects, economy, sustainability and optimization of design parameters by scientists. Performances of new technology thermal systems have improved and become more sustainable and environmentally less harmful with the help of these analyses.

Aircraft engines have also been under investigation in terms of performance, efficiency and environmental sustainability more recently, and require more development in this regard. For better engines, more detailed and various analyses need to be conducted in terms of thermodynamics point of view.

During literature review phase, it has been observed that many different and detailed studies have been conducted on performance of thermal systems, and observations on reasons which reduce the performance and efficiency have been done for different types of technologies. Also, it is further observed that some studies have been focused on losses and leakages in thermal systems, especially for ground-type power plants. However, it has been observed that effects of heat leakages on the performance of aircraft engines have not been investigated in the open literature.

It is known that aircraft engines have to operate at very cold media due to very high operating attitudes. Therefore, it has been considered that heat leakage from the engine to the ambient and within the engine can be significant. Hence, heat leakage can have significant effects on aircrafts engines in terms of performance and environmental effects.

During the literature review, recognizing the absence of a study focusing on effect of heat leakage on the performance of aircraft engines, and observing utilization of turbofan engines widely by most of the commercial aircrafts in today's technology,

and considering the environmental effects of these large engines' performance, it has been concluded that a new study is required focusing on effects of heat leakage on the performance of a turbofan engine. Moreover, it should be performed with the consideration of efficiency and environmental effects in terms of energy and exergy analyses so that designers of new engines can benefit from this study to understand the relation between heat leakage and performance of turbofan engines. This consideration constitutes the purpose and motivation of this thesis study, and possible future studies on the performance of aircraft engines.

## **1.2 Literature Review**

A detailed literature review has been conducted in order to gather comprehensive information on energy and exergy analyses for thermal systems, especially for aircraft engines.

The mechanics, aerothermodynamics and thermodynamics of gas turbine propulsion systems can be found in textbooks such as Cohen et al. (1996), Hünecke (2003), Oates (1998), Hill and Peterson (1992), Mattingly et al. (2002), Mattingly (2006), Baskharone (2006) and El-Sayed (2008). These textbooks also provide historical background for aircraft engines, developments and advances in this area, detailed information on different gas turbine propulsion engines and applications, detailed information on different configurations for turbofan engines and many numerical examples in addition to fundamental knowledge for aircraft engine analysis.

Also, widely utilized thermodynamics textbook Çengel and Boles (2005) gives detailed information, provides useful illustrations and applications on thermodynamics. One can learn almost all fundamental information on thermodynamics by utilizing this source. Moreover, it presents a comprehensive information on gas power cycles and introductory information on jet-propulsion cycles.

Additionally, importance of thermodynamic analysis of thermal systems and need for deepening these analyses by utilizing exergy concept have been stated by Bejan and Siems (2001), Dincer and Rosen (1998, 2005), Hepbasli (2008), Rosen (2002) and Rosen and Etele (2004).

In addition, optimization studies utilizing finite-time thermodynamics and ecological optimization of thermal systems studies have been performed in literature such as Chen et al. (2007), Durmayaz et al. (2004), Mollaoglu et al. (2009), Ust et al. (2006), Wang et al. (2011), Wang et al. (2014), Xia et al. (2006) and Zhang et al. (2007).

A performance optimization for a single-spool turbofan engine has been performed by Najjar and Al-Sharif (2006). Turbofan model utilized in this study includes polytropic efficiencies of turbomachinery, and excludes auxiliary power, bleed air and turbine cooling. Aim of the study is to minimize thrust specific fuel consumption as an objective function, by using four design parameters, namely bypass ratio, fan pressure ratio, overall pressure ratio and turbine inlet temperature. Optimization has been performed twice, once with introducing a minimum specific thrust criteria and optimizing thrust specific fuel consumption. In the second case, no specific thrust constraint has been introduced and only thrust specific fuel consumption optimization has been performed. It has been concluded that when optimization has been performed without a minimum specific thrust constraint, maximum bypass ratio and overall pressure ratio become limiting factors and this makes the optimization problem a two-dimensional one due to fan pressure ratio and turbine inlet temperature to be optimized as design parameters. In this configuration, it has been found that for optimum values of maximum turbine inlet temperature and fan pressure ratio, objective function takes better values with increasing bypass ratio and total pressure ratio. Moreover, small variations from optimum values of design parameters do not cause significant deterioration in thrust specific fuel consumption. When a minimum specific thrust constraint introduced to the problem, it has been observed that bypass ratio becomes no longer a limiting factor; hence, problem becomes a three-dimensional one with bypass ratio, fan pressure ratio and maximum turbine inlet temperature as the design parameters to be optimized.

An exergetic and exergoeconomic analysis of an aircraft jet engine has been conducted by Balli et al. (2008). In this paper, it has been reemphasized that exergy based performance analyses are more useful than energy based performance analyses for thermal systems especially for aircraft engines. Also, importance of exergoeconomic analysis has been indicated for cost-based point of view. Exergetic analyses of each component and the whole aircraft engine have been conducted and it has been concluded that the most exergy-destructive part of the engine is the

combustion chamber due to high level irreversibility of combustion process. Moreover, balance equations for exergoeconomic analysis have been developed; exergy cost and unit exergy cost of fuel and working fluid at each station have been calculated. Exergy cost is defined as unit exergy cost times exergy of flow at that station.

An exergetic analysis of an aircraft turbofan engine with an afterburner has been performed by Turgut et al. (2007). In their study, several exergetic performance parameters have been used and performance of each engine part has been calculated for ground level and cruise level altitudes. Their study has been conducted to investigate efficiencies and improvement potentials of each engine part considering increasing demand for aviation and jet fuel. It has been concluded that the most irreversible parts of the engine are afterburner, exhaust unit (nozzle) and combustion chamber respectively, due to high exergy destruction and low exergy efficiencies.

An exergy and thermoeconomic analysis of a mixed exhaust turbofan engine during a typical commercial flight has been conducted by Tona et al. (2010). In this study, two different approaches have been utilized, one is the exergetic performance of the whole engine for different phases of the flight (global model) and the other is the exergetic performance of each engine part (local model). In this detailed study, all parts and systems of aircraft have been defined carefully, and exergy flow analysis has been conducted for each component. It has been concluded in this study that exergetic efficiency is the highest in the cruise phase, while it is lowest in the landing. Also, it has been observed that combustion chamber and mixer (where bypass flow and core flow are mixed before leaving the engine) are responsible from the most of the exergy destruction, hence irreversibility in the system.

An optimization of energy and exergy of two-spool turbofan engines using genetic algorithms has been performed taking into account bleed air, cooling of the turbines, combustion process in the combustion chamber and polytropic efficiencies of rotation turbomachinery (fan, compressor and turbine) by Tai et al. (2014). In this study, three different objective functions have been utilized namely energy efficiency, exergy efficiency and combination of them. The aim of the study is to optimize the design of a turbofan engine in order to have the most efficient and effective system. It has been concluded that combination of energy and exergy efficiency as an objective function provides the best exergy efficiency and specific

thrust values; however, it does not provide the best results for energy efficiency and thrust specific fuel consumption. Also, when energy efficiency is the objective function alone, thrust specific fuel consumption reaches the minimum value. Moreover, authors have suggested including exergy efficiency too as an additional objective function for aircraft engine design since it helps to maximize utilization of the potential of the fuel efficiently.

An on-design analysis of high bypass turbofan engines study has been conducted by Turan et al. (2008). In this study, a new software program has been developed for parametric and performance analyzes of high bypass, unmixed, no afterburner turbofan engines. By using this program, objective functions of a turbofan engine such as specific thrust, thrust specific fuel consumption and efficiencies can be optimized. Design parameters such as compressor pressure ratio, fan pressure ratio, bypass ratio, Mach number for the flight, turbine inlet temperature etc. have been utilized; and variations of values of objective functions with respect to some design parameters have been analyzed with the help of this program. Also, plots of their objective functions with respect to selected design parameters have been illustrated in the paper, so that comparisons have been performed.

A first law of thermodynamics analysis of a low-bypass turbofan engine has been performed by Turan et al. (2014a). Fuel consumption and emissions of aircraft engines have been remarked and necessity of thermodynamically more efficient systems for a more sustainable environment has been defended. In the analysis, energy balance equations for each component of the engine have been developed, and energy flow rate calculations have been done. Also, temperature, pressure and mass flow rate values for each component have been calculated during the operation. Thrust specific fuel consumption, overall efficiency and component energy flows at maximum thrust level have been used as performance indicators of the engine. It has been concluded that maximum energy flow rate is observed in high-pressure turbine inlet (or combustion chamber exit) due to the combustion process with high fuel energy. Moreover, importance of the first law analysis of aircraft engines has been emphasized since fuel consumption and emissions, which can be assessed based on the first law analysis, have effects on environment and sustainability as well as on cost.



Some exergetic measures of a turbofan engine have been studied by Turan et al. (2014b). JT8D series turbofan engines have been selected to study, which are widely utilized low-bypass and twin-spool engines for commercial aircrafts. These engines have been in use since 1964 and some of the commercial aircrafts that have been powered by JT8D engines are 727, 737-100, 737-200 and MD-80 (Url-1). In this study, effects of aviation emissions and fuel consumption on the environment have been emphasized and importance of exergetic analysis for aircraft engines has been noticed. In the analysis, fuel depletion ratio, productivity lack ratio, fuel exergy factor, product exergy factor and improvement potential rates have been selected as exergetic measures for each part of the engine. Turbine cooling and auxiliary power requirements have not been taken into account in the study. Exergetic performances of each component have been calculated, and it has been concluded that combustion chamber is the most irreversible unit of the engine and it has the highest potential for improvement. Moreover, it has also been noted that exergo-economic and exergo-environmental analyses for turbofan engines would be useful to have more comprehensive conclusions.

An exergetic analysis of an aircraft turbojet engine with an afterburner has been conducted by Ehyaei et al. (2013). Analysis has been performed for both ground level and an altitude of 11,000 m, and each unit of the engine has been considered separately. Moreover, air inlet velocity to the engine has also been taken into consideration. System has been described in detail and fundamental information has been provided for thermodynamic analysis of aircraft engines including exergetic analysis. Exergetic efficiencies and entropy generation rates of the engine parts have been plotted to observe relative performances of these engine units. It has been concluded that the most exergy-efficient unit is the compressor and the least one is the afterburner for both altitudes. Moreover, it has been observed that reducing the velocity decreases the exergy efficiency at sea level.

Aydın et al. (2013a) has studied exergo-sustainability indicators of a turboprop aircraft for different phases of a flight. In this study, role of the aviation sector in the global warming and emissions has been emphasized, and importance of exergetic analysis for better sustainability has been remarked. Flight of a turboprop engine has been divided into steps, and performance of the aircraft in terms of exergo-sustainability has been evaluated. Exergy efficiency, waste exergy ratio, recoverable

exergy rate, exergy destruction factor, environmental effect factor and exergetic sustainability index have been utilized as the exergo-sustainability indicators of the turboprop engine. Turboprop engine analyzed in this study consists of a propeller, compressor, combustion chamber and two turbines one of which drives the compressor and the other one drives the propeller. Thrust is produced both by exhaust gases and by propeller. It has been concluded that the worse performance in terms of sustainability is seen during taxi and landing phases of the flight, where taxi is the phase when aircraft is moving on the ground with its own power before and after a flight. Moreover, it has been remarked in this study that it is important to understand the relations between exergetic sustainability and phases of the flight to further improve the performance and savings, and that exergetic performance indicators are useful tools for understanding the environmental effects of aircrafts.

An exergy based ecological optimization of a turbofan engine has been performed by Tanbay et al. (2015). In this study, a new performance indicator has been defined, namely the Coefficient of Ecological Performance *CEP*, and calculated by propulsive power per unit exergy destruction rate. Additionally, specific thrust, overall efficiency, exergy destruction factor and exergetic sustainability index have been selected as the other performance indicators while *CEP* has been considered as the main performance indicator. Combustion process has been modeled as finite-rate heat transfer from a hot source, and heat exchanger effectiveness has also been considered. Compressor pressure ratio, fan pressure ratio, bypass ratio and turbine inlet temperature have been used as design parameters and optimum range for these parameters have been calculated.

Considering these studies in the literature, this thesis has been commenced. In the same scope, some contents of the thesis has been presented in the 7<sup>th</sup> International Ege Energy Symposium (Colakoglu et al, 2014). Moreover, it has been accepted for publication in the International Journal of Exergy (Colakoglu et al, in press).

## **2. SELECTED FUNDAMENTAL CONCEPTS OF THERMODYNAMICS UTILIZED IN THE THESIS**

Before proceeding with the details of the thesis, a brief review of some fundamental information on thermodynamics will certainly be useful. This information may be considered as the basics for the thermodynamic analysis of aircraft engines.

### **2.1 Enthalpy**

Enthalpy is defined as a combination property consisting of internal energy and flow work of a flowing fluid in or out of a system. Flow work is known as work required for a fluid to push it in or out of an open system, and defined as the product of volume and pressure of the fluid element to be pushed. Enthalpy represents the total energy of a flowing fluid stream when its potential and kinetic energies are neglected (Çengel and Boles, 2005). It is denoted by  $H$  having a unit of  $kJ$  and can be formulated with the combination of internal energy, pressure and volume as

$$H = U + PV \quad (2.1)$$

Specific enthalpy represents per unit mass of enthalpy and it is denoted by  $h$ . It is also called as enthalpy for simplicity and from now on, specific enthalpy will be referred as enthalpy within this thesis. Hence, unit of the enthalpy becomes  $kJ/kg$ .

Enthalpy is a very useful property for analysis of steady-flow devices, such as turbines, compressors, nozzles etc. Since it is assumed that no change with time occurs inside the control volume in the properties of the fluid, change in internal energy of the fluid with time equals to zero for steady-flow devices. For the fluid flowing in or out, enthalpy is used since it includes both the internal energy and the flow work together. Hence, the conservation of energy equation for a steady-flow process through a steady-flow device can be written as

$$\dot{Q} - \dot{W} = \sum_{out} \dot{m} (h + v^2/2 + gz) - \sum_{in} \dot{m} (h + v^2/2 + gz) \quad (2.2)$$

For ideal gases, enthalpy is a function of only temperature and the relation between these two properties may be written in differential form as

$$dh = c_p dT \quad (2.3)$$

where  $c_p$  is specific heat at constant pressure, and it is also a function of temperature for ideal gases.

If it is further assumed that the ideal gas is a calorically perfect gas, which means that specific heat is constant and not a function of temperature, then relation between enthalpy change and temperature change becomes

$$\Delta h = c_p \Delta T \quad (2.4)$$

hence relation between enthalpy and temperature becomes

$$h = c_p T \quad (2.5)$$

## 2.2 Stagnation (Total) Properties

As very well explained and illustrated by Çengel and Boles (2005), change in kinetic energy cannot be neglected for most high speed flows. When there is no significant elevation difference and no heat or work interaction, energy of the flowing fluid stream consists of two terms, namely enthalpy and kinetic energy. Sum of these two quantities is referred as stagnation (total) enthalpy and it can be regarded as the enthalpy of a flowing fluid stream when it is brought to rest adiabatically.

Stagnation enthalpy can be defined as

$$h_0 = h + \frac{v^2}{2} \quad (2.6)$$

Stagnation enthalpy change remains constant for a steady-flow process through a control volume when there is no work or heat interaction, and it yields

$$h_1 + \frac{v_1^2}{2} = h_2 + \frac{v_2^2}{2} \quad (2.7)$$

which means

$$h_{01} = h_{02} \quad (2.8)$$

When the fluid is brought to rest during the process mentioned above, then enthalpy and stagnation enthalpy becomes equal at the final state and this can be shown as

$$h_1 + \frac{v_1^2}{2} = h_2 = h_{02} \quad (2.9)$$

Stagnation temperature can be found from stagnation enthalpy by using temperature-enthalpy relation for an ideal gas with constant specific heats assumption. Substituting equation (2.5) for equation (2.6) yields

$$c_p T_0 = c_p T + \frac{v^2}{2} \quad (2.10)$$

then stagnation temperature becomes

$$T_0 = T + \frac{v^2}{2c_p} \quad (2.11)$$

By using the isentropic relation between the temperature and the pressure for an isentropic process, stagnation pressure of an ideal gas with constant specific heats can be found from

$$\frac{P_0}{P} = \left( \frac{T_0}{T} \right)^{k/(k-1)} \quad (2.12)$$

### 2.3 Speed of Sound and Mach Number

For ideal gases, speed of sound is a function of only temperature and it can be written as

$$c = \sqrt{kRT} \quad (2.13)$$

where  $k$  is the specific heat ratio and  $R$  is the gas constant for that specific ideal gas (Çengel and Boles,2005).

Mach number is defined as the ratio of velocity of the gas to the speed of sound and can be written as

$$M = \frac{v}{c} \quad (2.14)$$

## 2.4 Chocking at the Nozzle Exit

Thrust required for the propulsion of aircrafts is provided from the aircraft engines. Thrust has two components, namely momentum and pressure. Momentum component of thrust is provided by the difference between the inlet air velocity to the engine and exit air velocity from the engine. On the other hand, pressure component of the thrust is provided by the pressure difference between exit air at the exhaust and ambient air.

When the critical pressure of exhaust gases at the exit is larger than the ambient pressure, it is said that flow is choked at the nozzle exit. Then, speed of the exhaust gases is at the sonic speed and Mach number is equal to 1. This provides contribution to the thrust produced by the engine.

When the critical pressure of exhaust gases at the exit is less than the ambient pressure, then it is said that flow is unchoked. In this case, pressure of the exhaust gases is assumed to be equal to the ambient pressure and no thrust contribution is provided due to pressure difference (El-Sayed, 2008).

## 2.5 Entropy

Entropy may be assumed as molecular disorder level (Çengel and Boles, 2005). As it is valid also for energy, engineering studies deal with change in entropy not the exact value of entropy. Definition of entropy is based on its differential change during an internally reversible process as

$$dS = \left( \frac{\delta Q}{T} \right)_{int rev} \quad (2.15)$$

Hence, entropy change for a system during an internally reversible process from state 1 to state 2 can be written as

$$\Delta S = S_2 - S_1 = \int_1^2 \left( \frac{\delta Q}{T} \right)_{int rev} \quad (2.16)$$

Total entropy is denoted by  $S$  with the unit of  $kJ/K$  and entropy per unit mass (or only entropy) is denoted by  $s$  with the unit of  $kJ/kg K$ .

In real processes, increase of entropy principle states that some entropy is always created (or generated) during a real (irreversible) process and total entropy always increases in the universe. For a closed system, entropy change can be written during an irreversible process as

$$\Delta S = S_2 - S_1 = \int_1^2 \left( \frac{\delta Q}{T} \right) + S_{gen} \quad (2.17)$$

Constant specific heats assumption is a common practice for ideal gases, and it provides sufficiently accurate results when the temperature range is not larger than a few hundred degrees. Since specific heats of ideal gases change almost linearly with the temperature, it is reasonable to assume average specific heats within the temperature limits (Çengel and Boles, 2005). By using constant average specific heats assumption, entropy change of an ideal gas during a process is

$$s_2 - s_1 = c_{p,avg} \ln \frac{T_2}{T_1} - R \ln \frac{P_2}{P_1} \quad (2.18)$$

where  $c_{p,avg}$  is average specific heat at constant pressure of this specified ideal gas. When entropy is held constant during a process, the process is referred as an isentropic process and for an isentropic process of an ideal gas, it can be written that

$$\frac{T_2}{T_1} = \left( \frac{P_2}{P_1} \right)^{(k-1)/k} \quad (2.19)$$

For control volume analysis, an entropy balance equation can be written and rearranged as

$$\sum \frac{Q}{T} + \sum m_i s_i - \sum m_e s_e + S_{gen} = \Delta S_{CV} \quad (2.20)$$

and

$$\dot{S}_{gen} = \sum \dot{m}_e s_e - \sum \dot{m}_i s_i - \sum \frac{\dot{Q}_k}{T_k} \quad (2.21)$$

in the rate form for steady-flow processes.

## 2.6 Exergy

Exergy can be defined as the maximum amount of useful work that a system is assumed to deliver with a reversible process from a given state to dead state in a specified environment by Çengel and Boles (2005). Since there is no reversible process in real life practices, it is impossible to convert all of the exergy of a system to work without any loss. Nonflow exergy or closed system exergy,  $\phi$  on a unit-mass basis, in  $kJ kg^{-1}$  can be defined for closed systems as

$$\phi = (u - u_0) + P_0(v - v_0) - T_0(s - s_0) + \frac{v^2}{2} + gz \quad (2.22)$$

and exergy for a stream or stream exergy,  $\psi$  on unit-mass basis, in  $kJ kg^{-1}$  can be defined as

$$\psi = (h - h_0) - T_0(s - s_0) + \frac{v^2}{2} + gz \quad (2.23)$$

where  $(h - h_0) - T_0(s - s_0)$  is the thermophysical exergy component,  $v^2/2$  is the kinetic exergy component and  $gz$  is the potential exergy component. In a more general definition, exergy has also chemical exergy component that can be obtained in a unit-mass basis, in  $kJ kg^{-1}$  by

$$\dot{e}x_{chem} = \sum_i x_i e_i^{chem} + \bar{R}T_0 \sum_i x_i \ln x_i \quad (2.24)$$

for gas mixtures (such as air) including  $i$  different gases where  $x_i$  is mole fraction,  $e_i^{chem}$  is standard chemical exergy and  $\bar{R}$  is the universal gas constant (Szargut et al,



1988; Kotas, 1995; Turgut et al, 2007). Standard chemical exergy models can be found in literature. For technical liquid fuels, specific chemical exergy can be calculated on a unit mass basis as it is proposed by Szargut et al. (1988) and utilized by Kotas (1995), Szargut (2005) and Balli et al. (2008) as

$$e_{chem} = \varphi Q_{LHV} \quad (2.25)$$

where  $\varphi$  represents the ratio of specific chemical exergy of the fuel to lower heating value of the fuel,  $Q_{LHV}$  represents lower heating value of the fuel and formulation of  $\varphi$  for liquid fuels has been presented as

$$e_{chem} = Q_{LHV} \left[ 1.0401 + 0.1728 \frac{H}{C} + 0.0432 \frac{O}{C} + 0.2169 \frac{S}{C} \left( 1 - 2.0628 \frac{H}{C} \right) \right] \quad (2.26)$$

In equation (2.26),  $H$ ,  $C$ ,  $O$  and  $S$  are mass fractions of hydrogen, carbon, oxygen and sulphure in fuel. Fuel utilized in the thesis is kerosene (a widely utilized jet engine fuel) and chemical formula is assumed as  $C_{12}H_{23}$  (Balli et al, 2008; Turgut et al, 2007).

By using equation (2.26),  $\varphi$  is calculated as 1.067894 for kerosene.  $Q_{LHV}$  of kerosene is considered as 43,15 MJ per kg (Tanbay et al, 2013, 2015) and by using equation (2.25) specific chemical exergy of kerosene is calculated as 46,08 MJ per kg. In order to be in alignment with literature, specific chemical exergy of kerosene is assumed as 45.8 MJ per kg (Turgut et al, 2007, 2009b) with a 0.6% deviation from the calculated value, which is insignificant and ignorable. One can reach detailed information on oxidation of kerosene in Dagaut and Cathonnet (2006).

Also for further information, calculation details of  $\varphi$  according to equations (2.25) and (2.26), and formulation for calculating specific chemical exergy of solid fuels has been presented in Appendix A.

Dead state is the state of a system when it is in thermodynamic equilibrium with the environment. When a system is in dead state, then no temperature and pressure differences, no chemical reactions, no potential and kinetic energy differences, no unbalanced magnetic, electric and surface tension or other effects exist between the system and the environment. Restricted dead state is the state when the system is

completely in thermo-mechanical equilibrium with but it has a different chemical composition from its environment (Çengel and Boles, 2005).

Decrease of exergy principle states that in an irreversible process, exergy of an isolated system or the universe always decreases and this decrease is proportional to entropy generation of the universe and equal to exergy destruction (or irreversibility). Exergy destruction is always positive for real processes and zero for reversible processes and can be expressed as

$$X_{dest} = T_0 S_{gen} \geq 0 \quad (2.27)$$

For a system, exergy balance equation can be written as

$$X_{in} - X_{out} - X_{dest} = \Delta X_{system} \quad (2.28)$$

If the system is closed, then  $X_{in}$  and  $X_{out}$  terms does not include exergy transfer with mass transfer; however, for control volumes (open systems) it also includes exergy transfer with mass. Equation (2.28) can be rewritten for steady flow as below.

$$\dot{X}_{in} - \dot{X}_{out} - \dot{X}_{dest} = \frac{dX_{system}}{dt} \quad (2.29)$$

## 2.7 Brayton Cycle

Brayton cycle is the ideal cycle for gas-turbine engines, which was developed by George Brayton around 1870 (Çengel and Boles, 2005). It consists of processes in a compressor, a combustion chamber and a turbine for the open Brayton cycle and additionally a heat exchanger for the closed Brayton cycle. Open Brayton cycle is widely utilized cycle for gas turbine engines, which takes fresh air from the ambient and exhausts the burned gases to the atmosphere.

Steps of an ideal Brayton cycle can be summarized as

- Isentropic compression (in a compressor)
- Constant pressure heat addition (in a combustion chamber or heat exchanger)
- Isentropic expansion (in a turbine)

- Constant pressure heat rejection (in a heat exchanger for closed Brayton cycle or exhaust for the open Brayton cycle)

An open-cycle gas-turbine engine has been shown in Figure 2.1.

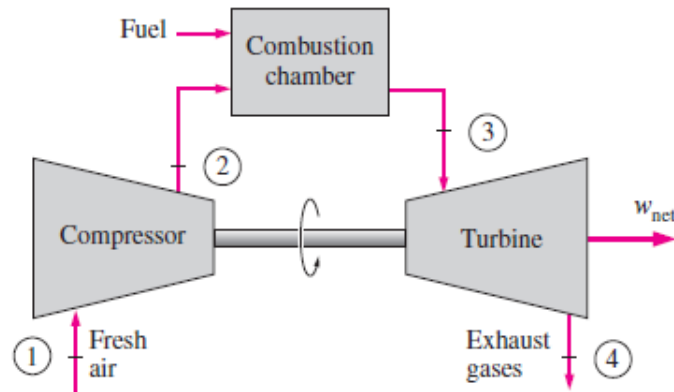


**Figure 2.1 :** An open-cycle gas-turbine engine (Çengel and Boles, 2005).

A closed-cycle gas-turbine engine and a T-s diagram for the Brayton cycle has been presented in Figure 2.2 and Figure 2.3.

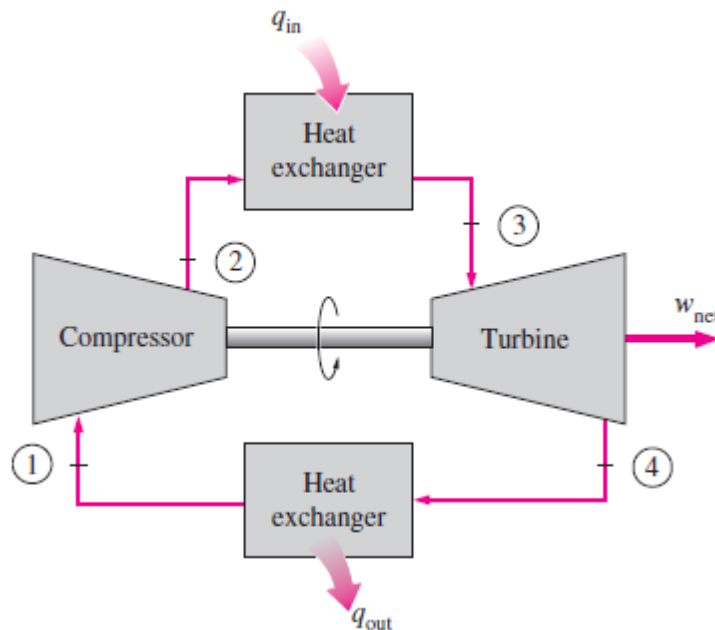


**Figure 2.2 :** A closed-cycle gas-turbine engine (Çengel and Boles, 2005).

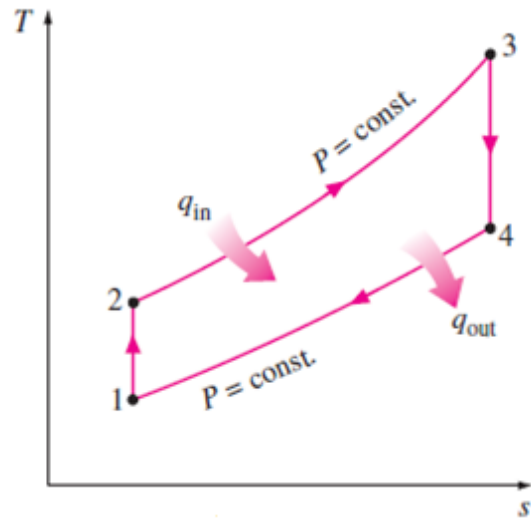


**Figure 2.3 :** T-s diagram for the ideal Brayton Cycle (Çengel and Boles, 2005).

### **3. A REVIEW OF PERFORMANCE INDICATORS USED IN THE THERMODYNAMIC ANALYSIS OF TURBOJET AND TURBOFAN CYCLES**

In this chapter, a brief introduction to turbojet engines and turbojet cycles has been presented in order to pass from Brayton cycle to jet propulsion cycle. Then, turbofan cycle and single-spool turbofan engines have been introduced in order to construct bases for twin-spool turbofan engines analyzed in the thesis. Moreover, selected thermodynamic analysis parameters utilized in literature for turbojet and turbofan engines have been introduced.

#### **3.1 Turbojet Cycle and Turbojet Engine**

Gas-turbine engines have been widely utilized for electricity production and aircraft propulsion. Idealized version of these gas-turbine cycles is Brayton cycle with four ideal processes described earlier. Aircraft engines utilize a special version of open Brayton cycle, which has a name of jet propulsion cycle. In both applications (both electricity production and aircraft propulsion), cycle consists of a compressor, a combustion chamber and a turbine; however, in aircraft engines there are also diffuser (intake) at the inlet and nozzle (exhaust) at the exit as additional parts (Çengel and Boles, 2005).

For the electricity production, gases are expanded in turbine as much as possible such that cycle produces net power that is more power than consumption of compressor. On the other hand, gas-turbine engines utilized in aircraft produces zero net power, which means that turbine produces just enough power to drive compressor. The reason is that the main purpose of the aircraft engines is not producing electricity but propel the aircraft. This has been realized by exhausting very hot gases with a very high velocity enough to propel the aircraft (Çengel and Boles, 2005; Tanbay et al, 2013). Steps of the processes a turbojet-engine (or an ideal turbojet) cycle can be summarized as

- Isentropic deceleration and compression of air at the diffuser
- Isentropic compression (much more compression than diffuser) in compressor
- Constant pressure combustion of fuel (or modelling as heat transfer to the air) in combustion chamber
- Isentropic expansion of combustion products (or modeling isentropic expansion of air by neglecting the burned fuel mass in the combustion products) in turbine (to provide the power consumption of the compressor on the same shaft and the auxiliary power requirement)
- Isentropic expansion and acceleration in nozzle
- Exhaust to the atmosphere

T-s diagram of an ideal jet propulsion cycle and a schematic illustration of a turbojet engine with its components have been presented in Figure 3.1 and Figure 3.2. Station numbering has been arranged such that

1. Diffuser inlet
2. Compressor inlet (diffuser exit)
3. Burner (combustion chamber) inlet (compressor outlet)
4. Turbine inlet (combustion chamber outlet)
5. Nozzle inlet (turbine outlet)
6. Nozzle exit

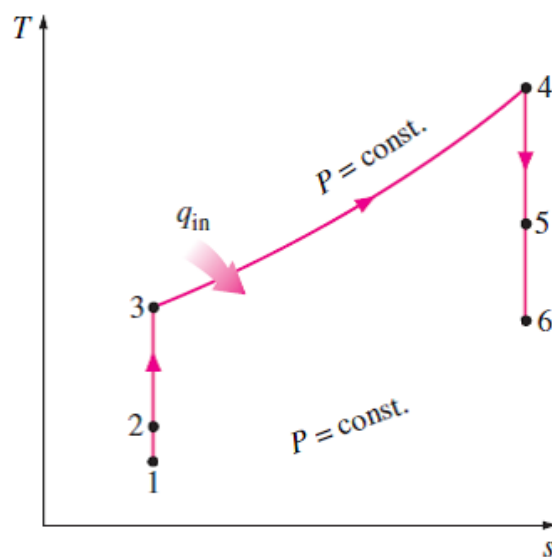


**Figure 3.1** : T-s diagram of an open ideal jet propulsion cycle.

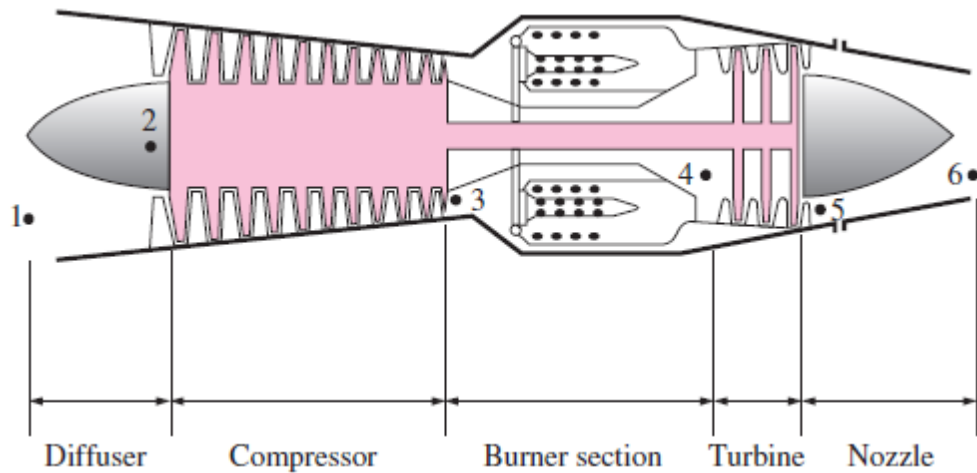


**Figure 3.2 :** A turbojet engine with its components (Çengel and Boles, 2005).

Moreover, in some cases an afterburner is also added to the exit of turbine before the gases enter to the nozzle in order to further increase the temperature of the gases such as in fighter aircrafts. Purpose of this application is to increase the thrust provided by the engine.

In contrast with the above ideal figure, in real life applications, cycles do not work ideally and some irreversibility occurs during operation such as pressure drop, heat leakage, friction etc. These effects cause deviations from the ideal operation of engines and should be considered for more realistic calculations.

### 3.2 Turbofan Cycle and Single-Spool Turbofan Engine

Turbofan engines are modified version of turbojet engines with a fan in the front of the engine and two separated streams along the engine. After passing the fan (F), one of the streams pass through the compressor (C), the combustion chamber (CC), the turbine (T) and the core nozzle (N). Meanwhile, the other stream directly goes through the fan nozzle (FN) after the fan without passing through C, CC and T; hence, it does not encounter the combustion process. This second stream is called as bypass stream. Bypass concept has been first introduced in the 1950s, and it has been successfully utilized since then. Turbofan engines have been powering both commercial aircrafts and fighter aircrafts. Moreover, turbofan engines provide greater thrust, improved fuel economy and lower noise level compared to turbojet engines (El-Sayed, 2008).

Processes of a turbofan cycle may be summarized as below considering the main (core) flow and bypass flow.

- Isentropic deceleration and compression of air at the diffuser (core and bypass air)
- Isentropic compression in fan (core and bypass air)

After the fan, bypass flow is separated and it goes through the fan nozzle with a process as

- Isentropic expansion and acceleration in fan nozzle (bypass flow)

On the other hand, main (core) flow continues its path with

- Isentropic compression in compressor (core flow)
- Constant pressure combustion (or modelling as heat transfer) in combustion chamber (core flow)
- Isentropic expansion in turbine (core flow)
- Isentropic expansion and acceleration in core nozzle (core flow)

These two streams (core flow and bypass flow) contribute to thrust produced by the engine together. In unmixed-type engines, these two streams leave the engine separately; while in mixed-type engines they are mixed before leaving the engine and exhausted together as a single stream.

Another difference between the turbojet and turbofan is that turbine in the turbojet drives the compressor; while, turbine in the single-spool turbofan drives the compressor and the fan together. Hence, power generated by the turbine of turbojet is equal to the power consumed by the compressor; on the other hand, power generated by the turbine of a single-spool turbofan engine is equal to the power consumed by the compressor plus power consumed by the fan. A schematic figure and a cross section of a turbofan engine is illustrated in Figure 3.3 and Figure 3.4.

### **3.3 Performance Indicators Utilized in the Thermodynamic Analysis of Turbojet and Turbofan Engines**

Parametric cycle analysis provides a useful tool for thermodynamic investigation of such systems. In parametric cycle analysis of aircraft engines, some objective functions (thrust specific fuel consumption, specific thrust etc.) are selected to



maximize or minimize and some design choices (compressor pressure ratio, bypass ratio etc.) are done with the existence of some flight conditions (temperature and pressure of the ambient air etc.) and some real-life limitations (maximum turbine inlet temperature etc.). By this way, predictions on performance indicators can be performed for aircraft engines (Mattingly et al, 2002).

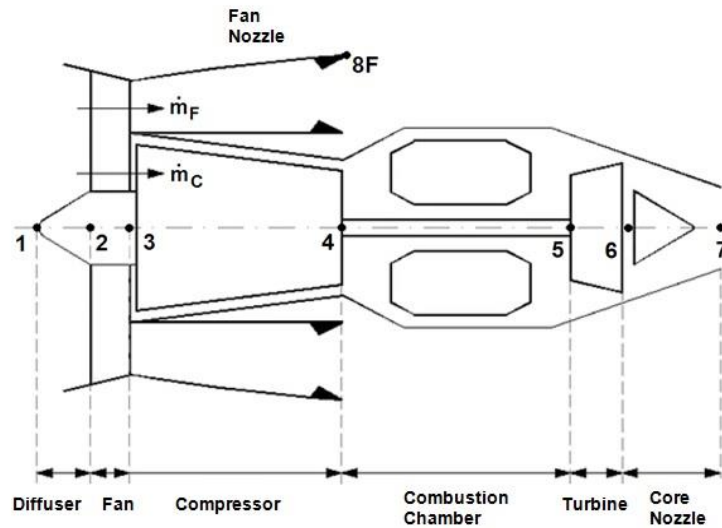


**Figure 3.3 :** A turbofan engine (Tanbay et al, 2015).

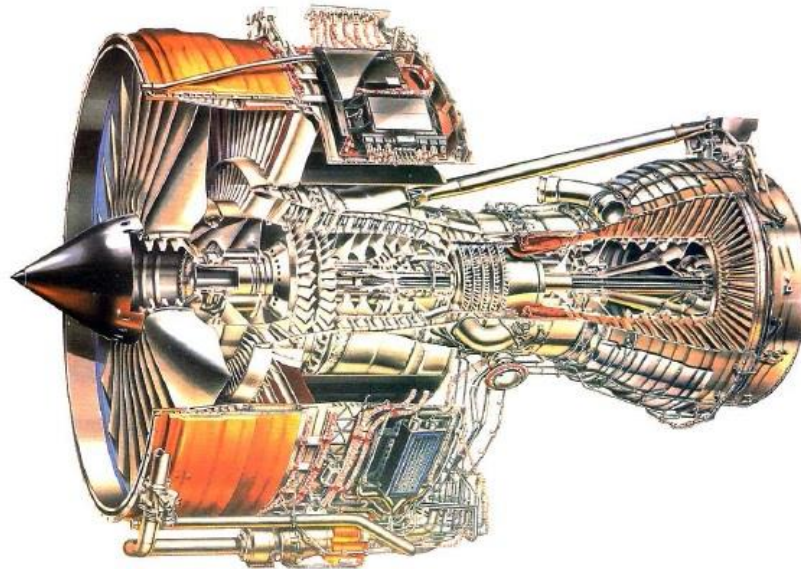


**Figure 3.4 :** Cross section of a turbofan engine (Rolls Royce, 1996).

When the open literature has been scanned, there are several performance indicators (or objective functions) utilized widely for performance analysis of turbojet and turbofan engines. Mattingly (2006) and El-Sayed (2008) have utilized thrust specific fuel consumption, specific thrust, propulsive efficiency, thermal efficiency and

overall efficiency as adequate performance indicators of a turbojet or turbofan engines considering the first law analysis of thermodynamics. T-s diagram for a turbofan engine has been presented in Figure 3.5. It has been utilized for the definitions for each of these performance indicators. Station numbering to be used is:

1. Diffuser inlet
2. Diffuser exit (fan inlet)
3. Fan exit (compressor inlet for core stream and fan nozzle inlet for bypass stream)
4. Compressor exit (combustion chamber inlet) for core stream
5. Combustion chamber exit (turbine inlet) for core stream
6. Turbine exit (core nozzle inlet) for core stream
7. Core nozzle exit for core stream
8. Fan nozzle exit for bypass stream

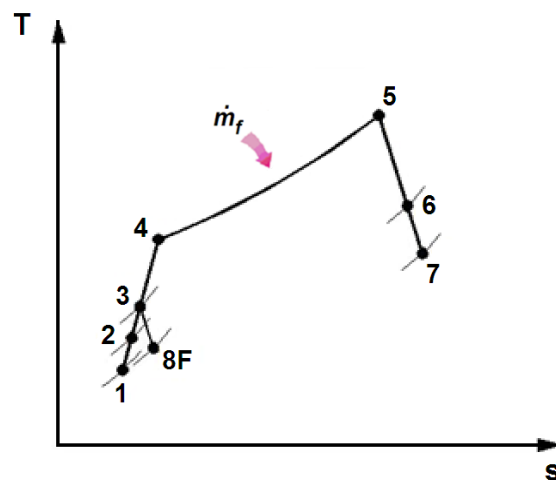


**Figure 3.5 :** T-s diagram of a turbofan engine.

### 3.3.1 Thrust specific fuel consumption (*TSFC*)

Thrust specific fuel consumption, *TSFC*, shows the amount of fuel consumption in order to produce one unit of thrust. It is a very helpful tool to analyze the efficiency of the engine in terms of fuel consumption comparing with thrust produced by burning this fuel. In the literature, it has been observed that several studies such as Hill and Peterson (1992), Mattingly et al. (2002), Hünecke (2003), Mattingly (2006),

Najjar and Al-Sharif (2006), El-Sayed (2008), Turan et al. (2008), Turan and Karakoc (2010) and Turan (2012) have utilized *TSFC* as a performance indicator. It can be defined as

$$TSFC = \frac{\text{Fuel consumption per unit time}}{\text{Total thrust}} = \frac{\dot{m}_f}{F} \quad (3.1)$$

where thrust is defined as

$$F = \dot{m}_c(v_7 - v_1) + \dot{m}_F(v_8 - v_1) + A_7(P_7 - P_1) + A_8(P_8 - P_1) \quad (3.2)$$

where  $\dot{m}_c(v_7 - v_1)$  is the momentum component by core stream,  $\dot{m}_F(v_8 - v_1)$  is the momentum component by bypass stream,  $A_7(P_7 - P_1)$  is the pressure component by core stream and  $A_8(P_8 - P_1)$  is the pressure component by bypass stream.  $\dot{m}_c$  and  $\dot{m}_F$  represents mass flow rates of air in core stream and bypass stream respectively.  $v_i$ ,  $A_i$  and  $P_i$  represents velocity of air at that station, area of corresponding exit station and pressure of the air for the specified station respectively.

### 3.3.2 Specific thrust ( $F_s$ )

Specific thrust,  $F_s$ , is a measure for how efficiently the engine produces thrust for each unit of air taken in by the engine inlet (Hünecke, 2003). Engines are required to be built larger when it is desired to suck more air at the inlet; in other words, the larger the engine, the larger the air sucking capacity. Therefore,  $F_s$  provides an evaluation for the engine size compared to its thrust production capacity. It has been utilized in the literature such as by Hill and Peterson (1992), Mattingly et al. (2002), Hünecke (2003), Mattingly (2006), Najjar and Al-Sharif (2006), El-Sayed (2008), Turan et al. (2008), Turan and Karakoc (2010) and Tanbay et al. (2013, 2015).  $F_s$  can be defined as

$$F_s = \frac{\text{Total thrust}}{\text{Total air mass flow in}} = \frac{F}{\dot{m}_c + \dot{m}_F} \quad (3.3)$$

### 3.3.3 Propulsive efficiency ( $\eta_P$ )

Propulsive efficiency,  $\eta_P$ , is defined by El-Sayed (2008) as the indicator of how efficiently the kinetic energy of air is converted to propulsive power in an engine.

Also, two different formulations for  $\eta_P$  have been presented by El-Sayed (2008). First expression is

$$\eta_P = \frac{\text{Propulsive power}}{\text{Propulsive power} + \text{power wasted in the exhaust}} \quad (3.4)$$

where

$$\text{Propulsive power} = \text{Total thrust} * \text{Air inlet velocity} = Fv_1 \quad (3.5)$$

so

$$\begin{aligned} \text{Power wasted in the exhaust} \\ = \frac{1}{2}(\dot{m}_c + \dot{m}_f)(v_7 - v_1)^2 + \frac{1}{2}(\dot{m}_F)(v_8 - v_1)^2 \end{aligned} \quad (3.6)$$

and the second expression is

$$\eta_P = \frac{\text{Propulsive power}}{\text{Rate of kinetic energy added to the air flow}} \quad (3.7)$$

where

$$\begin{aligned} \text{Rate of kinetic energy added to the air flow} \\ = \frac{1}{2}[(\dot{m}_c + \dot{m}_f)v_7^2 + \dot{m}_F v_8^2 - (\dot{m}_c + \dot{m}_F)v_1^2] \end{aligned} \quad (3.8)$$

El-Sayed (2008) stated that this second expression must not be used when the nozzles are choked since it comes out with results greater than unity. In other textbooks, the second expression for  $\eta_P$  has been utilized by Mattingly (2006) assuming the gases expand to ambient pressure at the nozzle; in other words, nozzles are not choked. Also, Hill and Peterson (1992) have already utilized the second expression in their textbook.

### 3.3.4 Thermal efficiency ( $\eta_{th}$ )

Thermal efficiency,  $\eta_{th}$ , is also another important performance indicator for aircraft engines. It may be defined as rate of kinetic energy addition to the air per unit of fuel energy consumed (Hill and Peterson, 1992). Thermal efficiency provides insight on

how efficiently the fuel energy is converted into kinetic energy in aircraft engines. El-Sayed (2008) defined  $\eta_{th}$  as

$$\eta_{th} = \frac{\text{Propulsive power} + \text{power wasted in the exhaust}}{\text{Rate of energy supplied by the fuel}} \quad (3.9)$$

where

$$\text{Rate of energy supplied by the fuel} = \dot{Q}_f = \dot{m}_f Q_{LHV} \quad (3.10)$$

and  $Q_{LHV}$  is the lower heating value of the fuel. It has been formulized by El-Sayed (2008) as

$$\eta_{th} = \frac{Fv_1 + \frac{1}{2}(\dot{m}_c + \dot{m}_f)(v_7 - v_1)^2 + \frac{1}{2}(\dot{m}_F)(v_8 - v_1)^2}{\dot{m}_f Q_{LHV}} \quad (3.11)$$

On the other hand, Hill and Peterson (1992) and Mattingly (2006) have utilized a different expression as

$$\eta_{th} = \frac{\text{Rate of kinetic energy added to the airflow}}{\text{Rate of energy supplied by the fuel}} \quad (3.12)$$

which yields

$$\eta_{th} = \frac{\frac{1}{2}[(\dot{m}_c + \dot{m}_f)v_7^2 + \dot{m}_F v_8^2 - (\dot{m}_c + \dot{m}_F)v_1^2]}{\dot{m}_f Q_{LHV}} \quad (3.13)$$

### 3.3.5 Overall efficiency ( $\eta_o$ )

Overall efficiency,  $\eta_o$ , has been defined as the product of propulsive efficiency and thermal efficiency by Hill and Peterson (1992), Mattingly (2006) and El-Sayed (2008). It may be interpreted as propulsive power produced by the engine per unit fuel energy consumed. Overall efficiency hence can be expressed as

$$\eta_o = \eta_P \eta_{th} = \frac{\text{Propulsive power}}{\text{Rate of energy supplied by the fuel}} = \frac{Fv_1}{\dot{m}_f Q_{LHV}} \quad (3.14)$$

Combustion process has been modelled as finite-rate heat transfer from a constant-temperature heat source to colder working fluid via a heat exchanger having

efficiency of  $\varepsilon_H$  by Tanbay et al. (2013, 2015). In these studies, instead of fuel addition and combustion, nearly-constant pressure heat addition process has been considered. Therefore, a different overall efficiency expression has been required due to absence of fuel combustion. It has been adopted as

$$\eta_o = \frac{\text{Propulsive power}}{\text{Max. rate of heat transfer possible from the heat source}} \quad (3.15)$$

and it has been expressed as

$$\eta_o = \frac{Fv_1}{\dot{m}_c c_p (T_{05} - T_{04}) / \varepsilon_H} \quad (3.16)$$

When it comes to the 2<sup>nd</sup> Law analysis of aircraft engines, there have been several performance indicators utilized in the open literature. These indicators will be explained below.

### 3.3.6 Exergetic efficiency ( $\eta_{ex}$ )

Exergetic efficiency,  $\eta_{ex}$ , has been proposed by Clarke and Horlock (1975) with the name of “rational efficiency”, utilized by Etele and Rosen (2001), which does not reflect the meaning sufficiently. Hence, it is renamed as “exergetic efficiency” by this thesis and presented with the same definition as

$$\text{Exergetic efficiency} = \frac{\text{Propulsive Power}}{\text{Exergy input rate}} \quad (3.17)$$

More generally it has been defined as rate of exergy recovered to rate of exergy supplied. In addition, it can be written by using exergy destruction rate. Exergetic efficiency can be expressed as

$$\text{Exergetic efficiency} = \frac{\text{Rate of exergy recovered}}{\text{Rate of exergy supplied}} = \frac{\dot{E}x_{recv}}{\dot{E}x_{supp}} \quad (3.18)$$

or

$$\eta_{ex} = 1 - \frac{\text{Rate of exergy destruction}}{\text{Rate of exergy supplied}} = 1 - \frac{\dot{E}x_{dest}}{\dot{E}x_{supp}} \quad (3.19)$$

Exergetic efficiency is a useful tool for the second law analysis of aircraft engines and it has been utilized by several studies such as Dincer and Rosen (2007), Turgut et al. (2007, 2009a, 2009b), Balli et al. (2008), Tona et al. (2010), Midilli and Dincer (2009), Midilli et al. (2011), Altuntas et al. (2012), Tai et al. (2014), Aydın et al. (2013a, 2013b, 2014a, 2014b), Aydın et al. (2012), Balli and Hepbasli (2013, 2014), Ehyaei et al. (2013), Turan et al. (2013, 2014b) and Yildirim et al. (2013).

### 3.3.7 Coefficient of ecological performance (*CEP*)

Coefficient of ecological performance, *CEP*, has been first introduced and presented by Tanbay et al. (2013, 2015). It has been defined as propulsive power per unit exergy destruction rate. It provides information on how much exergy is being destructed by the engine while producing propulsive power to propel the aircraft so that it gives insight on ecological performance of the engine. It has been expressed as

$$CEP = \frac{\text{Propulsive power}}{\text{Exergy destruction rate}} \quad (3.20)$$

or

$$CEP = \frac{Fv_1}{T_0\dot{S}_{gen}} \quad (3.21)$$

### 3.3.8 Exergy destruction factor ( $f_{exd}$ )

Exergy destruction factor,  $f_{exd}$ , is another exergetic performance indicator utilized in the literature. It has been introduced by Bejan et al. (1996). Connelly and Koshland (2001a, 2001b) used it as depletion number. Exergy destruction factor has been defined by Midilli and Dincer (2009) as an indicator for decrease in sustainability. It can be defined as exergy destruction rate per unit rate of exergy supplied and can be expressed as

$$f_{exd} = \frac{\dot{E}x_{dest}}{\dot{E}x_{supp}} \quad (3.22)$$

or by utilizing equation (3.19)

$$f_{exd} = 1 - \text{Exergetic efficiency} \quad (3.23)$$

Exergy destruction factor has been utilized in the literature by Dincer and Rosen (2007), Midilli and Dincer (2010), Midilli et al. (2011), Aydın et al. (2013a, 2014a), Turan et al. (2013) and Tanbay et al. (2015).

### 3.3.9 Waste exergy ratio ( $r_{wex}$ )

Waste exergy ratio,  $r_{wex}$ , has been defined as waste exergy rate per unit rate of exergy supplied by Midilli and Dincer (2009). It gives information on how much supplied exergy is wasted and it is better to have lower waste exergy ratios. It has been utilized by Midilli and Dincer (2010), Midilli et al. (2011), Aydın et al. (2013a, 2014a) and Turan et al. (2013). It may be expressed as

$$r_{wex} = \frac{\text{Total waste exergy output rate}}{\text{Rate of exergy supplied}} \quad (3.24)$$

### 3.3.10 Environmental effect (impact) factor ( $f_{eef}$ )

Environmental effect factor,  $f_{eef}$ , has been defined by Midilli and Dincer (2009) and utilized by Midilli and Dincer (2010), Midilli et al. (2011), Turan et al. (2013) and Aydın et al. (2013a, 2014a). It can be defined as an indicator of whether or not the waste exergy of the engine damages the environment. It can be expressed as

$$f_{eef} = \frac{\text{Waste exergy ratio}}{\text{Exergy efficiency}} \quad (3.25)$$

and by utilizing equations (3.24) and (3.18) it yields

$$f_{eef} = \frac{\text{Total waste exergy output rate}}{\text{Exergy output rate}} \quad (3.26)$$

### 3.3.11 Exergetic sustainability index ( $\theta_{exs}$ )

Exergetic sustainability index,  $\theta_{exs}$ , has been defined by Midilli and Dincer (2009) as reciprocal of environmental effect factor. Midilli and Dincer (2010), Midilli et al.



(2011), Aydın et al. (2013a, 2014a), Turan et al. (2013) and Tanbay et al. (2015) have utilized this indicator in the literature. It is expressed as

$$\theta_{exs} = \frac{1}{\text{Environmental effect factor}} \quad (3.27)$$

and by using equation (3.26) it yields

$$\theta_{exs} = \frac{\text{Exergy output rate}}{\text{Total waste exergy output rate}} \quad (3.28)$$

### 3.3.12 Improvement potential ( $I\dot{P}$ )

Improved potential,  $I\dot{P}$ , has been proposed by Van Gool (1997) and it can be defined as a performance measure that shows how much more exergy rate can be utilized instead of being lost or destructed. It has been used by Dincer and Rosen (2007), Turgut et al. (2007), Balli et al. (2008), Balli and Hepbasli (2013, 2014) and Turan et al. (2014b). It can be expressed as

$$I\dot{P} = (1 - \text{Exergetic efficiency})(\text{Exergy input rate} - \text{Exergy output rate}) \quad (3.29)$$

Improvement potential provides strong information on how much an engine or an engine unit can be improved in terms of exergy rate wasted. When it is utilized for comparison of engine units, it also provides information on which unit has the highest potential to be improved.

### 3.3.13 Relative irreversibility ( $\chi_i$ )

Relative irreversibility,  $\chi_i$ , is an exergetic performance parameter utilized when units of engine to be compared in terms of exergy destruction rates. Relative irreversibility of each unit can be calculated by dividing its own exergy destruction rate to total exergy destruction rate of the engine. By this way, it can be observed that what percentage of the exergy destruction is caused by which unit of the engine. Also, most irreversible unit can be revealed by using relative irreversibility. It has been proposed by Szargut et al. (2002) and utilized by Xiang et al. (2004), Dincer and

Rosen (2007), Turgut et al. (2007, 2009b), Balli et al. (2008), Balli and Hepbasli (2013), Aydın et al. (2014b). It can be expressed as

*Relative Irreversibility*

$$= \frac{\text{Exergy destruction rate of the } i^{\text{th}} \text{ unit}}{\text{Total exergy destruction rate}} \quad (3.30)$$

or

$$\text{Relative Irreversibility} = \frac{\dot{E}x_{dest,i}}{\dot{E}x_{dest}} \quad (3.31)$$

### 3.3.14 Fuel depletion ratio ( $\delta_i$ )

Fuel depletion ratio,  $\delta_i$ , has been a good exergetic performance indicator to analyze exergy destruction rates of engine units compared to exergy of the fuel consumed. It has been introduced by Bejan et al. (1996) and utilized by Xiang et al. (2004), Turgut et al. (2007, 2009b), Balli et al. (2008), Balli and Hepbasli (2013), Tai et al. (2014) and Turan et al. (2014b).

It can be defined as exergy destruction rate of each component divided by fuel exergy input, and can be expressed as

$$\text{Fuel Depletion Ratio} = \frac{\dot{E}x_{dest,i}}{\dot{E}x_{fuel}} \quad (3.32)$$

#### **4. THEORETICAL MODEL FOR THE THERMODYNAMIC ANALYSIS ABOUT THE EFFECT OF HEAT LEAKAGE ON THE OPTIMAL PERFORMANCE OF A TWIN-SPOOL TURBOFAN ENGINE**

In the previous chapters, simple Brayton cycle, jet propulsion cycle and simple turbofan cycle have been introduced. In this chapter, the theoretical model utilized for this thesis will be introduced and steps of a parametric cycle analysis will be determined in detail.

As mentioned earlier, single-spool turbofan engines have a fan and a bypass nozzle in addition to one compressor, combustion chamber and one turbine. In this configuration, fan and compressor are driven by turbine through a shaft between them. As a new technological step, another compressor-turbine couple has been introduced with another shaft in order to improve the performance of the turbofan engine and this new configuration is called as twin-spool turbofan engine.

In twin-spool turbofan engines, one spool is called as low pressure spool, and the second spool is called as high pressure spool. There have been two different configurations for twin-spool turbofan engines. In the first configuration, low pressure spool consists of a fan and a turbine, where turbine produces enough power to drive only the fan. High pressure spool consists of a compressor and a turbine for this configuration, and turbine drives the compressor. In short, this configuration can be generalized as low pressure turbine driving the fan, high pressure turbine driving the compressor. In the second configuration, low pressure spool consists of a fan, a low pressure compressor and a turbine, where the turbine produces power to drive fan and low pressure compressor. High pressure spool in this configuration consists of a high pressure compressor and a high pressure turbine, where the compressor is driven by the turbine (El-Sayed, 2008).

In this thesis, the second configuration has been utilized, and Figure 4.1 shows it schematically. Also a T-s diagram of this model has been shown in Figure 4.2.

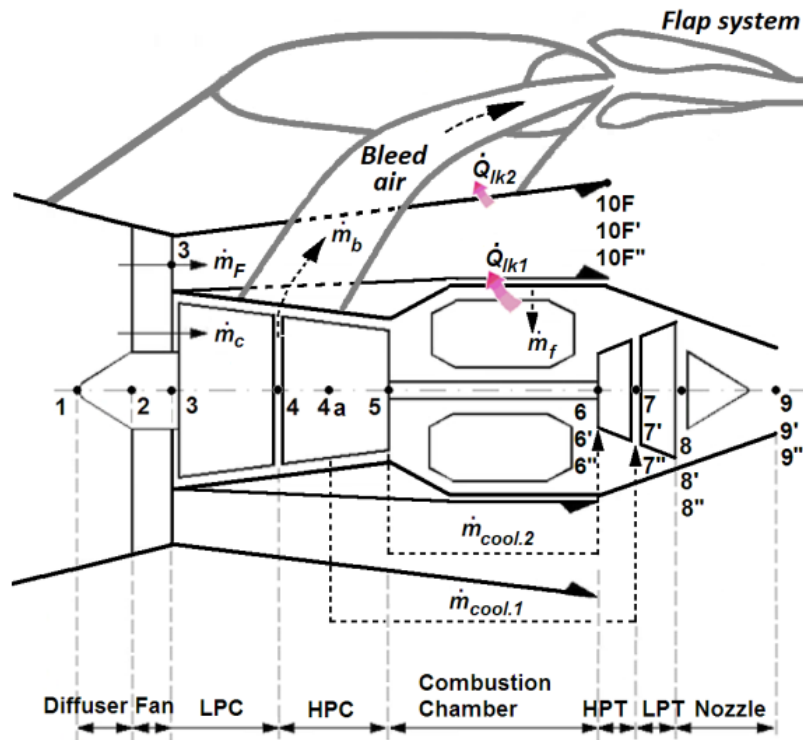


**Figure 4.1 :** The turbofan engine configuration and station numbering utilized in the thesis.

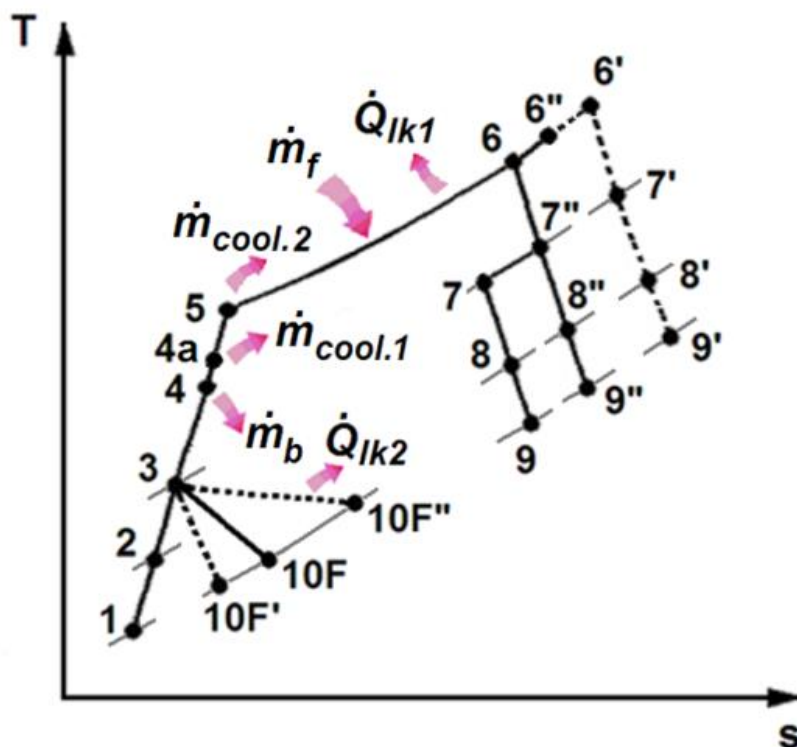


**Figure 4.2 :** T-s diagram of the turbofan engine cycle and corresponding station numbering utilized in the thesis.

## 4.1 Processes and Assumptions

Processes for this configuration can be expressed as in the following.

- 1-2: Air at environmental conditions is taken into engine through diffuser, slowed down and compressed. This process takes place adiabatically and irreversibly.
- 2-3: After leaving the diffuser, air is further compressed in fan via an adiabatic and irreversible process.
- 3-4: Part of this air, which has been introduced earlier as core flow, goes through the low-pressure compressor (LPC). In LPC, air is compressed via an adiabatic and irreversible process.
- Bleed air extraction: After LPC, air is split into two streams. First stream is taken out of the engine in order to provide in-cabin pressure and anti-icing, to drive flap system and to be utilized in environmental control unit. This air taken out of the engine and utilized in several applications is called as bleed air. Bleed air is always taken before air enters into combustion process as it is still colder and fresher than combustion products.
- 4-5: Second stream continues to be further compressed in high-pressure compressor (HPC) via an adiabatic and irreversible compression process. Some of the air is taken out from some intermediate stage of compressor (stage 4a) in order to cool low-pressure turbine (LPT). Other part continues through core of the engine.
- 5-6<sup>''</sup>: After leaving the HPC, some part of the air proceeds through combustion chamber (CC). Fuel is added to air, and this high-pressure fuel-air mixture is burned with a slight pressure loss due to friction in CC and some heat leakage occurs from hot CC to colder bypass air skirting. Some other part is taken to cool high-pressure turbine (HPT) bypassing the CC without any combustion.
- 6<sup>''</sup>-6: Cooling air for HPT is added to the combustion products before entering HPT in order to reduce temperature of the flow. This process protects turbine blades from very high temperature of combustion that is above metallurgical limits of turbine blades.

- 6-7<sup>''</sup>: After the cooling, high-pressure high-temperature combustion products enters into HPT. These gases expand via an adiabatic and irreversible expansion process in HPT; by this way, HPT produces enough shaft power to drive HPC and some auxiliary equipment of aircraft.
- 7<sup>''</sup>-7: Cooling air for LPT is added to the combustion products proceeding through core of the engine before entering LPT. This operation may not exist for all engines utilized today.
- 7-8: Core flow leaving the HPT proceeds through LPT for further expanding. In LPT, an adiabatic and irreversible expansion process takes place and shaft power produced by LPT drives the fan and LPC.
- 8-9: After leaving the LPT, combustion gases expand in the core nozzle and leave the engine at a very high velocity in order to provide propulsive power to propel the aircraft.
- 3-10F: The real path that is followed by the bypass air, which has been separated after leaving the fan. In this process, some heat is leaked from CC and added to bypass air as mentioned earlier. It has been called as heat leakage one, and denoted as  $\dot{Q}_{LK1}$ . Also, some heat is lost from bypass air to ambient air during this process, which has been called as heat leakage two, and denoted as  $\dot{Q}_{LK2}$ . This process is an irreversible expansion process realized in fan nozzle, and air leaves the fan nozzle contributing to propulsive power.
- 3-10F<sup>'</sup>: This is an imaginary path that would be followed by bypass air if there were no heat leakages from CC to bypass air, and no heat leakages from bypass air to ambient air. Bypass air would expand in fan nozzle adiabatically (i.e no heat addition from CC and no heat loss to the ambient) and contribute to propulsive power by leaving the engine with a high velocity.
- 3-10F<sup>''</sup>: This is a similar imaginary expansion process path followed by bypass air in fan nozzle. This time there is heat leakage from CC to bypass air,  $\dot{Q}_{LK1}$ , but no heat leakage from bypass air to the ambient air,  $\dot{Q}_{LK2}$ . In other words, in this imaginary path, bypass air receives  $\dot{Q}_{LK1}$  but does not lose  $\dot{Q}_{LK2}$ .

Assumptions made for this twin-spool turbofan engine have been expressed as in the following.

- An open irreversible turbofan cycle is considered.
- Air and combustion gases are ideal gases with the same constant specific heats ( $k = 1.359$  and  $c_p = 1086 \text{ J kg}^{-1} \text{ K}^{-1}$ ).
- The cruise phase of the flight is considered.
- All processes are steady-flow processes.
- Differential-pressure-change based irreversibility correction factor for adiabatic compression process of turbomachinery (fan, LPC, HPC, HPT, and LPT) have been taken into account (Cohen et al, 1996).
- Cooling process causes some efficiency losses in turbines (Mattingly et al. 2002).
- LPT cooling has been taken as zero (Mattingly et al. 2002).
- Only chemical exergy of fuel and kinetic exergy of incoming air have been considered.
- Potential exergy of fuel and air have been neglected since there is no elevation difference from the environment (Ehyaie et al, 2013).
- Physical exergy of fuel due to very high pressures has been neglected because of being small figures such as 0.03-0.06 MW (Turgut et al, 2007).
- Physical exergy of incoming air has been considered as zero (Turgut et al, 2007; Ehyaie et al, 2013).
- Lower heating value of the fuel (kerosene) is considered to be 43.15 MJ per kg as utilized by Tanbay et al. (2013, 2015).
- Specific chemical exergy of the fuel (kerosene) is considered to be 45.8 MJ per kg as utilized by Turgut et al. (2007, 2009b).
- Auxiliary power requirements provided from the engine is assumed to be constant as 350 kW.

## 4.2 Mass Flow Rates and Ratios

As described above, there are several streams in the engine such as core air, bypass air, cooling air, bleed air etc. When analyzing the performance of turbofan engines and performing parametric cycle analysis, it becomes very important to denote these streams separately and define some dimensionless mass flow ratios as applied by Mattingly et al. (2002) and El-Sayed (2008). By this way analysis becomes more

practical to apply and easy to follow and understand. All mass flow rates according to assumed model have been illustrated in Table 4.1.

**Table 4.1** : Mass flow rates.

Stations	Mass Flow Rates
Total air at the engine inlet	$\dot{m}_c + \dot{m}_F$
Bypass air through fan nozzle	$\dot{m}_F$
Bleed air	$\dot{m}_b$
Cooling air for LPT	$\dot{m}_{cool1}$
Cooling air for HPT	$\dot{m}_{cool2}$
Air at the core before bleeding	$\dot{m}_c$
Air at the core after bleeding	$\dot{m}_c - \dot{m}_b$
Air at the core after LPT cooling extraction	$\dot{m}_c - \dot{m}_b - \dot{m}_{cool1}$
Air at the core after HPT cooling extraction	$\dot{m}_c - \dot{m}_b - \dot{m}_{cool1} - \dot{m}_{cool2}$
Fuel added in CC	$\dot{m}_f$
Combustion product gases after combustion	$\dot{m}_c - \dot{m}_b - \dot{m}_{cool1} - \dot{m}_{cool2} + \dot{m}_f$
Mass flow rate at the HPT inlet	$\dot{m}_c - \dot{m}_b - \dot{m}_{cool1} + \dot{m}_f$
Mass flow rate at the LPT inlet, nozzle inlet and exhaust	$\dot{m}_c - \dot{m}_b + \dot{m}_f$

According to above mass flow rates, some practical dimensionless mass flow ratios to be utilized in analysis can be defined. One of the most important mass flow ratios in analyzing turbofan engines is bypass air ratio. It can be defined as

$$\beta = \frac{\text{mass flow rate of bypass air}}{\text{mass flow rate of core air}} = \frac{\dot{m}_F}{\dot{m}_c} \quad (4.1)$$

This ratio is also important for the size of the turbofan engines since it determines how much air will flow through bypass nozzle compared to core stream. This ratio has an important role on determination of size of the fan unit.

Another ratio that will be utilized is bleed air ratio. As it has been mentioned above, bleed air is extracted after LPC. In general, it can be utilized in providing in-cabin pressure, in anti-icing application, in environmental control unit and flap system. As indicated earlier, it should be fresh air because it is utilized in pressurizing the cabin air. Since bleed air is extracted from core stream, a dimensionless ratio can be defined as

$$\gamma = \frac{\text{mass flow rate of bleed air extracted}}{\text{mass flow rate of core air}} = \frac{\dot{m}_b}{\dot{m}_c} \quad (4.2)$$



After bleed air is extracted after LPC and before HPC, cooling air is extracted from one of the HPC stages. This extraction is done before the pressure of air gets too high for LPT air. If this extraction is done from very last stages of HPC, then the pressure of extracted air for cooling the LPT would be too high. In this situation, it would require a throttling process to drop its pressure to the level of LPT entrance, and power spent for compressing this cooling air would be wasted. Therefore, cooling air one for LPT is extracted from one of the stages of HPC convenient for LPT pressure level, and cooling air ratio-1 can be defined as

$$\theta_1 = \frac{\text{mass flow rate of cooling air for LPT}}{\text{mass flow rate of core air}} = \frac{\dot{m}_{cool1}}{\dot{m}_c} \quad (4.3)$$

After the extraction of cooling air for LPT, pressure of the core air continues to increase through HPC and reaches maximum at the end of HPC. At this point, pressure is nearly the same as pressure of HPT inlet (only a slight pressure drop occurs in CC). Therefore cooling air for HPT is extracted from core air after HPT before entering CC. In the same fashion, cooling air ratio-2 can be expressed as

$$\theta_2 = \frac{\text{mass flow rate of cooling air for HPT}}{\text{mass flow rate of core air}} = \frac{\dot{m}_{cool2}}{\dot{m}_c} \quad (4.4)$$

After all extractions have been realized, core air enters into CC and fuel is added to air. Combustion takes place with this air-fuel mixture and temperature rises to very high degrees. Determination of mass flow rate of fuel is closely related with the maximum temperature level allowed for HPT inlet, due to metallurgical constraints. Fuel to air ratio can be defined as

$$\begin{aligned} \alpha &= \frac{\text{mass flow rate of fuel added in CC}}{\text{mass flow rate of core air entering into CC}} \\ &= \frac{\dot{m}_f}{\dot{m}_c - \dot{m}_b - \dot{m}_{cool1} - \dot{m}_{cool2}} \end{aligned} \quad (4.5)$$

### 4.3 Heat Leakage Rates and Ratios

In this thesis, two types of heat leakages have been modeled as stated above. First one is heat leakage from CC to bypass air denoted as  $\dot{Q}_{LK1}$ . This leakage is a lost for core air because it is a lost energy from potential of fuel energy to be supplied to core air. On the other hand, this lost heat is received by bypass air, so it constitutes a gain

for bypass air. Therefore, as  $\dot{Q}_{LK1}$  increases, losses of CC and gains of bypass air increases in terms of heat transfer.

Second heat leakage modeled in this study is heat leakage from bypass air to ambient air denoted as  $\dot{Q}_{LK2}$ . This leakage is lost from engine to environment; therefore, as this leakage increases, energy loss of bypass air increases.

In order to be able to perform cycle analysis and performance assessment of the turbofan engine, these two heat leakages stated above are required to be defined and well expressed. They are very important for energy balances in CC and fan nozzle. Therefore, they are required to be formulized before starting cycle analysis.

As it can be seen in Figure 4.1 and Figure 4.2, when CC is considered as control volume to be analyzed, air after bleeding and cooling extractions enter into CC and fuel is added to this air. Combustion takes place inside CC and some heat,  $\dot{Q}_{LK1}$ , is lost to bypass air during this process. Fuel energy added during the combustion process can be defined as follows.

$$\dot{Q}_f = \dot{m}_f Q_{LHV} \quad (4.6)$$

in kJ/s where  $\dot{m}_f$  is mass flow rate of fuel (kg/s) added in CC, and  $Q_{LHV}$  is lower heating value of the fuel in kJ/kg.

As observed in T-s diagram of the turbofan engine in Figure 4.2, combustion process would end at point 6' if there were no heat leakage from CC, which is  $\dot{Q}_{LK1}$ . The real process, however, ends at point 6'' due to this heat loss. In other words, state of working fluid would be carried to state 6' instead of state 6'' with released energy of the fuel during combustion if there were no  $\dot{Q}_{LK1}$ . Therefore energy equation in CC can be expressed in two forms, one with  $\dot{Q}_{LK1}$  term and one without it by utilizing the first law of thermodynamics energy conservation equation for steady-flow processes as described in Chapter 2, and written in the form of equation (2.2) as

$$\dot{Q} - \dot{W} = \sum_{out} \dot{m} (h + v^2/2 + gz) - \sum_{in} \dot{m} (h + v^2/2 + gz) \quad (4.7)$$

Equation (4.7) can be modified by eliminating potential energy term due to no elevation difference and using stagnation enthalpy instead of enthalpy and velocity terms separated. Therefore, without heat leakage term it yields

$$\dot{Q}_{5 \text{ to } 6'} - \dot{W}_{5 \text{ to } 6'} = \dot{m}_{6'}(h_{06'}) - \dot{m}_5(h_{05}) \quad (4.8)$$

Simplifying equation (4.8) by canceling the work term since there is no work interaction in CC, writing mass flow rates explicitly and using equation (2.5) it yields

$$\begin{aligned} \dot{Q}_f &= (\dot{m}_c - \dot{m}_b - \dot{m}_{cool1} - \dot{m}_{cool2} + \dot{m}_f)c_p T_{06'} \\ &\quad - (\dot{m}_c - \dot{m}_b - \dot{m}_{cool1} - \dot{m}_{cool2})c_p T_{05} \end{aligned} \quad (4.9)$$

where  $\dot{Q}_f$  is heat addition to CC shown in equation (4.6). The same energy balance can be written with heat leakage term as

$$\dot{Q}_{5 \text{ to } 6''} - \dot{W}_{5 \text{ to } 6''} = \dot{m}_{6''}(h_{06''}) - \dot{m}_5(h_{05}) \quad (4.10)$$

and by eliminating work term it becomes

$$\begin{aligned} \dot{Q}_f - \dot{Q}_{LK1} &= (\dot{m}_c - \dot{m}_b - \dot{m}_{cool1} - \dot{m}_{cool2} + \dot{m}_f)c_p T_{06''} \\ &\quad - (\dot{m}_c - \dot{m}_b - \dot{m}_{cool1} - \dot{m}_{cool2})c_p T_{05} \end{aligned} \quad (4.11)$$

Then, to find an expression for heat leakage  $\dot{Q}_{LK1}$ , equation (4.9) can be substituted into equation (4.11) which yields

$$\begin{aligned} &(\dot{m}_c - \dot{m}_b - \dot{m}_{cool1} - \dot{m}_{cool2} + \dot{m}_f)c_p T_{06'} \\ &\quad - (\dot{m}_c - \dot{m}_b - \dot{m}_{cool1} - \dot{m}_{cool2})c_p T_{05} - \dot{Q}_{LK1} \\ &= (\dot{m}_c - \dot{m}_b - \dot{m}_{cool1} - \dot{m}_{cool2} + \dot{m}_f)c_p T_{06''} \\ &\quad - (\dot{m}_c - \dot{m}_b - \dot{m}_{cool1} - \dot{m}_{cool2})c_p T_{05} \end{aligned} \quad (4.12)$$

Eliminating the same terms from both sides of the equation (4.12) and rearranging yields

$$\dot{Q}_{LK1} = (\dot{m}_c - \dot{m}_b - \dot{m}_{cool1} - \dot{m}_{cool2} + \dot{m}_f)c_p (T_{06'} - T_{06''}) \quad (4.13)$$

which mathematically proves that temperature difference between state 6' and state 6'' is caused by heat leakage from CC during combustion,  $\dot{Q}_{LK1}$ . As described earlier and can be seen from Figure 4.2, combustion process would increase the state of working fluid up until to 6' but it can only reach state 6'' due to  $\dot{Q}_{LK1}$ .

As described earlier, heat leakage from the CC is received by bypass air. Therefore, energy lost from combustion process causes an energy gain in fan nozzle process. By utilizing energy balance equation of fan nozzle process,  $\dot{Q}_{LK1}$  can be defined in an

alternative way. To do this, energy balance equation of process 3-10F' and 3-10F'' can be written and rearrangements can provide a second way to express  $\dot{Q}_{LK1}$ . As described earlier, process 3-10F' is an imaginary adiabatic process in fan nozzle; while, process 3-10F'' is the one when there is  $\dot{Q}_{LK1}$ .

By utilizing equation (4.7), energy balance equation of process 3-10F' can be written in the following form as

$$\dot{Q}_{3 \text{ to } 10F'} - \dot{W}_{3 \text{ to } 10F'} = \dot{m}_{10F'}(h_{10F'} + \frac{v_{10F'}^2}{2}) - \dot{m}_{03}(h_{03}) \quad (4.14)$$

Since this process is an adiabatic one, heat transfer term will be eliminated. Moreover, there is no work interaction during expansion process in fan nozzle, so work term will also be eliminated. Since mass flow rate both in the inlet and at the exit of fan nozzle has been denoted by  $\dot{m}_F$  and air has been assumed to be a calorically perfect gas, equation (4.14) can be reduced to

$$0 = (\dot{m}_F c_p T_{10F'} + \dot{m}_F \frac{v_{10F'}^2}{2}) - \dot{m}_F c_p T_{03} \quad (4.15)$$

Now, energy balance equation will be written for process 3-10F'' in which  $\dot{Q}_{LK1}$  will be included. Utilizing equation (4.7) again, energy balance equation can be written as

$$\dot{Q}_{3 \text{ to } 10F''} - \dot{W}_{3 \text{ to } 10F''} = \dot{m}_{10F''}(h_{10F''} + \frac{v_{10F''}^2}{2}) - \dot{m}_{03}(h_{03}) \quad (4.16)$$

During this process no work interaction takes place, and the only heat transfer is heat leakage from CC to fan nozzle, which is  $\dot{Q}_{LK1}$ . Again, the mass flow rate of the air is  $\dot{m}_F$  and air has been considered as a calorically perfect gas so equation (4.16) becomes

$$\dot{Q}_{LK1} = (\dot{m}_F c_p T_{10F''} + \dot{m}_F \frac{v_{10F''}^2}{2}) - \dot{m}_F c_p T_{03} \quad (4.17)$$

Subtracting equation (4.15) from equation (4.17) yields

$$\dot{Q}_{LK1} = \dot{m}_F c_p (T_{10F''} - T_{10F'}) + \dot{m}_F (\frac{v_{10F''}^2 - v_{10F'}^2}{2}) \quad (4.18)$$

Equation (4.18) proves that heat leakage from CC to fan nozzle causes the energy difference between state 10F'' and state 10F'. If there were no heat leakage one,  $\dot{Q}_{LK1}$ , then process in the fan nozzle could not reach 10F'', instead it would end at state 10F'.

Now, heat leakage ratio one can be defined since heat leakage one has been expressed. Definition of heat leakage ratio one,  $\varepsilon_{LK1}$ , may start from the most basic point of view of loss. For the combustion process, purpose is to increase the temperature (energy) of the working fluid with all energy released from the fuel within the limitations. Any part of energy released from the fuel but could not be utilized for the energy increase of the fluid would be considered as "loss". Hence, heat leakage ratio can be defined as follows.

$$\varepsilon_{LK1} = 1 - \frac{\text{Rate of thermal energy increase of the flow in CC}}{\text{Rate of total thermal energy released from the fuel}} \quad (4.19)$$

Energy of the flowing fluid increases to 6'' from 5 considering the heat leakage. Therefore, energy difference of the fluid between state 6'' and state 5 will be written on numerator of the equation (4.19). Also, fuel energy released has already been expressed in equation (4.9), so it will be substituted for the denominator of the equation (4.19). Hence, it becomes

$$\varepsilon_{LK1} = 1 - \frac{\dot{m}_{6''}(h_{06''}) - \dot{m}_5(h_{05})}{\dot{m}_{6'}(h_{06'}) - \dot{m}_5(h_{05})} \quad (4.20)$$

or explicitly

$$= 1 - \frac{(\dot{m}_C - \dot{m}_b - \dot{m}_{cool1} - \dot{m}_{cool2} + \dot{m}_f)c_p T_{06''} - (\dot{m}_C - \dot{m}_b - \dot{m}_{cool1} - \dot{m}_{cool2})c_p T_{05}}{(\dot{m}_C - \dot{m}_b - \dot{m}_{cool1} - \dot{m}_{cool2} + \dot{m}_f)c_p T_{06'} - (\dot{m}_C - \dot{m}_b - \dot{m}_{cool1} - \dot{m}_{cool2})c_p T_{05}} \quad (4.21)$$

Eliminating  $c_p$  terms and rearranging yields

$$\varepsilon_{LK1} = \frac{(\dot{m}_C - \dot{m}_b - \dot{m}_{cool1} - \dot{m}_{cool2} + \dot{m}_f)(T_{06'} - T_{06''})}{(\dot{m}_C - \dot{m}_b - \dot{m}_{cool1} - \dot{m}_{cool2} + \dot{m}_f)T_{06'} - (\dot{m}_C - \dot{m}_b - \dot{m}_{cool1} - \dot{m}_{cool2})T_{05}} \quad (4.22)$$

Dividing by  $\dot{m}_C - \dot{m}_b - \dot{m}_{cool1} - \dot{m}_{cool2}$  term in order to utilize fuel to air ratio,  $\alpha$ , defined in equation (4.5), it becomes

$$\begin{aligned} \varepsilon_{LK1} &= \frac{\frac{(\dot{m}_c - \dot{m}_b - \dot{m}_{cool1} - \dot{m}_{cool2} + \dot{m}_f)}{(\dot{m}_c - \dot{m}_b - \dot{m}_{cool1} - \dot{m}_{cool2})} (T_{06'} - T_{06''})}{\frac{(\dot{m}_c - \dot{m}_b - \dot{m}_{cool1} - \dot{m}_{cool2} + \dot{m}_f)}{(\dot{m}_c - \dot{m}_b - \dot{m}_{cool1} - \dot{m}_{cool2})} T_{06'} - \frac{(\dot{m}_c - \dot{m}_b - \dot{m}_{cool1} - \dot{m}_{cool2})}{(\dot{m}_c - \dot{m}_b - \dot{m}_{cool1} - \dot{m}_{cool2})} T_{05}} \end{aligned} \quad (4.23)$$

and using equation (4.5) it can be simplified to

$$\varepsilon_{LK1} = \frac{(1 + \alpha)(T_{06'} - T_{06''})}{(1 + \alpha)T_{06'} - T_{05}} \quad (4.24)$$

As mentioned earlier, heat leakage from the bypass air (during fan nozzle process) to the ambient air has been modeled as the heat leakage two, and can be denoted by  $\dot{Q}_{LK2}$ . This energy is completely lost from bypass air, and it causes a change in exit state of the flowing fluid.

As already described, 10F'' is exit state of fan nozzle process when there is no  $\dot{Q}_{LK2}$  (but  $\dot{Q}_{LK1}$  still exists). On the other hand, in the real process  $\dot{Q}_{LK2}$  exists and the exit state is 10F. Therefore, an expression for  $\dot{Q}_{LK2}$  can be found by writing energy balance equations for process 3-10F'' and process 3-10F. Equation (4.17) is the energy balance equation for the process 3-10F'' where only  $\dot{Q}_{LK1}$  exists. For the process 3-10F, equation (4.9) can be utilized and it can be written as

$$\dot{Q}_{3 \text{ to } 10F} - \dot{W}_{3 \text{ to } 10F} = \dot{m}_{10F} \left( h_{10F} + \frac{v_{10F}^2}{2} \right) - \dot{m}_{03} (h_{03}) \quad (4.25)$$

In the real process,  $\dot{Q}_{LK1}$  and  $\dot{Q}_{LK2}$  exists together so heat transfer term will be replaced by these two heat leakage terms.  $\dot{Q}_{LK1}$  term increases the energy of bypass flow; however,  $\dot{Q}_{LK2}$  causes the bypass flow to lose energy. Moreover, in fan nozzle process, no work interaction occurs so work term will be cancelled. It can be rewritten as

$$\dot{Q}_{LK1} - \dot{Q}_{LK2} = (\dot{m}_F c_p T_{10F} + \dot{m}_F \frac{v_{10F}^2}{2}) - \dot{m}_F c_p T_{03} \quad (4.26)$$

Substituting equation (4.17) into equation (4.26) yields

$$\begin{aligned} & (\dot{m}_F c_p T_{10F''} + \dot{m}_F \frac{v_{10F''}^2}{2}) - \dot{m}_F c_p T_{03} - \dot{Q}_{LK2} \\ & = (\dot{m}_F c_p T_{10F} + \dot{m}_F \frac{v_{10F}^2}{2}) - \dot{m}_F c_p T_{03} \end{aligned} \quad (4.27)$$

and rearranging yields

$$\dot{Q}_{LK2} = \dot{m}_F \left[ c_p (T_{10F''} - T_{10F}) + \frac{v_{10F''}^2 - v_{10F}^2}{2} \right] \quad (4.28)$$

Heat leakage ratio two, indicated by  $\varepsilon_{LK2}$  has been defined as heat leakage ratio from the bypass air to the ambient air earlier. This time, heat leakage ratio has been expressed by dividing the realized heat leakage amount to the maximum theoretical heat leakage amount for the process in fan nozzle. Hence,

$$\begin{aligned} & \varepsilon_{LK2} \\ & = \frac{\text{Heat loss due to the second heat leakage}}{\text{Max. theoretical heat loss due to the second heat leakage}} \end{aligned} \quad (4.29)$$

Numerator of the equation (4.29) has already been defined in equation (4.28). Now, maximum theoretical heat loss due to the second heat leakage is to be calculated. According to the second law of thermodynamics, heat transfer occurs from the high temperature source to low temperature sink. Therefore, in this case, energy loss occurs from the bypass air (higher temperature) to the ambient air (lower temperature). Ambient air can be considered as an infinitely large thermal sink compared to energy lost from the bypass air. Therefore, heat loss from the bypass air can occur until the temperature of bypass air goes down to that of the ambient air. In other words, bypass air may lose its excess energy to ambient air until it reaches the temperature level of the ambient air. It can also be defined by utilizing station numbering such that exit state 10F'' decreases down to 10F with the realized heat leakage two, and it would further decrease down to state 1 (ambient air state) in the limiting case. Hence, energy difference between these two states constitutes the maximum amount of energy transfer (heat loss) amount. Equation (4.28) can be rewritten for 10F''-1 instead of 10F''-10F as follows.

$$\dot{Q}_{LK2,max} = \dot{m}_F \left[ c_p(T_{10F''} - T_1) + \frac{v_{10F''}^2 - v_1^2}{2} \right] \quad (4.30)$$

Then, heat leakage ratio two becomes

$$\varepsilon_{LK2} = \frac{\dot{m}_F \left[ c_p(T_{10F''} - T_{10F}) + \frac{v_{10F''}^2 - v_{10F}^2}{2} \right]}{\dot{m}_F \left[ c_p(T_{10F''} - T_1) + \frac{v_{10F''}^2 - v_1^2}{2} \right]} \quad (4.31)$$

and finally eliminating  $\dot{m}_F$  terms yields

$$\varepsilon_{LK2} = \frac{\left[ c_p(T_{10F''} - T_{10F}) + \frac{v_{10F''}^2 - v_{10F}^2}{2} \right]}{\left[ c_p(T_{10F''} - T_1) + \frac{v_{10F''}^2 - v_1^2}{2} \right]} \quad (4.32)$$

#### 4.4 Power Consumption and Production Balances

As indicated in Chapter 3, main purpose of the turbofan engine is not to produce excess power but to propel the aircraft. Therefore, turbines produce just enough power to drive power-consuming turbomachinery on the same shaft. In this thesis, selected configuration of turbofan engine was that low pressure spool consists of Fan, LPC and LPT, and high pressure spool consists of HPC and HPT.

In addition to these main turbomachinery, an aircraft engine also provides power for some auxiliary requirements such as electric and hydraulic systems (Tona et al, 2010). This feature has been defined by Mattingly et al. (2002) as power takeoff (extraction) for accessories. In this thesis, power requirement for auxiliary equipment has been considered to be extracted from high pressure spool; therefore, HPT produces power to drive HPC and auxiliary equipment.

As explained by Çengel and Boles (2005) and assumed in this thesis, turbomachinery works adiabatically and all processes are steady-flow processes. Therefore, heat transfer term in general energy conservation equation (the first law of thermodynamics) vanishes when it is written for adiabatic fan, compressors and turbines. Also, enthalpy terms are written as stagnation enthalpy without considering the velocity (hence kinetic energy) term as shown in equation (2.6).



#### 4.4.1 Power consumed by fan

In the light of the explanation presented under Section 4.4 and equation 4.7, the energy balance equation of the process 2-3 which occurs in fan can be written as

$$\dot{Q}_{2-3} - \dot{W}_{2-3} = \sum_{out} \dot{m} (h_{0,out}) - \sum_{in} \dot{m} (h_{0,in}) \quad (4.33)$$

Due to adiabatic process and calorically perfect gas assumption, it can be rewritten as

$$-\dot{W}_F = (\dot{m}_c + \dot{m}_F)c_p T_{03} - (\dot{m}_c + \dot{m}_F)c_p T_{02} \quad (4.34)$$

where mass flow rate at both inlet and exit of the fan is  $\dot{m}_c + \dot{m}_F$  as shown in Table 4.1. Since fan consumes power, it has been seen that work term has a negative sign. When it is considered as consumption and rewritten in a more compact expression, the magnitude of power consumed by the fan becomes

$$\dot{W}_F = (\dot{m}_c + \dot{m}_F)c_p (T_{03} - T_{02}) \quad (4.35)$$

#### 4.4.2 Power consumed by LPC

Utilizing the same approach, heat transfer term will be eliminated in energy conservation equation for LPC. Also, process starts at state 3 with a mass flow rate of  $\dot{m}_c$  and ends at state 4 with the same mass flow rate. Therefore, with the same steps done for the fan, power consumed by LPC can be written as follows.

$$\dot{W}_{LPC} = \dot{m}_c c_p (T_{04} - T_{03}) \quad (4.36)$$

#### 4.4.3 Power consumed by HPC

Adiabatic compression process in HPC starts at station 4 with a mass flow rate of  $\dot{m}_c - \dot{m}_b$  since bleed air has been extracted just before air enters into HPC as shown in Figure 4.1. Until the air extraction for LPT at station 4a in an amount of  $\dot{m}_{cool1}$ , mass flow rate is constant at  $\dot{m}_c - \dot{m}_b$ . Therefore, between the states of 4 and 4a, HPC consumes power in an amount of

$$\dot{W}_{HPC,4-4a} = (\dot{m}_c - \dot{m}_b)c_p (T_{04a} - T_{04}) \quad (4.37)$$

After cooling air for LPT extracted at 4a, there remains  $\dot{m}_c - \dot{m}_b - \dot{m}_{cool1}$  amount of mass flow rate in compressor, which is further compressed until the state 5. Therefore, HPC power consumption after cooling air extraction can be written as

$$\dot{W}_{HPC,4a-5} = (\dot{m}_c - \dot{m}_b - \dot{m}_{cool1})c_p(T_{05} - T_{04a}) \quad (4.38)$$

Hence, total power consumed by HPC can be found by summing up the right hand sides of the equations (4.37) and (4.38) since they represent the power consumption starting from the beginning of HPC until the turbine cooling air extraction and from extraction to the exit of the HPC respectively.

$$\begin{aligned} \dot{W}_{HPC} = & (\dot{m}_c - \dot{m}_b)c_p(T_{04a} - T_{04}) \\ & + (\dot{m}_c - \dot{m}_b - \dot{m}_{cool1})c_p(T_{05} - T_{04a}) \end{aligned} \quad (4.39)$$

Cooling air for HPT extraction occurs at station 5 just after the compression in HPC before entering into CC for combustion process. This extracted air, in a mass flow rate of  $\dot{m}_{cool2}$ , will be added to working fluid again, after combustion process before entering HPT.

#### 4.4.4 Power produced by HPT

Starting point of the adiabatic expansion process in HPT is point 6 because of two effects. Firstly, due to the heat leakage one during combustion process in CC, ending point of the process cannot reach 6' but reach 6''. Secondly, cooling air for HPT decreases the temperature of the working fluid after combustion (before entering HPT) from 6'' to 6. Adiabatic expansion process in HPT ends at point 7''. Therefore, power produced by the HPT is calculated by writing the energy balance of process 6-7'' as follows.

$$\dot{Q}_{6-7''} - \dot{W}_{6-7''} = \sum_{out} \dot{m} (h_{0,out}) - \sum_{in} \dot{m} (h_{0,in}) \quad (4.40)$$

Adiabatic process and calorically perfect gas assumption makes the equation (4.40)

$$\begin{aligned} -\dot{W}_{HPT} = & (\dot{m}_c - \dot{m}_b - \dot{m}_{cool1} + \dot{m}_f)c_p T_{07''} \\ & - (\dot{m}_c - \dot{m}_b - \dot{m}_{cool1} + \dot{m}_f)c_p T_{06} \end{aligned} \quad (4.41)$$

rearranging equation (4.41) yields

$$\dot{W}_{HPT} = (\dot{m}_c - \dot{m}_b - \dot{m}_{cool1} + \dot{m}_f)c_p(T_{06} - T_{07''}) \quad (4.42)$$

where mass flow rate at the inlet and exit of HPT is  $\dot{m}_c - \dot{m}_b - \dot{m}_{cool1} + \dot{m}_f$  as shown in Table 4.1 On the other hand, quantity calculated by equation (4.42) is equal to power consumed by HPC and auxiliary power requirement, since HPT drives HPC and auxiliary equipment being on the same shaft.

As indicated by Mattingly et al. (2002), mechanical efficiency is defined for power transmitting components such as shafts, gears etc. It has been defined considering losses due to windage, bearing friction and seal drag. It can be expressed generally as

$$\eta_M = \frac{\text{Mechanical power output}}{\text{Mechanical power input}} \quad (4.43)$$

where  $\eta_M$  represents mechanical efficiency. For HPT, it can be written that

$$\eta_{M2} = \frac{\text{Mechanical power transmitted to HPC and aux. equipment}}{\text{Mechanical power produced by HPT}} \quad (4.44)$$

where  $\eta_{M2}$  represents mechanical efficiency of high pressure spool (shaft). It has been considered that power transmission to auxiliary equipment is provided by another shaft, and mechanical efficiency of auxiliary equipment power extraction can be written as

$$\eta_{aux} = \frac{\text{Auxiliary power requirement } (\dot{W}_{aux})}{\text{Mechanical power extracted from HPT for aux. equipment}} \quad (4.45)$$

or

$$\begin{aligned} & \text{Mechanical power extracted from HPT for aux. equipment} \\ &= \frac{\dot{W}_{aux}}{\eta_{aux}} \end{aligned} \quad (4.46)$$

By substituting equation (4.46) into equation (4.44) and rewriting yields

$$\eta_{M2} = \frac{\dot{W}_{HPC} + \dot{W}_{aux}/\eta_{aux}}{\dot{W}_{HPT}} \quad (4.47)$$

and finally becomes

$$\dot{W}_{HPT} = \frac{\dot{W}_{HPC} + \dot{W}_{aux}/\eta_{aux}}{\eta_{M2}} \quad (4.48)$$

Equations (4.42) and (4.48) can be equated as follows.

$$\frac{\dot{W}_{HPC} + \dot{W}_{aux}/\eta_{aux}}{\eta_{M2}} = (\dot{m}_c - \dot{m}_b - \dot{m}_{cool1} + \dot{m}_f)c_p(T_{06} - T_{07''}) \quad (4.49)$$

#### 4.4.5 Power produced by LPT

After adiabatic expansion process in HPT, cooling air for LPT is added to working fluid and state of working fluid becomes 7 instead of 7''. Therefore, adiabatic expansion process from state 7 to 8 occurs in LPT. Energy balance equation can be written for process 7-8 as

$$\dot{Q}_{7-8} - \dot{W}_{7-8} = \sum_{out} \dot{m} (h_{0,out}) - \sum_{in} \dot{m} (h_{0,in}) \quad (4.50)$$

and

$$-\dot{W}_{LPT} = (\dot{m}_c - \dot{m}_b + \dot{m}_f)c_p T_{08} - (\dot{m}_c - \dot{m}_b + \dot{m}_f)c_p T_{07} \quad (4.51)$$

and rearranging yields

$$\dot{W}_{LPT} = (\dot{m}_c - \dot{m}_b + \dot{m}_f)c_p(T_{07} - T_{08}) \quad (4.52)$$

For the low pressure spool, mechanical efficiency can be written by utilizing equations (4.43) and (4.44) as

$$\eta_{M1} = \frac{\text{Mechanical power transmitted to LPC and Fan}}{\text{Mechanical power produced by LPT}} \quad (4.53)$$

or

$$\eta_{M1} = \frac{\dot{W}_{LPC} + \dot{W}_F}{\dot{W}_{LPT}} \quad (4.54)$$

and rearranging yields

$$\dot{W}_{LPT} = \frac{\dot{W}_{LPC} + \dot{W}_F}{\eta_{M1}} \quad (4.55)$$

Equations (4.52) and (4.55) can be equated as

$$\frac{\dot{W}_{LPC} + \dot{W}_F}{\eta_{M1}} = (\dot{m}_c - \dot{m}_b + \dot{m}_f)c_p(T_{07} - T_{08}) \quad (4.56)$$

#### 4.4.6 Thrust and propulsive power

As mentioned earlier, thrust and hence propulsive power are the main purposes of an aircraft engine to propel the aircraft. Therefore, thrust and propulsive power constitute important parameters for aircraft engine analysis. In chapter 3, a single-spool turbofan engine has been utilized to demonstrate simple equations for thrust and propulsive power. Now, formulations of thrust and propulsive power are to be determined for the particular turbofan engine configuration utilized in this thesis. These two parameters are utilized in calculations of objective functions of this thesis; hence, they are very important.

##### 4.4.6.1 Thrust

As expressed in equation (3.2), thrust consists of momentum component and pressure component both for core nozzle and for bypass nozzle, when considering a turbofan engine. For the configuration utilized in this thesis, thrust can be written part by part as follows.

###### a. Core nozzle momentum component

Core air enters into engine at the mass flow rate of  $\dot{m}_c$  at state 1 and leaves from the core nozzle at the mass flow rate of  $\dot{m}_c - \dot{m}_b + \dot{m}_f$  at state 9 as seen from Table 4.1 and Figure 4.1. Exit velocity of the core flow is  $v_9$  and inlet velocity is  $v_1$ . Therefore core nozzle momentum part of the thrust is

$$F_1 = (\dot{m}_c - \dot{m}_b + \dot{m}_f)v_9 - \dot{m}_c v_1 \quad (4.57)$$

b. Core nozzle pressure component

Since inlet condition is 1 and exit condition is 9 for core flow in this thesis, utilizing the third term of the equation (3.2), second part of the thrust can be written as

$$F_2 = A_9(P_9 - P_1) \quad (4.58)$$

where  $A_9$  is exit area of core nozzle and can be calculated via general mass flow rate equation as performed by El-Sayed (2008), Mattingly et al. (2002) and Cohen et al. (1996).

$$\dot{m} = \rho v A \quad (4.59)$$

for this specific case it can be written as

$$\dot{m}_c - \dot{m}_b + \dot{m}_f = \rho_9 v_9 A_9 \quad (4.60)$$

rearranging yields

$$A_9 = \frac{\dot{m}_c - \dot{m}_b + \dot{m}_f}{\rho_9 v_9} \quad (4.61)$$

where  $\rho_9$  is the density of core flow at the core nozzle exit and it can be calculated by utilizing ideal gas equation of state, due to ideal gas assumption. Hence,

$$\frac{P_9}{\rho_9} = RT_9 \quad (4.62)$$

$$\rho_9 = \frac{P_9}{RT_9} \quad (4.63)$$

where  $R$  is the gas constant of air. As explained in detail in Chapter 2, pressure component of thrust is active only when choking at the nozzle exit occurs. If nozzle is not choked, then pressure contribution in thrust equation becomes zero.

c. Bypass nozzle momentum component

Bypass air enters into engine at state 1 at a mass flow rate of  $\dot{m}_F$ , and leaves bypass nozzle at state 10F at the same mass flow rate. Exit velocity of the bypass flow is  $v_{10F}$  and inlet velocity is  $v_1$ . Therefore, third part of the thrust is

$$F_3 = \dot{m}_F(v_{10F} - v_1) \quad (4.64)$$

d. Bypass nozzle pressure component

As applied in equation (4.58), pressure component of thrust for bypass nozzle can be written considering inlet as state 1 and exit as state 10F as follows.

$$F_4 = A_{10F}(P_{10F} - P_1) \quad (4.65)$$

where  $A_{10F}$  is the exit area of bypass nozzle and can be calculated by mass flow rate equation as written in equation (4.59).

$$\dot{m}_F = \rho_{10F}v_{10F}A_{10F} \quad (4.66)$$

so

$$A_{10F} = \frac{\dot{m}_F}{\rho_{10F}v_{10F}} \quad (4.67)$$

where  $\rho_{10F}$  is the density of air at bypass nozzle exit and can be calculated by ideal gas equation of state as follows.

$$\rho_{10F} = \frac{P_{10F}}{RT_{10F}} \quad (4.68)$$

Combining all of the above four components, thrust equation for this particular turbofan configuration becomes

$$F = F_1 + F_2 + F_3 + F_4 \quad (4.69)$$

or

$$F = (\dot{m}_c - \dot{m}_b + \dot{m}_f)v_9 - \dot{m}_c v_1 + \dot{m}_F(v_{10F} - v_1) + A_9(P_9 - P_1) + A_{10F}(P_{10F} - P_1) \quad (4.70)$$

#### 4.4.6.2 Propulsive power

Propulsive power has been expressed in Chapter 3 as thrust multiplied by aircraft velocity (i.e. inlet velocity of air) as in equation (3.5). Therefore, propulsive power for this particular turbofan engine is

$$\dot{W}_p = v_1 [(\dot{m}_c - \dot{m}_b + \dot{m}_f)v_9 - \dot{m}_c v_1 + \dot{m}_F(v_{10F} - v_1) + A_9(P_9 - P_1) + A_{10F}(P_{10F} - P_1)] \quad (4.71)$$

Since thrust is a force, it is in units of N or kN; and propulsive power is a power, it is in units of W or kW.

#### 4.4.7 Thrust specific fuel consumption, specific thrust and overall efficiency

As explained in Chapter 3, there have been several performance parameters that utilized as an objective function in thermodynamic analysis of aircraft engines. There have been explained five broadly utilized parameters that are based on the first law of thermodynamics point of view. These parameters were thrust specific fuel consumption, specific thrust, propulsive efficiency, thermal efficiency and overall efficiency. As mentioned earlier, overall efficiency is multiplication of thermal efficiency and propulsive efficiency.

In this thesis, three of them have been selected as appropriate performance indicators considering the first law of thermodynamics. These indicators are thrust specific fuel consumption, specific thrust and overall efficiency.

##### 4.4.7.1 Thrust specific fuel consumption (*TSFC*)

By utilizing equation (3.1) it can be written as

$$TSFC = \frac{\dot{m}_f}{F} \quad (4.72)$$

and substituting equation (4.70) into equation (4.72) yields

$$TSFC = \frac{\dot{m}_f}{(\dot{m}_c - \dot{m}_b + \dot{m}_f)v_9 - \dot{m}_c v_1 + \dot{m}_F(v_{10F} - v_1) + A_9(P_9 - P_1) + A_{10F}(P_{10F} - P_1)} \quad (4.73)$$

Unit of *TSFC* is g kN<sup>-1</sup>s<sup>-1</sup>.

##### 4.4.7.2 Specific thrust (*F<sub>s</sub>*)

By utilizing equation (3.3) it can be written as

$$F_s = \frac{F}{\dot{m}_c + \dot{m}_F} \quad (4.74)$$



and substituting equation (4.70) into equation (4.74) yields  $F_s$  in units of  $\text{Ns kg}^{-1}$  as

$$F_s = \frac{(\dot{m}_c - \dot{m}_b + \dot{m}_f)v_9 - \dot{m}_c v_1 + \dot{m}_F(v_{10F} - v_1) + A_9(P_9 - P_1) + A_{10F}(P_{10F} - P_1)}{\dot{m}_c + \dot{m}_F} \quad (4.75)$$

#### 4.4.7.3 Overall efficiency ( $\eta_o$ )

It has been considered in this thesis that aircraft engine provides power for auxiliary equipment in addition to propulsive power. Therefore, useful power produced by the engine definition has been extended to propulsive power and auxiliary power. Therefore, equation (3.14) can be rewritten as

$$\eta_o = \frac{\dot{W}_p + \dot{W}_{aux}}{\dot{m}_f Q_{LHV}} \quad (4.76)$$

and substituting equation (4.71) into equation (4.76) yields

$$\eta_o = \frac{v_1 [(\dot{m}_c - \dot{m}_b + \dot{m}_f)v_9 - \dot{m}_c v_1 + \dot{m}_F(v_{10F} - v_1)]}{\dot{m}_f Q_{LHV}} + \frac{v_1 [A_9(P_9 - P_1) + A_{10F}(P_{10F} - P_1)] + \dot{W}_{aux}}{\dot{m}_f Q_{LHV}} \quad (4.77)$$

#### 4.4.8 Thermodynamic property relations

In order to be able to perform the thermodynamic analysis, all thermodynamic states have to be determined. Starting from the state 1, all states have been determined one after another. Temperatures, pressure, isentropic or polytropic efficiencies, velocities and mass flow rates have been determined where they are necessary. By this way, all parameters that constitute objective functions have been accessed. However, it is necessary to determine operating conditions of the engine before start analyzing the parts one by one.

##### 4.4.8.1 Operating conditions, design parameters and performance parameters utilized in the thesis

Operating conditions, design and performance parameters utilized in this thesis has been shown in Table 4.2. These values have been selected by utilizing references Cohen et al. (1996), El-Sayed (2008), Mattingly et al. (2002), Mattingly (2006) and

Tanbay et al. (2013, 2015) which includes many real-life examples and results of experimental studies that characterize a typical twin-spool turbofan engine of a large commercial aircraft. Values of design and performance parameters are constant as in Table 4.2 when they are not variable.

**Table 4.2 :** Operating conditions, design and performance parameters.

Operating Conditions	Value
$T_1$	216.8 K
$P_1$	22.7 kPa
$M_1$	0.85 Ma
$\dot{m}_c$	100 kg s <sup>-1</sup>
Design Parameters	Value
$r_{LPC}$	3.5
$r_{HPC}$	5.0
$r_{C,Total}$	17.5
$r_F$	1.7
$\beta$	6
$\gamma$	0.03
$\theta_1$	0.00
$\theta_2$	0.05
$\dot{W}_{auxHP}$	350 kW
$T_{max}$	1300 K
Performance Parameters	Value
$\varepsilon_{LK1}$	0.02
$\varepsilon_{LK2}$	0.02
$e_F$	0.90
$e_{LPC}$	0.90
$e_{HPC}$	0.90
$e_{HPT}$	0.88
$e_{LPT}$	0.90
$r_D$	0.95
$\eta_N$	0.95
$\eta_{FN}$	0.95
$\eta_{M1}$	0.98
$\eta_{M2}$	0.98
$\eta_{auxHP}$	0.98
$\Delta P_{CC}/P_{05}$	0.02

#### 4.4.8.2 Diffuser

An adiabatic irreversible deceleration process occurs in diffuser of the turbofan engine from state 1 to state 2. Some pressure losses occur due to friction and due to shock waves (only for supersonic speeds) during this process. Temperature and pressure at the inlet (state 1) is known since they are ambient air's values at flight altitude. Temperature and pressure of the ambient air is taken as 216.8 K and 22.7 kPa respectively at 11,000 m altitude for the cruise phase (Cohen et al, 1996). Inlet velocity (flight Mach number) is assumed constant at 0.85 Ma, since commercial aircrafts' cruise speed is around this figure (Cohen et al, 1996; Mattingly, 2006). Exit conditions have to be calculated by using inlet conditions and thermodynamic relations for the process. A schematic illustration of a diffuser has been shown in Figure 4.3.

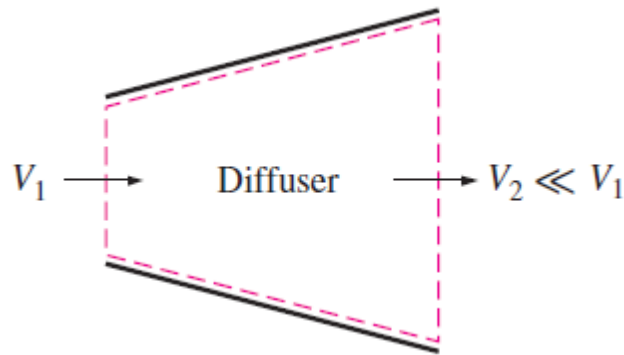


**Figure 4.3 :** A diffuser (Çengel and Boles, 2005).

Energy equation for this process can be written as

$$\dot{Q}_{1-2} - \dot{W}_{1-2} = \sum_{out} \dot{m} (h_{0,out}) - \sum_{in} \dot{m} (h_{0,in}) \quad (4.78)$$

Since there is no work interaction and process is adiabatic, heat and work terms vanish. Remaining stagnation enthalpy terms yield

$$h_{01} = h_{02} \quad (4.79)$$

and hence

$$T_{01} = T_{02} \quad (4.80)$$

By using equation (2.11), stagnation temperature relation can be written as

$$T_{01} = T_{02} = T_1 + \frac{v_1^2}{2c_p} \quad (4.81)$$

$T_{02}$  represents the stagnation temperature at the exit of diffuser for an irreversible adiabatic process. If the process was reversible (i.e. isentropic and adiabatic), stagnation temperature would be  $T_{02s}$  and related stagnation enthalpy would be  $h_{02s}$ . In this case, isentropic efficiency of the diffuser can be written as

$$\eta_D = \frac{h_{02s} - h_1}{h_{02} - h_1} \quad (4.82)$$

by eliminating  $c_p$  terms due to the calorically perfect gas assumption, it becomes

$$\eta_D = \frac{T_{02s} - T_1}{T_{02} - T_1} \quad (4.83)$$

by rearranging equation (4.81), below can be written

$$T_{02} - T_1 = \frac{v_1^2}{2c_p} \quad (4.84)$$

substituting equation (4.84) into denominator of equation (4.83) yields

$$\eta_D = \frac{T_{02s} - T_1}{\frac{v_1^2}{2c_p}} \quad (4.85)$$

then rearranging to draw  $T_{02s}$  yields

$$T_{02s} = T_1 + \eta_D \frac{v_1^2}{2c_p} \quad (4.86)$$

On the other hand, by using isentropic process relation between temperature and pressure as shown in equation (2.12), it can be written that

$$\frac{P_{02}}{P_1} = \left( \frac{T_{02s}}{T_1} \right)^{k/(k-1)} \quad (4.87)$$

by considering  $P_{02} = P_{02s}$ .

Substituting equation (4.86) into equation (4.87) yields

$$\frac{P_{02}}{P_1} = \left( \frac{T_1 + \eta_D \frac{v_1^2}{2c_p}}{T_1} \right)^{k/(k-1)} \quad (4.88)$$

or it can be written as

$$\frac{P_{02}}{P_1} = \left( 1 + \eta_D \frac{v_1^2}{2c_p T_1} \right)^{k/(k-1)} \quad (4.89)$$

By utilizing equation (2.13) and equation (2.14), it can be written that

$$M_1 = \frac{v_1}{\sqrt{kRT_1}} \quad (4.90)$$

then by rearranging

$$v_1^2 = M_1^2 kRT_1 \quad (4.91)$$

Also, below arrangements can be done considering  $R$ ,  $k$ ,  $c_p$  and  $c_v$ , which are gas constant, specific heat ratio, specific heats under constant pressure and constant volume respectively (Çengel and Boles, 2005).

$$R = c_p - c_v \quad (4.92)$$

dividing by  $c_p$

$$\frac{R}{c_p} = 1 - \frac{c_v}{c_p} \quad (4.93)$$

also

$$k = \frac{c_p}{c_v} \quad (4.94)$$

so

$$\frac{c_v}{c_p} = \frac{1}{k} \quad (4.95)$$

substituting equation (4.95) into equation (4.93) yields

$$\frac{R}{c_p} = 1 - \frac{1}{k} \quad (4.96)$$

or

$$\frac{R}{c_p} = \frac{k-1}{k} \quad (4.97)$$

Substituting equation (4.91) into equation (4.89) yields

$$\frac{P_{02}}{P_1} = \left( 1 + \eta_D \frac{M_1^2 k R T_1}{2 c_p T_1} \right)^{k/(k-1)} \quad (4.98)$$

cancelling  $T_1$  terms and substituting equation (4.97) into equation (4.98) yields

$$\frac{P_{02}}{P_1} = \left( 1 + \eta_D \frac{M_1^2 k (k-1)}{2k} \right)^{k/(k-1)} \quad (4.99)$$

and cancelling  $k$  terms results in

$$\frac{P_{02}}{P_1} = \left( 1 + \eta_D \frac{M_1^2 (k-1)}{2} \right)^{k/(k-1)} \quad (4.100)$$

In equation (4.100), purpose is to find  $P_{02}$ , the exit state pressure, by using the known parameters  $P_1$ ,  $M_1$  and  $k$ . However,  $\eta_D$  is not known and below steps have been performed to find an expression for it. Dividing both sides of equation (4.81) by  $T_1$  term yields

$$\frac{T_{02}}{T_1} = 1 + \frac{v_1^2}{2c_p T_1} \quad (4.101)$$

and substituting equation (4.91) into equation (4.101)

$$\frac{T_{02}}{T_1} = 1 + \frac{M_1^2 k R T_1}{2 c_p T_1} \quad (4.102)$$

simplifying and substituting equation (4.97) yields

$$\frac{T_{02}}{T_1} = 1 + \frac{M_1^2 (k-1)}{2} \quad (4.103)$$

It has been already shown in equation (4.81) that  $T_{02} = T_{01}$ . Using this equality, equation (4.103) can be rewritten as

$$\frac{T_{01}}{T_1} = 1 + \frac{M_1^2(k-1)}{2} \quad (4.104)$$

In Chapter 2, an equation for stagnation pressure and temperature have been defined as equation (2.12). By utilizing this equation, left side of the equation (4.104) can be written as

$$\frac{P_{01}}{P_1} = \left(\frac{T_{01}}{T_1}\right)^{k/(k-1)} \quad (4.105)$$

so substituting equation (4.104) into equation (4.105) yields

$$\frac{P_{01}}{P_1} = \left(1 + \frac{M_1^2(k-1)}{2}\right)^{k/(k-1)} \quad (4.106)$$

The left side of equation (4.95) can be disintegrated into two parts as

$$\frac{P_{02}}{P_1} = \frac{P_{02}}{P_{01}} \frac{P_{01}}{P_1} \quad (4.107)$$

where stagnation pressure ratio of the diffuser,  $r_D$  is

$$r_D = \frac{P_{02}}{P_{01}} \quad (4.108)$$

This pressure ratio is also known as pressure recovery factor and it has two components as follows.

$$r_D = r_{D,f} r_{D,s} \quad (4.109)$$

In the right hand side of equation (4.109), first term,  $r_{D,f}$ , refers to pressure recovery against decreasing effect of friction and it is a known parameter (less than but close to 1) as seen in Table 4.2. On the other hand, second term,  $r_{D,s}$ , refers to pressure recovery against decreasing effect of shock waves when the Mach number is above 1. As mentioned by Cohen et al. (1996) and Mattingly (2006),  $r_{D,s}$  has been formulized as

$$r_{D,s} = 1 \quad \text{when } M < 1 \quad (4.110)$$

and

$$r_{D,s} = 1 - 0.075(M - 1)^{1.35} \quad \text{when } 1 < M < 5 \quad (4.111)$$

Since in this thesis Mach number of the flight has been assumed as constant at 0.85,  $r_{D,s}$  is considered as equal to unity, so it does not have any effects on equation (4.109).

After accessing stagnation pressure ratio of diffuser, substituting equations (4.106) and (4.108) into equation (4.107) yields

$$\frac{P_{02}}{P_1} = r_D \left( 1 + \frac{M_1^2(k-1)}{2} \right)^{k/(k-1)} \quad (4.112)$$

and substituting equation (4.100) into equation (4.112), one can reach an equation with the only unknown, isentropic efficiency of the diffuser as

$$\left( 1 + \eta_D \frac{M_1^2(k-1)}{2} \right)^{k/(k-1)} = r_D \left( 1 + \frac{M_1^2(k-1)}{2} \right)^{k/(k-1)} \quad (4.113)$$

taking the power of  $(k-1)/k$  of both sides yields

$$1 + \eta_D \frac{M_1^2(k-1)}{2} = (r_D)^{(k-1)/k} \left( 1 + \frac{M_1^2(k-1)}{2} \right) \quad (4.114)$$

drawing the isentropic efficiency of diffuser and leaving it alone on the left side yields

$$\eta_D = \frac{\left( 1 + \frac{M_1^2(k-1)}{2} \right) (r_D)^{(k-1)/k} - 1}{\frac{M_1^2(k-1)}{2}} \quad (4.115)$$

By this equation, one can calculate  $P_{02}$ , stagnation pressure at the exit of diffuser by using equation (4.100). Calculation of  $T_{02}$  has already been demonstrated in equation (4.103). Hence, state of air at the diffuser exit is known without any unknowns remaining after performing above calculations.

#### 4.4.8.3 Fan

An adiabatic irreversible compression process occurs in fan from state 2 to state 3. Temperature and pressure of the air rises due to this compression process. Stagnation



properties at the inlet of fan have been calculated above as exit properties of diffuser. Here, aim is to utilize inlet properties of fan (exit properties of diffuser) and determining the properties at the exit of fan by applying adiabatic irreversible process relations. Schematic illustration of a turbofan has been presented in Figure 4.4.

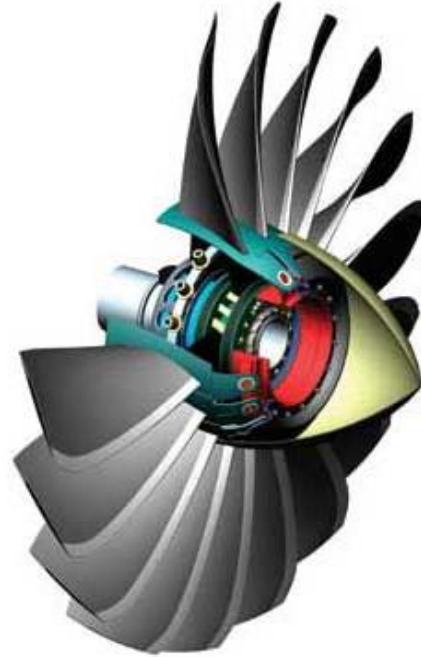


**Figure 4.4 :** A turbofan (Langston, 2011).

Fan is one of the rotating machinery in the turbofan engine and it works with a predetermined pressure ratio. In other words, exit stagnation pressure over inlet stagnation pressure of fan is determined by designers and it is an input for cycle analysis. This predetermined ratio is called as pressure ratio of fan and can be written as

$$r_F = \frac{P_{03}}{P_{02}} \quad (4.116)$$

In order to find exit stagnation temperature, there should be a link between pressure ratios and temperature ratios for compression process in fan. In some studies in literature, isentropic relation between temperature and pressure has been utilized directly assuming the compression process in fan is adiabatic and reversible so isentropic. However, in the thesis the process in fan is considered as adiabatic but irreversible. Therefore, instead of directly utilizing the isentropic relation between

temperature ratios and pressure ratios as it is, a corrected version of isentropic relation has been utilized in the thesis.

In order to find a correction, literature review has been performed. In Mattingly (2006) it has been shown that isentropic efficiency of a multistage compressor is a function of compressor pressure ratio, pressure ratio of each stage and isentropic efficiency of each stage as

$$\eta_c = \frac{r_c^{\left(\frac{k-1}{k}\right)} - 1}{\prod_{j=1}^N \left\{ 1 + \left(\frac{1}{\eta_{sj}}\right) \left( r_{sj}^{\left(\frac{k-1}{k}\right)} - 1 \right) \right\} - 1} \quad (4.117)$$

In equation (4.117),  $\eta_c$  is compressor isentropic efficiency,  $r_c$  is compressor pressure ratio, N is the total number of stages,  $\eta_{sj}$  is isentropic efficiency of  $j^{\text{th}}$  stage of compressor and  $r_{sj}$  is pressure ratio of  $j^{\text{th}}$  stage of compressor. Derivation of equation (4.117) has been shown in Appendix B.

For a specific compressor having a specific pressure ratio, specific number of stages, specific isentropic efficiency of each stage and specific pressure ratio of each stage; a constant and already-known isentropic efficiency of compressor could be determined and utilized in calculations. This constant isentropic efficiency of compressor would be the figure of merit for this component, and would be utilized to link the temperature and pressure ratios at the exit and inlet of the component.

However, in parametric cycle analysis, since compressor pressure ratio is one of the variables as being a design parameter, a constant isentropic efficiency is not the case for such a hypothetical component which may have any pressure ratio between two specified values. The same concern is also valid for fan and turbines due to having variable compression or expansion ratios in parametric cycle analysis. Therefore, it is a common practice to utilize another figure of merit for turbomachinery that is constant for variable compression (or expansion) ratios in literature. This figure of merit is named polytropic efficiency and has been utilized by many studies and textbooks such as Cohen et al. (1996), Najjar and Al-Sharif (2006), Mattingly (2006), El-Sayed (2008) and Tai et al. (2014).

Firstly, isentropic efficiency has been defined for a fan, then polytropic efficiency has been defined and derived for a fan. Also relation between isentropic efficiency and polytropic efficiency has been shown.

Isentropic efficiency for a fan can be defined considering a specific compression ratio as

$$\eta_F = \frac{\text{work required for reversible (ideal)adiabatic compression}}{\text{work required for real compression}} \quad (4.118)$$

which can be rewritten in terms of stagnation enthalpies as

$$\eta_F = \frac{h_{03s} - h_{02}}{h_{03} - h_{02}} \quad (4.119)$$

or eliminating constant  $c_p$  and rewriting in terms of temperatures

$$\eta_F = \frac{T_{03s} - T_{02}}{T_{03} - T_{02}} \quad (4.120)$$

Dividing by  $T_{02}$  it becomes

$$\eta_F = \frac{\frac{T_{03s}}{T_{02}} - 1}{\frac{T_{03}}{T_{02}} - 1} \quad (4.121)$$

and using isentropic relation for temperature and pressure ratios, it becomes

$$\eta_F = \frac{\left(\frac{P_{03}}{P_{02}}\right)^{(k-1)/k} - 1}{\frac{T_{03}}{T_{02}} - 1} \quad (4.122)$$

and lastly, using equation (4.116), equation (4.122) has been shown as

$$\eta_F = \frac{(r_F)^{(k-1)/k} - 1}{\frac{T_{03}}{T_{02}} - 1} \quad (4.123)$$

As stated before, this definition is valid for a specific fan having an already-determined pressure ratio.

Before starting derivation of polytropic efficiency, it is important to note that polytropic efficiency utilized in the thesis should not be perceived as the efficiency

of a compression or an expansion process which also includes heat transfer (i.e. polytropic process) as its name suggests. Instead, it is actually a correction factor for isentropic property relations between temperatures and pressures when the process is adiabatic but not reversible. The name of the polytropic efficiency would be more correctly expressed as “differential-pressure-change based correction factor for irreversibility of an isentropic relation”, “differential-pressure-change based irreversibility correction factor for an isentropic relation” or briefly “differential-pressure-change based irreversibility correction factor” in order not to cause any confusion with polytropic process including heat transfer.

Differential-pressure-change based irreversibility correction factor for adiabatic compression process in a fan can be defined as

$$e_F = \frac{\text{work required for ideal (isentropic) compression for a diff. pressure change}}{\text{work required for real compression for a diff. pressure change}} \quad (4.124)$$

By utilizing equation (4.124) and considering equation (4.35), differential-pressure-change based irreversibility correction factor for adiabatic compression process of fan can be expressed as

$$e_F = \frac{dh_{0s}}{dh_0} \quad (4.125)$$

or

$$e_F = \frac{dT_{0s}}{dT_0} \quad (4.126)$$

where subscript  $s$  represents the ideal (isentropic) process. Utilizing the general equation for entropy change of an ideal gas as given in Çengel and Boles (2005),

$$ds = c_p \frac{dT}{T} - R \frac{dP}{P} \quad (4.127)$$

dividing by  $R$  and utilizing the relation expressed in equation (4.97) yields

$$\frac{ds}{R} = \frac{k}{k-1} \frac{dT}{T} - \frac{dP}{P} \quad (4.128)$$

If the process is assumed to be isentropic, then it means that  $ds = 0$  and temperature takes subscript  $s$  as in equation (4.126). Then,

$$0 = \frac{k}{k-1} \frac{dT_s}{T} - \frac{dP}{P} \quad (4.129)$$

This relation can also be written for stagnation properties as

$$0 = \frac{k}{k-1} \frac{dT_{0s}}{T_0} - \frac{dP_0}{P_0} \quad (4.130)$$

rearranging yields

$$\frac{dT_{0s}}{T_0} = \frac{k-1}{k} \frac{dP_0}{P_0} \quad (4.131)$$

dividing equation (4.126) by  $T_0$  yields

$$e_F = \frac{dT_{0s}/T_0}{dT_0/T_0} \quad (4.132)$$

Now, equation (4.131) is substituted into equation (4.132) as

$$e_F = \frac{\frac{k-1}{k} \frac{dP_0}{P_0}}{dT_0/T_0} \quad (4.133)$$

rearranging

$$\frac{dT_0}{T_0} = \frac{k-1}{ke_F} \frac{dP_0}{P_0} \quad (4.134)$$

integrating between state 2 to state 3 yields

$$\ln \frac{T_{03}}{T_{02}} = \frac{k-1}{ke_F} \ln \frac{P_{03}}{P_{02}} \quad (4.135)$$

then it becomes

$$\frac{T_{03}}{T_{02}} = \left( \frac{P_{03}}{P_{02}} \right)^{\left( \frac{k-1}{k} \right) \frac{1}{e_F}} \quad (4.136)$$

then by using pressure ratio of fan definition as in equation (4.116),  $T_{03}$  can be found by

$$T_{03} = T_{02} \left[ r_F^{\left( \frac{k-1}{k} \right) \frac{1}{e_F}} \right] \quad (4.137)$$

Value of differential-pressure-change based irreversibility correction factor for adiabatic compression (or expansion) process is an input that is already known and considered as constant for any turbomachinery, and values used in this thesis have been shown in Table 4.2.

Therefore, with the known fan pressure ratio and differential-pressure-change based irreversibility correction factor for adiabatic compression process of fan, inlet temperature  $T_{02}$  has been utilized to calculate exit temperature  $T_{03}$ .

In order to write a relation between differential-pressure-change based irreversibility correction factor for adiabatic compression process and isentropic efficiency, equation (4.136) and equation (4.116) have been substituted into equation (4.123) as

$$\eta_F = \frac{(r_F)^{\left(\frac{k-1}{k}\right)} - 1}{(r_F)^{\left(\frac{k-1}{k}\right)\frac{1}{e_F}} - 1} \quad (4.138)$$

Equation (4.138) clearly shows the relation between constant differential-pressure-change based irreversibility correction factor for adiabatic compression process (figure of merit for turbomachinery), variable fan pressure ratio and variable fan isentropic efficiency. In case of requirement, isentropic efficiency of fan can be calculated by using equation (4.138) for a specific fan pressure ratio. In the thesis, it has not been required to do so for turbomachinery (fan, LPC, HPC, HPT, LPT); instead, exit pressure and exit temperature values have been calculated by using equation (4.116) and equation (4.137) respectively. The same approach has been considered for compressors and turbines.

#### 4.4.8.4 LPC and HPC

Air enters into LPC at pressure  $P_{03}$  and temperature  $T_{03}$ . After an adiabatic and irreversible compression process, air leaves LPC at  $P_{04}$ ,  $T_{04}$  respectively. Schematic illustration of a twin-spool axial compressor has been presented in Figure 4.5.

Compression ratio or pressure ratio of LPC is an input, since it is a design parameter as for the fan. Pressure ratio of LPC can be expressed as

$$r_{LPC} = \frac{P_{04}}{P_{03}} \quad (4.139)$$

Utilization of differential-pressure-change based irreversibility correction factor for adiabatic compression process and steps for determination of the exit temperature formula is the same as fan, since both in fan and in LPC air goes under an adiabatic and irreversible compression process with work input. Therefore equation (4.124) is also valid for LPC and equation (4.137) can be written for LPC as

$$T_{04} = T_{03} \left[ r_{LPC}^{\left(\frac{k-1}{k}\right)} e_{LPC} \right] \quad (4.140)$$

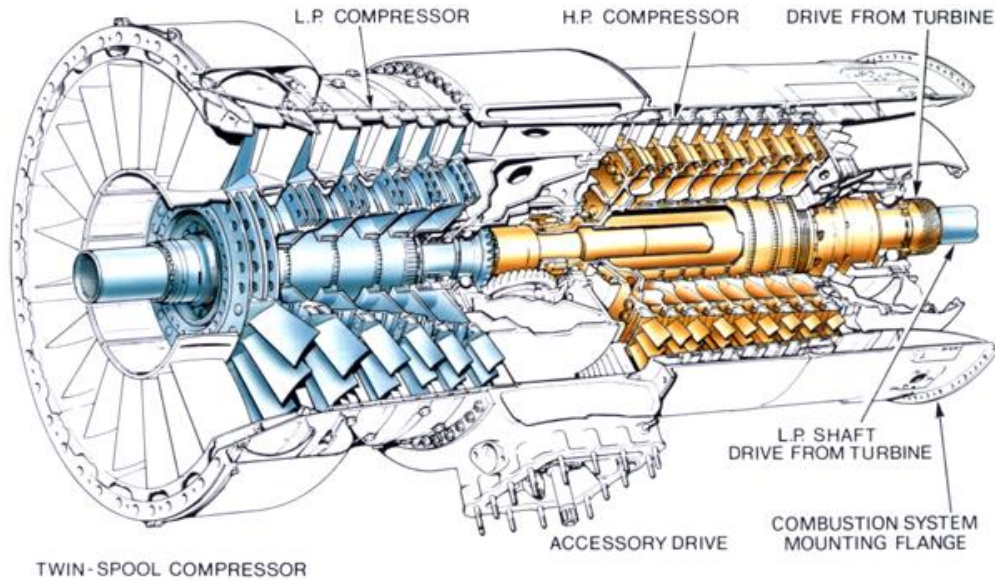


**Figure 4.5 :** A twin-spool axial compressor (Rolls Royce, 1996).

where  $e_{LPC}$  is differential-pressure-change based irreversibility correction factor for adiabatic compression process of LPC. Now, pressure and temperature have been determined at the LPC exit, which is inlet of HPC. HPC has been considered in two parts. One part is from state 4 to state 4a until the cooling air for LPT is drawn. Second part is from state 4a to state 5 until the end of HPC. For both of these parts of HPC, pressure ratio is predetermined (design parameter) and can be written as

$$r_{HPC1} = \frac{P_{04a}}{P_{04}} \quad (4.141)$$

$$r_{HPC2} = \frac{P_{05}}{P_{04a}} \quad (4.142)$$

Then, total compressor pressure ratio becomes

$$r_{C,Total} = \frac{P_{04}}{P_{03}} * \frac{P_{04a}}{P_{04}} * \frac{P_{05}}{P_{04a}} \quad (4.143)$$

or by simplifying it becomes

$$r_{C,Total} = \frac{P_{05}}{P_{03}} \quad (4.144)$$

since  $r_{C,Total}$  is the ratio of exit pressure of compressor (exit of HPC) to the inlet pressure of compressor (inlet of LPC). In addition to section 4.4.8.1, it has to be clarified that when total compressor pressure ratio,  $r_{C,Total}$ , is considered as variable, one of the components of compressor has been kept constant and the other component has been varied. Namely, the compressor pressure ratio for LPC has been kept constant at 2.5 and the compressor pressure ratio for HPC has been varied within 1 and 13.4 so that total compressor pressure ratio has covered the values between 2.5 and 33.5 when it is considered as variable.

As for fan and LPC, adiabatic irreversible compression process with work input is valid for HPC; therefore, temperature relations can be written as

$$T_{04a} = T_{04} \left[ r_{HPC1}^{\left(\frac{k-1}{k}\right) \frac{1}{e_{HPC}}} \right] \quad (4.145)$$

$$T_{05} = T_{04a} \left[ r_{HPC2}^{\left(\frac{k-1}{k}\right) \frac{1}{e_{HPC}}} \right] \quad (4.146)$$

where  $e_{HPC}$  is differential-pressure-change based irreversibility correction factor for adiabatic compression process of HPC.

#### 4.4.8.5 Combustion chamber

After leaving the HPC, second cooling air (cooling air for HPT) is drawn at state 5 before entering combustion chamber. The mass flow rate for HPT cooling extraction is  $\dot{m}_{cool2}$  as seen in Table 4.1 Then, mass flow rate of remaining air flow is  $\dot{m}_c - \dot{m}_b - \dot{m}_{cool1} - \dot{m}_{cool2}$  and this amount goes under the combustion process. During the combustion process,  $\dot{m}_f$  is the mass flow rate of fuel added. Therefore at state 5, mass flow rate of air at the CC inlet is  $\dot{m}_c - \dot{m}_b - \dot{m}_{cool1} - \dot{m}_{cool2}$  and at state 6' it



is  $\dot{m}_c - \dot{m}_b - \dot{m}_{cool1} - \dot{m}_{cool2} + \dot{m}_f$ . Schematic illustration of a combustion chamber has been presented in Figure 4.6.

Due to metallurgical constraints, maximum temperature allowed at the CC outlet is limited and it is a design parameter which is determined during the design phase of the engine (Mattingly, 2006). Therefore, it is given as an input to the thermodynamic cycle analysis of the turbofan engine. In this thesis, value of  $T_{06'}$  (maximum temperature at CC exit) has been considered as an input and shown in Table 4.2.

In order to reach that temperature with known CC inlet temperature, mass flow rate of fuel has to be adjusted such that it will carry the temperature of the flow to predetermined  $T_{06'}$  level from different CC inlet temperatures. Therefore, two expressions have been developed for the mass flow rate of fuel and fuel to air ratio respectively. Right hand sides of these two expressions are composed of known parameters, so  $\dot{m}_f$  and  $\alpha$  can be calculated depending on the inlet temperature of CC and predesigned exit temperature.

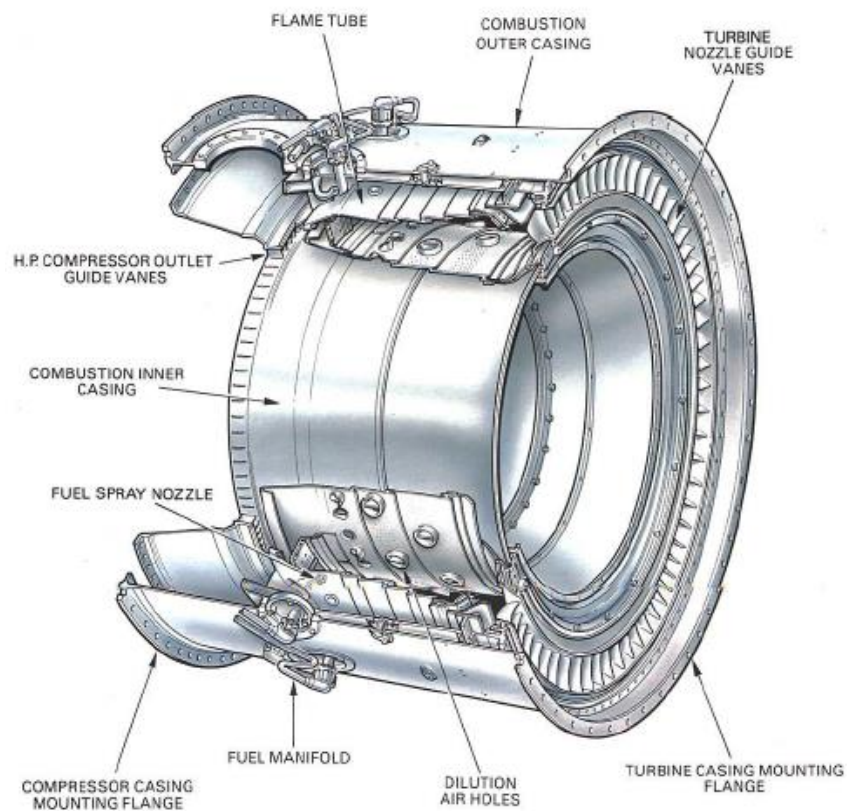


**Figure 4.6 :** An annular combustion chamber (Rolls Royce, 1996).

Substituting equation (4.6) into equation (4.9) yields

$$\begin{aligned} \dot{m}_f Q_{LHV} = & (\dot{m}_C - \dot{m}_b - \dot{m}_{cool1} - \dot{m}_{cool2} + \dot{m}_f) c_p T_{06'} \\ & - (\dot{m}_C - \dot{m}_b - \dot{m}_{cool1} - \dot{m}_{cool2}) c_p T_{05} \end{aligned} \quad (4.147)$$

Rearrangement yields

$$(\dot{m}_C - \dot{m}_b - \dot{m}_{cool1} - \dot{m}_{cool2}) c_p (T_{06'} - T_{05}) = \dot{m}_f (Q_{LHV} - c_p T_{06'}) \quad (4.148)$$

so

$$\dot{m}_f = \frac{(\dot{m}_C - \dot{m}_b - \dot{m}_{cool1} - \dot{m}_{cool2}) c_p (T_{06'} - T_{05})}{Q_{LHV} - c_p T_{06'}} \quad (4.149)$$

Dividing by  $(\dot{m}_C - \dot{m}_b - \dot{m}_{cool1} - \dot{m}_{cool2})$  in order to utilize equation (4.5) yields

$$\alpha = \frac{c_p (T_{06'} - T_{05})}{Q_{LHV} - c_p T_{06'}} \quad (4.150)$$

In order to find  $T_{06''}$ , which is the temperature level fallen from maximum temperature level  $T_{06'}$  due to heat leakage one,  $\varepsilon_{LK1}$  has to be utilized.  $\varepsilon_{LK1}$  has been considered as an input in this thesis. Three different values for  $\varepsilon_{LK1}$  have been selected, 0%, 2% and 4%. Effects of  $\varepsilon_{LK1}$  on the performance of the engine have been investigated on these three scenarios. In equation (4.24), a mathematical relation has been established between calculated air to fuel ratio  $\alpha$ , calculated CC inlet temperature  $T_{05}$ , predetermined maximum CC outlet temperature  $T_{06'}$ , heat leakage ratio one  $\varepsilon_{LK1}$  and temperature level after heat leakage  $T_{06''}$ . Rearranging equation (4.24)

$$\varepsilon_{LK1} [(1 + \alpha) T_{06'} - T_{05}] = (1 + \alpha) (T_{06'} - T_{06''}) \quad (4.151)$$

Then

$$T_{06'} - T_{06''} = \frac{\varepsilon_{LK1} [(1 + \alpha) T_{06'} - T_{05}]}{1 + \alpha} \quad (4.152)$$

And so

$$T_{06''} = T_{06'} - \frac{\varepsilon_{LK1}[(1 + \alpha)T_{06'} - T_{05}]}{1 + \alpha} \quad (4.153)$$

Then, exit pressure of CC has to be calculated since temperature and fuel consumption values have been determined. As expressed by Mattingly (2006) and El-Sayed (2008), there exists a pressure loss in the CC mainly due to friction. This loss may be a few percent in total and it has been assumed to be 2% in this thesis as indicated in Table 4.2. Due to this loss, pressure ratio of CC can be written as

$$\frac{P_{06''}}{P_{05}} < 1 \quad (4.154)$$

Then, to reach an expression

$$P_{06''} = P_{05} - \Delta P_{CC} \quad (4.155)$$

or rearranging yields

$$P_{06''} = P_{05} \left( 1 - \frac{\Delta P_{CC}}{P_{05}} \right) \quad (4.156)$$

where  $\Delta P_{CC}$  is the pressure loss in the combustion chamber.

#### 4.4.8.6 HPT and LPT

An adiabatic irreversible process takes place in each of HPT and LPT. After CC, HPT is the next component to proceed for core flow. As mentioned earlier, combustion products after combustion are mixed with cooling air two before entering into HPT. After cooling effect, flow comes to state 6 and it is the inlet state of HPT. Schematic illustration of a twin-turbine has been presented in Figure 4.7.

Since the pressure of cooling air and core flow is nearly the same, it can be written that

$$P_{06} = P_{06''} \quad (4.157)$$

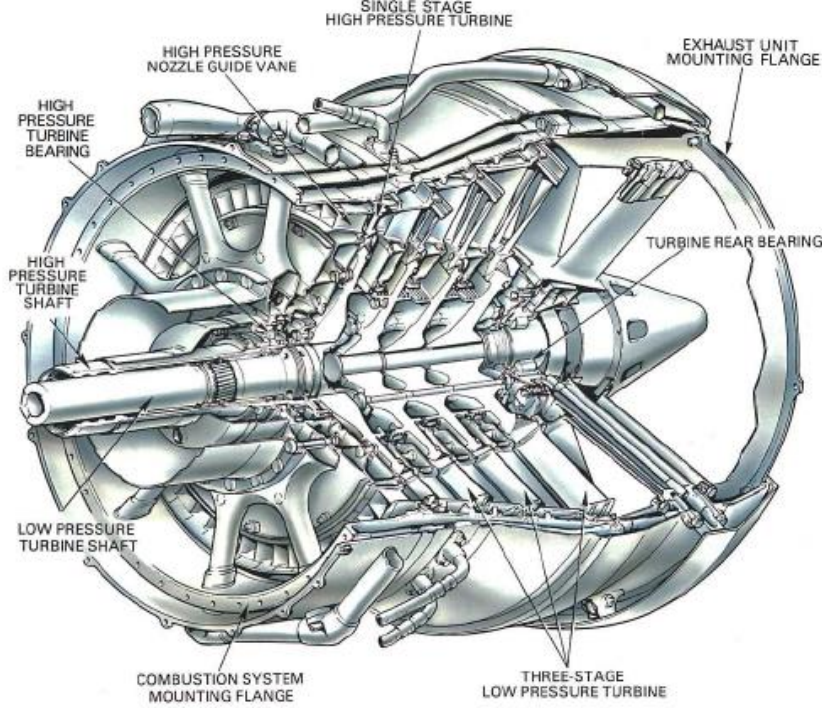


**Figure 4.7 :** A twin-turbine (Rolls Royce, 1996).

Also, in order to find the temperature at state 6, energy balance equation has been written for the inlet of HPT. Cooling air enters with temperature  $T_{05}$  since it was taken out from state 5 and mass flow rate  $\dot{m}_{cool2}$ . On the other hand, core flow enters with  $T_{06''}$  since it has dropped from state 6' to state 6'' due to heat leakage one. Mass flow rate of the core flow is  $\dot{m}_C - \dot{m}_b - \dot{m}_{cool1} - \dot{m}_{cool2} + \dot{m}_f$  since fuel has been added in CC. The resulting temperature at the HPT inlet is  $T_{06}$  after cooling. Total mass flow rate that enters HPT is summation of above mentioned two streams resulting in  $\dot{m}_C - \dot{m}_b - \dot{m}_{cool1} + \dot{m}_f$ . Then equation is

$$\begin{aligned} \dot{m}_{cool2}c_pT_{05} + (\dot{m}_C - \dot{m}_b - \dot{m}_{cool1} - \dot{m}_{cool2} + \dot{m}_f)c_pT_{06''} \\ = (\dot{m}_C - \dot{m}_b - \dot{m}_{cool1} + \dot{m}_f)c_pT_{06} \end{aligned} \quad (4.158)$$

cancelling  $c_p$  terms and dividing by  $\dot{m}_C - \dot{m}_b - \dot{m}_{cool1} + \dot{m}_f$  term in order to solve for  $T_{06}$  yields

$$T_{06} = \frac{\dot{m}_{cool2}T_{05} + (\dot{m}_C - \dot{m}_b - \dot{m}_{cool1} - \dot{m}_{cool2} + \dot{m}_f)T_{06''}}{(\dot{m}_C - \dot{m}_b - \dot{m}_{cool1} + \dot{m}_f)} \quad (4.159)$$

By calculating the temperature and the pressure at state 6, inlet conditions at the HPT inlet have been determined. Equation (4.49) can be rearranged to solve for  $T_{07''}$  which is the exit temperature of HPT.

$$T_{06} - T_{07''} = \frac{W_{HPC} + \dot{W}_{aux}/\eta_{aux}}{\eta_{M2}(\dot{m}_c - \dot{m}_b - \dot{m}_{cool1} + \dot{m}_f)c_p} \quad (4.160)$$

then substituting equation (4.39) into equation (4.160) yields

$$\begin{aligned} T_{06} - T_{07''} \\ = \frac{(\dot{m}_c - \dot{m}_b)c_p(T_{04a} - T_{04}) + (\dot{m}_c - \dot{m}_b - \dot{m}_{cool1})c_p(T_{05} - T_{04a}) + (\dot{W}_{aux}/\eta_{aux})}{\eta_{M2}(\dot{m}_c - \dot{m}_b - \dot{m}_{cool1} + \dot{m}_f)c_p} \end{aligned} \quad (4.161)$$

eliminating  $c_p$  terms and solving for  $T_{07''}$  yields

$$\begin{aligned} T_{07''} \\ = T_{06} - \frac{(\dot{m}_c - \dot{m}_b)(T_{04a} - T_{04}) + (\dot{m}_c - \dot{m}_b - \dot{m}_{cool1})(T_{05} - T_{04a}) + \frac{\dot{W}_{aux}}{\eta_{aux}}}{\eta_{M2}(\dot{m}_c - \dot{m}_b - \dot{m}_{cool1} + \dot{m}_f)} \end{aligned} \quad (4.162)$$

Since temperature at HPT exit has been calculated, pressure at HPT exit has to be calculated to access thermodynamic state of HPT exit. As done for fan and compressors, differential-pressure-change based irreversibility correction factor for adiabatic expansion process has been utilized for turbines in this thesis. By utilizing differential-pressure-change based irreversibility correction factor for adiabatic expansion process, a relation has been calculated between temperatures and pressures of inlet and exit of turbines. differential-pressure-change based irreversibility correction factor for adiabatic expansion process has been defined by Mattingly (2006) as

$$\begin{aligned} e_{HPT} \\ = \frac{\text{actual HPT work for a differential pressure change}}{\text{ideal (isentropic) HPT work for a differential pressure change}} \end{aligned} \quad (4.163)$$

then by utilizing equation (4.126)

$$e_{HPT} = \frac{dT_0}{dT_{0s}} \quad (4.164)$$

dividing by  $T_0$  and utilizing equation (4.131) yields

$$e_{HPT} = \frac{dT_0/T_0}{dT_{0s}/T_0} \quad (4.165)$$

and

$$e_{HPT} = \frac{dT_0/T_0}{\frac{k-1}{k} \frac{dP_0}{P_0}} \quad (4.166)$$

then

$$\frac{dT_0}{T_0} = \frac{e_{HPT}(k-1)}{k} \frac{dP_0}{P_0} \quad (4.167)$$

integrating between state 7'' and state 6

$$\ln \frac{T_{07''}}{T_{06}} = \frac{e_{HPT}(k-1)}{k} \ln \frac{P_{07''}}{P_{06}} \quad (4.168)$$

then it becomes

$$\frac{T_{07''}}{T_{06}} = \left( \frac{P_{07''}}{P_{06}} \right)^{\frac{(k-1)e_{HPT}}{k}} \quad (4.169)$$

Solving for  $P_{07''}$  yields

$$P_{07''} = P_{06} \left( \frac{T_{07''}}{T_{06}} \right)^{\frac{k}{(k-1)e_{HPT}}} \quad (4.170)$$

where  $e_{HPT}$  is differential-pressure-change based irreversibility correction factor for adiabatic expansion process of high pressure turbine. So, exit temperature and pressure at HPT exit have been calculated with equations (4.157) and (4.165). After HPT, core flow proceeds to LPT; however, cooling air for LPT is added to this core flow before entering into LPT. Therefore temperature,  $T_{07}$  and pressure,  $P_{07}$  at the LPT inlet have to be determined by considering the effects of cooling air for LPT.

As explained for HPT, cooling air for LPT also has a pressure level close to the core air proceeding to LPT. Therefore it can be written that

$$P_{07} = P_{07''} \quad (4.171)$$

Energy balance equation can be written for LPT entrance as done for HPT entrance. Cooling air has been drawn from state 4a with a mass flow rate of  $\dot{m}_{cool1}$ . Also, core air proceeding to LPT is at state 7'' with a mass flow rate of  $\dot{m}_c - \dot{m}_b - \dot{m}_{cool1} + \dot{m}_f$ . As a result, inlet state of LPT is state 7 and mass flow rate is summation of these two streams. Then, energy conservation equation at LPT entrance yields

$$\begin{aligned} (\dot{m}_c - \dot{m}_b - \dot{m}_{cool1} + \dot{m}_f)c_p T_{07''} + \dot{m}_{cool1}c_p T_{04a} \\ = (\dot{m}_c - \dot{m}_b + \dot{m}_f)c_p T_{07} \end{aligned} \quad (4.172)$$

eliminating  $c_p$  terms and dividing by  $\dot{m}_c - \dot{m}_b + \dot{m}_f$  in order to solve for  $T_{07}$  yields

$$T_{07} = \frac{(\dot{m}_c - \dot{m}_b - \dot{m}_{cool1} + \dot{m}_f)T_{07''} + \dot{m}_{cool1}T_{04a}}{\dot{m}_c - \dot{m}_b + \dot{m}_f} \quad (4.173)$$

Temperature and pressure have been calculated for LPT inlet. Then, those of LPT exit have to be calculated. In order to calculate temperature at the LPT exit, equation (4.55) can be utilized. When equations (4.35), (4.36) and (4.52) are substituted into equation (4.55), it yields

$$\begin{aligned} (\dot{m}_c - \dot{m}_b + \dot{m}_f)c_p(T_{07} - T_{08}) \\ = \frac{\dot{m}_c c_p(T_{04} - T_{03}) + (\dot{m}_c + \dot{m}_F)c_p(T_{03} - T_{02})}{\eta_{M1}} \end{aligned} \quad (4.174)$$

where  $T_{08}$  is the temperature to be determined. Cancelling  $c_p$  terms and dividing by  $\dot{m}_c - \dot{m}_b + \dot{m}_f$  yield

$$T_{07} - T_{08} = \frac{\dot{m}_c(T_{04} - T_{03}) + (\dot{m}_c + \dot{m}_F)(T_{03} - T_{02})}{\eta_{M1}(\dot{m}_c - \dot{m}_b + \dot{m}_f)} \quad (4.175)$$

or

$$T_{08} = T_{07} - \frac{\dot{m}_c(T_{04} - T_{03}) + (\dot{m}_c + \dot{m}_F)(T_{03} - T_{02})}{\eta_{M1}(\dot{m}_c - \dot{m}_b + \dot{m}_f)} \quad (4.176)$$

Then, in order to calculate exit pressure of LPT,  $P_{08}$ , the same relation has been utilized as for HPT exit. Therefore, by utilizing equation (4.170) it can be written that

$$P_{08} = P_{07} \left( \frac{T_{08}}{T_{07}} \right)^{\frac{k}{(k-1) e_{LPT}}} \quad (4.177)$$

where  $e_{LPT}$  is differential-pressure-change based irreversibility correction factor for adiabatic expansion process of the low pressure turbine.

#### 4.4.8.7 Core nozzle

After HPT and LPT, core air proceeds to core nozzle before leaving the engine. Air is expanded and accelerated to a very high velocity in order to provide thrust and produce propulsive power for the aircraft. Air enters at state 8 and leaves the engine at state 9. Schematic illustration of core nozzle has been illustrated in Figure 4.8.

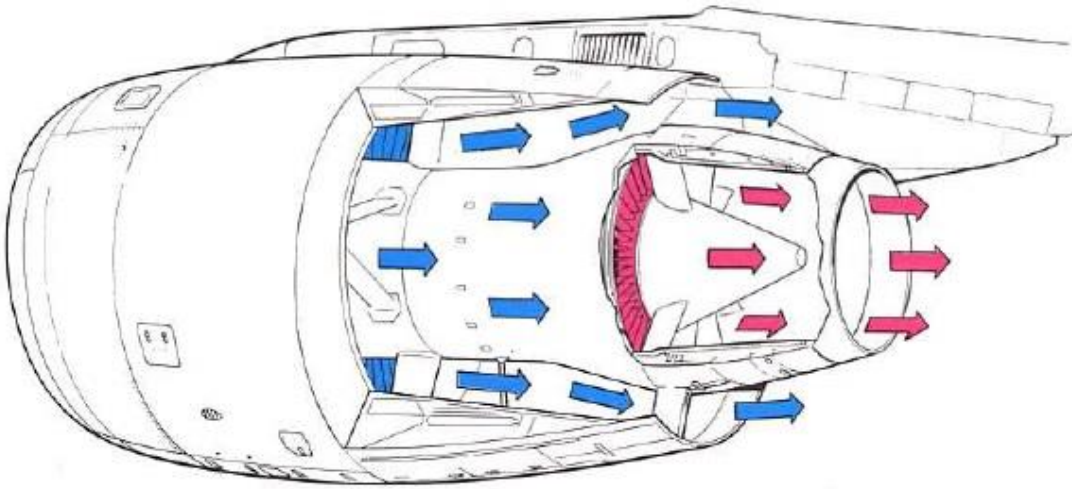


**Figure 4.8 :** A nozzle or exhaust (inner red arrows show core nozzle) (Rolls Royce, 1996).

As mentioned in Chapter 2, exit condition of air from nozzle differs with respect to expansion level (i.e. exit pressure level). If the critical pressure is above or equal to the environment pressure, then it is said that flow is choked. Otherwise, it is unchoked. This critical pressure yields the pressure where Mach number at the exit is equal to unity (Cohen et al, 1996). It can be calculated as

$$h_{08} = h_{09} = h_{cr} + \frac{v_{cr}^2}{2} \quad (4.178)$$

can be written since the process is adiabatic and no work interaction occurs. Then due to calorically perfect gas assumption it becomes

$$T_{08} = T_{cr} + \frac{v_{cr}^2}{2c_p} \quad (4.179)$$



By using equation (2.13) and (2.14), since  $M = 1$  at critical conditions

$$v_{cr} = c = \sqrt{kRT_{cr}} \quad (4.180)$$

Substituting equation (4.180) into equation (4.179) yields

$$T_{08} = T_{cr} + \frac{kRT_{cr}}{2c_p} \quad (4.181)$$

Utilizing equation (4.97) and cancelling  $k$  terms yield

$$T_{08} = T_{cr} \left( 1 + \frac{k-1}{2} \right) \quad (4.182)$$

or

$$T_{08} = T_{cr} \left( \frac{k+1}{2} \right) \quad (4.183)$$

then  $T_{cr}$  becomes

$$T_{cr} = T_{08} \frac{2}{k+1} \quad (4.184)$$

or it can be written as

$$T_{cr} = T_{08} \left( 1 - \frac{k-1}{k+1} \right) \quad (4.185)$$

Critical temperature has been calculated in terms of core nozzle inlet temperature. To link the critical pressure to temperature, isentropic efficiency of core nozzle  $\eta_N$  has to be utilized. It has been defined by Çengel and Boles (2005) as

$$\eta_N = \frac{\text{Actual kinetic energy at the nozzle exit}}{\text{Ideal kinetic energy at the nozzle exit}} \quad (4.186)$$

so it can be written as

$$\eta_N = \frac{h_{cr} - h_{08}}{h_{cr,s} - h_{08}} \quad (4.187)$$

where subscript  $s$  represents the isentropic case. Due to calorically perfect gas assumption it can be written as

$$\eta_N = \frac{T_{cr} - T_{08}}{T_{cr,s} - T_{08}} \quad (4.188)$$

Dividing right hand side by  $T_{08}$  and then cancelling yields

$$\eta_N = \frac{\frac{T_{cr}}{T_{08}} - 1}{\frac{T_{cr,s}}{T_{08}} - 1} \quad (4.189)$$

Into the numerator of equation (4.189), equation (4.185) can be substituted. Then it becomes

$$\eta_N = \frac{1 - \frac{k-1}{k+1} - 1}{\frac{T_{cr,s}}{T_{08}} - 1} \quad (4.190)$$

Also, utilizing isentropic temperature-pressure relation it can written that

$$\frac{T_{cr,s}}{T_{08}} = \left(\frac{P_{cr}}{P_{08}}\right)^{\frac{k-1}{k}} \quad (4.191)$$

Substituting equation (4.191) into equation (4.190) yields

$$\eta_N = \frac{-\frac{k-1}{k+1}}{\left(\frac{P_{cr}}{P_{08}}\right)^{\frac{k-1}{k}} - 1} \quad (4.192)$$

Rearranging to solve for  $P_{cr}$

$$\eta_N \left[ \left(\frac{P_{cr}}{P_{08}}\right)^{\frac{k-1}{k}} - 1 \right] = -\frac{k-1}{k+1} \quad (4.193)$$

and

$$\left(\frac{P_{cr}}{P_{08}}\right)^{\frac{k-1}{k}} = 1 - \frac{1}{\eta_N} \left(\frac{k-1}{k+1}\right) \quad (4.194)$$

then

$$P_{cr} = P_{08} \left[ 1 - \frac{1}{\eta_N} \left( \frac{k-1}{k+1} \right) \right]^{\frac{k}{k-1}} \quad (4.195)$$

So, critical pressure has been calculated. If the critical pressure is above or equal to the ambient pressure, where  $P_{cr} \geq P_1$ , then the flow is choked. Mach number is equal to unity that is  $M = 1$  and  $v^2 = kRT$  is valid. In this case, exit pressure  $P_{09}$  is equal to critical pressure that is  $P_{09} = P_{cr}$ . Then using equation (4.184) and velocity definition it becomes

$$T_{09} = T_{08} \frac{2}{k+1} \quad (4.196)$$

and

$$v_9 = \sqrt{kRT_9} \quad (4.197)$$

If the critical pressure is less than the ambient pressure, which is  $P_{cr} < P_1$ , then flow is said to be unchoked. Pressure at the exit is assumed to be equal to ambient pressure that is  $P_{09} = P_1$ . Temperature at the nozzle exit can be calculated in this case as follows. By using equation (4.186)

$$\eta_N = \frac{h_{08} - h_9}{h_{08} - h_{9s}} \quad (4.198)$$

then

$$\eta_N = \frac{T_{08} - T_9}{T_{08} - T_{9s}} \quad (4.199)$$

and it becomes

$$\eta_N = \frac{1 - \frac{T_9}{T_{08}}}{1 - \frac{T_{9s}}{T_{08}}} \quad (4.200)$$

Utilizing the isentropic relation in equation (4.191) and substituting it into equation (4.200) yields

$$\eta_N = \frac{1 - \frac{T_9}{T_{08}}}{1 - \left(\frac{P_9}{P_{08}}\right)^{\left(\frac{k-1}{k}\right)}} \quad (4.201)$$

then

$$1 - \frac{T_9}{T_{08}} = \eta_N \left( 1 - \left(\frac{P_9}{P_{08}}\right)^{\left(\frac{k-1}{k}\right)} \right) \quad (4.202)$$

or

$$\frac{T_9}{T_{08}} = 1 - \eta_N \left( 1 - \left(\frac{P_9}{P_{08}}\right)^{\left(\frac{k-1}{k}\right)} \right) \quad (4.203)$$

and finally

$$T_9 = T_{08} \left[ 1 - \eta_N \left( 1 - \left(\frac{P_9}{P_{08}}\right)^{\left(\frac{k-1}{k}\right)} \right) \right] \quad (4.204)$$

and velocity can be found by

$$h_9 + \frac{v_9^2}{2} = h_{08} \quad (4.205)$$

calorically perfect gas assumption yields

$$T_9 + \frac{v_9^2}{2c_p} = T_{08} \quad (4.206)$$

and rearranging yields

$$v_9^2 = (T_{08} - T_9)2c_p \quad (4.207)$$

then

$$v_9 = \sqrt{2c_p(T_{08} - T_9)} \quad (4.208)$$

or

$$v_9 = \sqrt{2c_p T_{08} \left(1 - \frac{T_9}{T_{08}}\right)} \quad (4.209)$$

Substituting equation (4.203) into equation (4.209) finally yields

$$v_9 = \sqrt{2c_p \eta_N T_{08} \left[1 - \left(\frac{P_9}{P_{08}}\right)^{(k-1)/k}\right]} \quad (4.210)$$

So, for both of the scenarios temperatures, pressures and velocities have been calculated by utilizing critical pressure.

#### 4.4.8.8 Fan nozzle

As mentioned earlier, after passing the fan component, some of the air proceeds directly to fan nozzle without passing through compressor, combustion chamber, turbine and core nozzle sequence. Fan nozzle process is an expansion process where air is accelerated in order to contribute to thrust. State 3 is the inlet state of air and 10F is the real exit state where both heat leakage from CC to bypass air (i.e. heat leakage one) and heat leakage from bypass air to ambient air (i.e. heat leakage two) occurs. Moreover, imaginary state 10F' represents the adiabatic case and imaginary 10F'' represents the exit state when there is only heat leakage one. Schematic illustration of fan nozzle has been illustrated in Figure 4.9.

As done for core nozzle and shown in equation (4.195), critical pressure for fan nozzle can be written considering the inlet state is 3 as follows.

$$P_{cr} = P_{03} \left[1 - \frac{1}{\eta_{FN}} \left(\frac{k-1}{k+1}\right)\right]^{\frac{k}{k-1}} \quad (4.211)$$

As mentioned above for core nozzle, if the critical pressure is greater or equal to the ambient pressure at the fan nozzle exit (i.e.  $P_{cr} \geq P_1$ ) then the flow is said to be choked. In this case, exit pressure is assigned to critical pressure. So, it can be written that

$$P_{10F'} = P_{10F''} = P_{10F} = P_{cr} \quad (4.212)$$

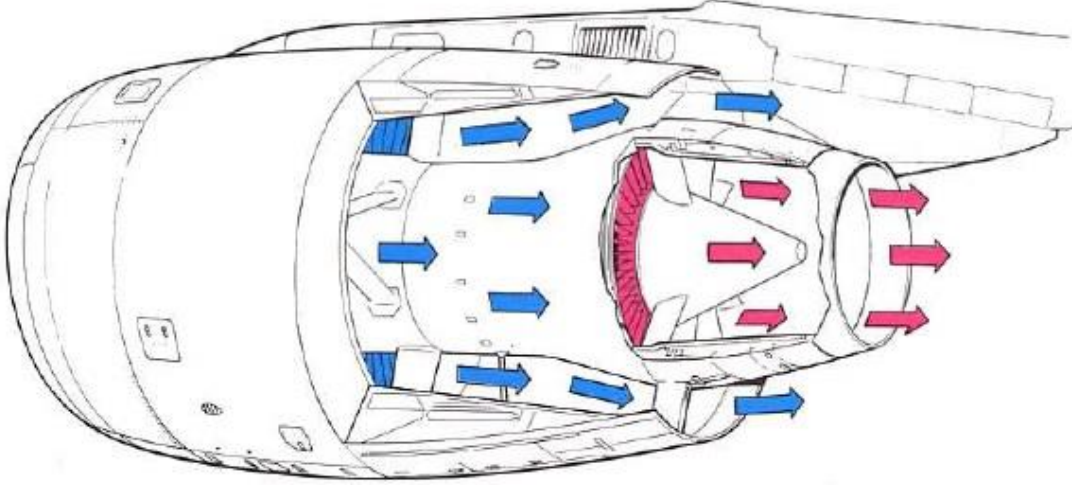


**Figure 4.9** : A nozzle or exhaust (outer blue arrows show fan nozzle) (Rolls Royce, 1996).

Since at the critical conditions Mach number is equal to unity and equation (4.192) is also valid. Therefore it yields the following.

$$v_{10F'} = \sqrt{kRT_{10F'}} \quad (4.213)$$

$$v_{10F''} = \sqrt{kRT_{10F''}} \quad (4.214)$$

$$v_{10F} = \sqrt{kRT_{10F}} \quad (4.215)$$

When it comes to determination of temperatures, firstly  $T_{10F'}$  has been calculated by utilizing equation (4.196) since it is the adiabatic case. Then, the case that includes heat leakage from CC to bypass air,  $T_{10F''}$ , has been calculated by utilizing  $T_{10F'}$ . After,  $T_{10F}$  has been reached which is the case that includes both heat leakage one and heat leakage two. By utilizing equation (4.196)

$$T_{10F'} = \frac{2}{k+1} T_{03} \quad (4.216)$$

In order to find an expression for  $T_{10F''}$ , equations (4.13) and (4.18) have been equated, so it yields

$$\begin{aligned} & (\dot{m}_c - \dot{m}_b - \dot{m}_{cool1} - \dot{m}_{cool2} + \dot{m}_f)c_p(T_{06'} - T_{06''}) \\ & = \dot{m}_F c_p(T_{10F''} - T_{10F'}) + \dot{m}_F \left( \frac{v_{10F''}^2 - v_{10F'}^2}{2} \right) \end{aligned} \quad (4.217)$$

Dividing both sides by  $c_p \dot{m}_F$  it becomes

$$\begin{aligned} & \frac{(\dot{m}_c - \dot{m}_b - \dot{m}_{cool1} - \dot{m}_{cool2} + \dot{m}_f)(T_{06'} - T_{06''})}{\dot{m}_F} \\ &= (T_{10F''} - T_{10F'}) + \frac{v_{10F''}^2 - v_{10F'}^2}{2c_p} \end{aligned} \quad (4.218)$$

Then, by utilizing equation (4.5), mass flow rate of fuel can be rewritten and equation (4.218) becomes

$$\begin{aligned} & \frac{(\dot{m}_c - \dot{m}_b - \dot{m}_{cool1} - \dot{m}_{cool2})(1 + \alpha)(T_{06'} - T_{06''})}{\dot{m}_F} \\ &= (T_{10F''} - T_{10F'}) + \frac{v_{10F''}^2 - v_{10F'}^2}{2c_p} \end{aligned} \quad (4.219)$$

Then dividing left hand side of the equation (4.219) by  $\dot{m}_c$  and utilizing mass flow ratio equations (4.2), (4.3), (4.4) and lastly (4.1) yields

$$\begin{aligned} & \frac{(1 - \gamma - \theta_1 - \theta_2)(1 + \alpha)(T_{06'} - T_{06''})}{\beta} \\ &= (T_{10F''} - T_{10F'}) + \frac{v_{10F''}^2 - v_{10F'}^2}{2c_p} \end{aligned} \quad (4.220)$$

Then, substituting equations (4.216), (4.214) and (4.213) into equation (4.220) yields

$$\begin{aligned} & \frac{(1 - \gamma - \theta_1 - \theta_2)(1 + \alpha)(T_{06'} - T_{06''})}{\beta} \\ &= T_{10F''} - \frac{2}{k+1} T_{03} + \frac{kRT_{10F''} - kR \frac{2}{k+1} T_{03}}{2c_p} \end{aligned} \quad (4.221)$$

or

$$\begin{aligned} & \frac{(1 - \gamma - \theta_1 - \theta_2)(1 + \alpha)(T_{06'} - T_{06''})}{\beta} \\ &= T_{10F''} - \frac{2}{k+1} T_{03} + \frac{kR(T_{10F''} - \frac{2}{k+1} T_{03})}{2c_p} \end{aligned} \quad (4.222)$$

By utilizing equation (4.97) and substituting it into equation (4.222) yields

$$\begin{aligned} & \frac{(1 - \gamma - \theta_1 - \theta_2)(1 + \alpha)(T_{06'} - T_{06''})}{\beta} \\ &= T_{10F''} - \frac{2}{k+1}T_{03} + \frac{(k-1)(T_{10F''} - \frac{2}{k+1}T_{03})}{2} \end{aligned} \quad (4.223)$$

Then regrouping right hand side yields

$$\begin{aligned} & \frac{(1 - \gamma - \theta_1 - \theta_2)(1 + \alpha)(T_{06'} - T_{06''})}{\beta} \\ &= \left(1 + \frac{k-1}{2}\right)T_{10F''} - \frac{2}{k+1}T_{03} - \frac{k-1}{2} \frac{2}{k+1}T_{03} \end{aligned} \quad (4.224)$$

Rearranging the terms with  $T_{03}$  yield

$$\frac{(1 - \gamma - \theta_1 - \theta_2)(1 + \alpha)(T_{06'} - T_{06''})}{\beta} = \left(\frac{k+1}{2}\right)T_{10F''} - T_{03} \quad (4.225)$$

Then final form yields

$$T_{10F''} = \frac{2}{k+1} \left( \frac{(1 - \gamma - \theta_1 - \theta_2)(1 + \alpha)(T_{06'} - T_{06''})}{\beta} + T_{03} \right) \quad (4.226)$$

Then, in order to find  $T_{10F}$  by using  $T_{10F''}$ , heat leakage ratio two,  $\varepsilon_{LK2}$  has been utilized. Substituting equations (4.91), (4.214) and (4.215) into (4.32) yields

$$\varepsilon_{LK2} = \frac{c_p(T_{10F''} - T_{10F}) + \frac{kRT_{10F''} - kRT_{10F}}{2}}{c_p(T_{10F''} - T_1) + \frac{kRT_{10F''} - M_1^2 kRT_1}{2}} \quad (4.227)$$

Rearranging yields

$$\varepsilon_{LK2} = \frac{\left(\frac{c_p + kR}{2}\right)(T_{10F''} - T_{10F})}{\left(\frac{c_p + kR}{2}\right)(T_{10F''} - M_1^2 T_1)} \quad (4.228)$$

Eliminating equal terms in the numerator and denominator yields

$$\varepsilon_{LK2} = \frac{(T_{10F''} - T_{10F})}{(T_{10F''} - M_1^2 T_1)} \quad (4.229)$$



or equation (4.229) can be rewritten as

$$\varepsilon_{LK2}(T_{10F''} - M_1^2 T_1) = T_{10F''} - T_{10F} \quad (4.230)$$

Then,

$$\varepsilon_{LK2} T_{10F''} - T_{10F''} = \varepsilon_{LK2} M_1^2 T_1 - T_{10F} \quad (4.231)$$

and finally

$$T_{10F} = (1 - \varepsilon_{LK2}) T_{10F''} + \varepsilon_{LK2} M_1^2 T_1 \quad (4.232)$$

Hence, all thermodynamic states have been determined and all required properties have been calculated for the thermodynamic cycle analysis.

#### 4.4.9 Coefficient of ecological performance, entropy generation rate and exergy destruction factor

As defined and expressed in equations (3.20) and (3.21) under Chapter 3, *CEP* is a measure that provides insight on how much power has been utilized from the engine for each unit of exergy destroyed. In this thesis, it has been assumed that engine does not only provide propulsive power but also provides auxiliary power to aircraft. Therefore, auxiliary power provided by the engine has also been added to the definition of *CEP* and it has been updated for this thesis as

$$CEP = \frac{\text{Propulsive power} + \text{Auxiliary power}}{\text{Exergy destruction rate}} \quad (4.233)$$

And in mathematical form,

$$CEP = \frac{\dot{W}_P + \dot{W}_{aux}}{\dot{E}x_{dest}} \quad (4.234)$$

where  $\dot{W}_P$  has been given in equation (4.71),  $\dot{W}_{aux}$  is a constant power level for an ordinary commercial aircraft and  $\dot{E}x_{dest}$  is

$$\dot{E}x_{dest} = T_1 \dot{S}_{gen} \quad (4.235)$$

It is clear that  $\dot{S}_{gen}$  has to be calculated first in order to reach  $\dot{E}x_{dest}$ .

Entropy generation rate can be determined by writing the entropy balance equation for the turbofan engine considering it as a control volume. Equation (2.21) has been utilized for determination of entropy generation rate since it includes inlet flows, exit flows and heat transfer terms which represent the steady-flow turbofan engine.

Inlet flows that have been considered are core flow and bypass flow at state 1. Moreover, fuel has also been considered as an inlet flow. It has been assumed that properties of the fuel are the same as air due to small fuel to air ratio and for simplification. Therefore, entropy property of the fuel has been assumed to be the average of states 5 and 6'' for simplification.

Exit flows that have been considered are air at the core flow exit, air at the fan nozzle exit and bleed air. Exit states of fan nozzle, core nozzle and bleed air are state 10F, state 9 and state 4 respectively.

Heat transfer terms that have been considered are heat transfer in CC and in fan nozzle. Increase in the flow energy of the core air during combustion process has been considered as the heat transferred to the engine, and heat lost to the surrounding from the fan nozzle is considered as the heat transferred from the engine. Hence, components of equation (2.21) can be written in the following form.

$$\sum \dot{m}_e s_e = [\dot{m}_F s_{10F} + (\dot{m}_c - \dot{m}_b + \dot{m}_f) s_9 + \dot{m}_b s_{04}] \quad (4.236)$$

where  $s_{10F}$  is the entropy of the bypass air at the fan nozzle exit,  $s_9$  is the entropy of the core air at the core nozzle exit and  $s_{04}$  is the entropy of the bleed air.

$$\sum \dot{m}_i s_i = \left[ (\dot{m}_F + \dot{m}_c) s_1 + \dot{m}_f \frac{(s_{05} + s_{06''})}{2} \right] \quad (4.237)$$

where  $s_1$  is the entropy of the air at the engine inlet,  $s_{05}$  and  $s_{06''}$  are the entropy values at the CC inlet and outlet. Entropy term due to heat transfer for the CC can be written as

$$\sum_1 \frac{\dot{Q}_k}{T_k} = \frac{(\dot{m}_c - \dot{m}_b - \dot{m}_{cool1} - \dot{m}_{cool2} + \dot{m}_f) c_p T_{06'}}{T_{06'}} - \frac{(\dot{m}_c - \dot{m}_b - \dot{m}_{cool1} - \dot{m}_{cool2}) c_p T_{05}}{T_{06'}} \quad (4.238)$$

and, entropy term due to heat transfer from fan nozzle can be written as

$$\sum_2 \frac{\dot{Q}_k}{T_k} = - \frac{\dot{m}_F \left[ c_p (T_{10F''} - T_{10F}) + \frac{v_{10F''}^2 - v_{10F}^2}{2} \right]}{T_1} \quad (4.239)$$

Therefore, combining all the terms above yields

$$\begin{aligned} \dot{S}_{gen} = & \left[ \dot{m}_F s_{10F} + (\dot{m}_c - \dot{m}_b + \dot{m}_f) s_9 + \dot{m}_b s_{04} \right] \\ & - \left[ (\dot{m}_F + \dot{m}_c) s_1 + \dot{m}_f \frac{(s_{05} + s_{06''})}{2} \right] \\ & - \frac{(\dot{m}_c - \dot{m}_b - \dot{m}_{cool1} - \dot{m}_{cool2} + \dot{m}_f) c_p T_{06'}}{T_{06}'} \\ & - \frac{(\dot{m}_c - \dot{m}_b - \dot{m}_{cool1} - \dot{m}_{cool2}) c_p T_{05}}{T_{06}'} \\ & + \frac{\dot{m}_F \left[ c_p (T_{10F''} - T_{10F}) + \frac{v_{10F''}^2 - v_{10F}^2}{2} \right]}{T_1} \end{aligned} \quad (4.240)$$

In order to solve equation (4.240), entropy terms have been coupled with respect to their mass flow rates. Entropy change formulation of an ideal gas has been utilized to solve these couples as shown in equation (2.18). All couples have been shown and written explicitly as

$$\dot{m}_F s_{10F} - \dot{m}_F s_1 = \dot{m}_F \left( c_p \ln \frac{T_{10F}}{T_1} - R \ln \frac{P_{10F}}{P_1} \right) \quad (4.241a)$$

$$\dot{m}_c s_9 - \dot{m}_c s_1 = \dot{m}_c \left( c_p \ln \frac{T_9}{T_1} - R \ln \frac{P_9}{P_1} \right) \quad (4.241b)$$

$$\dot{m}_b s_{04} - \dot{m}_b s_9 = \dot{m}_b \left( c_p \ln \frac{T_{04}}{T_9} - R \ln \frac{P_{04}}{P_9} \right) \quad (4.241c)$$

$$\frac{\dot{m}_f}{2} s_9 - \frac{\dot{m}_f}{2} s_{05} = \frac{\dot{m}_f}{2} \left( c_p \ln \frac{T_9}{T_{05}} - R \ln \frac{P_9}{P_{05}} \right) \quad (4.241d)$$

$$\frac{\dot{m}_f}{2} s_9 - \frac{\dot{m}_f}{2} s_{06''} = \frac{\dot{m}_f}{2} \left( c_p \ln \frac{T_9}{T_{06''}} - R \ln \frac{P_9}{P_{06''}} \right) \quad (4.241e)$$

Then, substituting equations (4.241a) through (4.241e) into equation (4.240) yields

$$\begin{aligned}
\dot{S}_{gen} = & \dot{m}_F \left( c_p \ln \frac{T_{10F}}{T_1} - R \ln \frac{P_{10F}}{P_1} \right) + \dot{m}_c \left( c_p \ln \frac{T_9}{T_1} - R \ln \frac{P_9}{P_1} \right) \\
& + \dot{m}_b \left( c_p \ln \frac{T_{04}}{T_9} - R \ln \frac{P_{04}}{P_9} \right) + \frac{\dot{m}_f}{2} \left( c_p \ln \frac{T_9}{T_{05}} - R \ln \frac{P_9}{P_{05}} \right) \\
& + \frac{\dot{m}_f}{2} \left( c_p \ln \frac{T_9}{T_{06''}} - R \ln \frac{P_9}{P_{06''}} \right) \\
& - \frac{(\dot{m}_c - \dot{m}_b - \dot{m}_{cool1} - \dot{m}_{cool2} + \dot{m}_f) c_p T_{06'}}{T_{06'}} \\
& - \frac{(\dot{m}_c - \dot{m}_b - \dot{m}_{cool1} - \dot{m}_{cool2}) c_p T_{05}}{T_{06'}} \\
& + \frac{\dot{m}_F \left[ c_p (T_{10F''} - T_{10F}) + \frac{v_{10F''}^2 - v_{10F}^2}{2} \right]}{T_1}
\end{aligned} \tag{4.242}$$

Then, taking out  $c_p$  terms and utilizing mass flow ratio equations (4.1), (4.2), (4.3), (4.4) and (4.5), equation (4.242) can be written in the following form.

$$\begin{aligned}
\dot{S}_{gen} = & \dot{m}_c c_p \left\{ \beta \left( \ln \frac{T_{10F}}{T_1} - \frac{R}{c_p} \ln \frac{P_{10F}}{P_1} \right) + \left( \ln \frac{T_9}{T_1} - \frac{R}{c_p} \ln \frac{P_9}{P_1} \right) + \gamma \left( \ln \frac{T_{04}}{T_9} - \frac{R}{c_p} \ln \frac{P_{04}}{P_9} \right) \right. \\
& + \frac{\alpha(1 - \gamma - \theta_1 - \theta_2)}{2} \left( \ln \frac{T_9}{T_{06''}} - \frac{R}{c_p} \ln \frac{P_9}{P_{06''}} \right) \\
& + \frac{\alpha(1 - \gamma - \theta_1 - \theta_2)}{2} \left( \ln \frac{T_9}{T_{05}} - \frac{R}{c_p} \ln \frac{P_9}{P_{05}} \right) \\
& - \frac{(1 - \gamma - \theta_1 - \theta_2)[(1 + \alpha)T_{06'} - T_{05}]}{T_{06'}} \\
& \left. + \frac{\beta \left( T_{10F''} - T_{10F} + \frac{v_{10F''}^2 - v_{10F}^2}{2c_p} \right)}{T_1} \right\}
\end{aligned} \tag{4.243}$$

or by using equation (4.97) and utilizing the natural logarithm property to write the equation (4.243) in more compact form yields

$$\begin{aligned}
\dot{S}_{gen} = \dot{m}_c c_p \left\{ \ln \left( \frac{T_{10F}}{T_1} \right)^\beta - \ln \left( \frac{P_{10F}}{P_1} \right)^{\beta \left( \frac{k-1}{k} \right)} + \ln \frac{T_9}{T_1} - \ln \left( \frac{P_9}{P_1} \right)^{\frac{k-1}{k}} + \ln \left( \frac{T_{04}}{T_9} \right)^\gamma \right. \\
- \ln \left( \frac{P_{04}}{P_9} \right)^{\gamma \left( \frac{k-1}{k} \right)} + \ln \left( \frac{T_9}{T_{06''}} \right)^{\frac{\alpha(1-\gamma-\theta_1-\theta_2)}{2}} \\
- \ln \left( \frac{P_9}{P_{06''}} \right)^{\left( \frac{k-1}{k} \right) \frac{\alpha(1-\gamma-\theta_1-\theta_2)}{2}} + \ln \left( \frac{T_9}{T_{05}} \right)^{\frac{\alpha(1-\gamma-\theta_1-\theta_2)}{2}} \\
- \ln \left( \frac{P_9}{P_{05}} \right)^{\left( \frac{k-1}{k} \right) \frac{\alpha(1-\gamma-\theta_1-\theta_2)}{2}} \\
- \frac{(1-\gamma-\theta_1-\theta_2)[(1+\alpha)T_{06'} - T_{05}]}{T_{06'}} \\
\left. + \frac{\beta \left( T_{10F''} - T_{10F} + \frac{v_{10F''}^2 - v_{10F}^2}{2c_p} \right)}{T_1} \right\} \quad (4.244)
\end{aligned}$$

or it can be written in the common natural logarithm base as

$$\begin{aligned}
\dot{S}_{gen} \\
= \dot{m}_c c_p \left\{ \ln \frac{\left( \frac{T_{10F}}{T_1} \right)^\beta \frac{T_9}{T_1} \left( \frac{T_{04}}{T_9} \right)^\gamma \left( \frac{T_9}{T_{06''}} \right)^{\frac{\alpha(1-\gamma-\theta_1-\theta_2)}{2}} \left( \frac{T_9}{T_{05}} \right)^{\frac{\alpha(1-\gamma-\theta_1-\theta_2)}{2}}}{\left( \frac{P_{10F}}{P_1} \right)^{\beta \left( \frac{k-1}{k} \right)} \left( \frac{P_9}{P_1} \right)^{\frac{k-1}{k}} \left( \frac{P_{04}}{P_9} \right)^{\gamma \left( \frac{k-1}{k} \right)} \left( \frac{P_9}{P_{06''}} \right)^{\left( \frac{k-1}{k} \right) \frac{\alpha(1-\gamma-\theta_1-\theta_2)}{2}} \left( \frac{P_9}{P_{05}} \right)^{\left( \frac{k-1}{k} \right) \frac{\alpha(1-\gamma-\theta_1-\theta_2)}{2}}} \right. \\
\left. - \frac{(1-\gamma-\theta_1-\theta_2)[(1+\alpha)T_{06'} - T_{05}]}{T_{06'}} + \frac{\beta \left( T_{10F''} - T_{10F} + \frac{v_{10F''}^2 - v_{10F}^2}{2c_p} \right)}{T_1} \right\} \quad (4.245)
\end{aligned}$$

Finally it becomes

$$\begin{aligned}
\dot{S}_{gen} = \dot{m}_c c_p \left\{ \ln \left[ \left( \frac{T_{10F}}{T_1} \right)^\beta \frac{T_9}{T_1} \left( \frac{T_{04}}{T_9} \right)^\gamma \left( \frac{T_9}{T_{06''}} \right)^{\frac{\alpha(1-\gamma-\theta_1-\theta_2)}{2}} \left( \frac{T_9}{T_{05}} \right)^{\frac{\alpha(1-\gamma-\theta_1-\theta_2)}{2}} \left( \frac{P_1}{P_{10F}} \right)^{\beta \left( \frac{k-1}{k} \right)} \right. \right. \\
\left. \left. \left( \frac{P_1}{P_9} \right)^{\frac{k-1}{k}} \left( \frac{P_9}{P_{04}} \right)^{\gamma \left( \frac{k-1}{k} \right)} \left( \frac{P_{06''}}{P_9} \right)^{\left( \frac{k-1}{k} \right) \frac{\alpha(1-\gamma-\theta_1-\theta_2)}{2}} \left( \frac{P_{05}}{P_9} \right)^{\left( \frac{k-1}{k} \right) \frac{\alpha(1-\gamma-\theta_1-\theta_2)}{2}} \right] \right. \\
- \frac{(1-\gamma-\theta_1-\theta_2)[(1+\alpha)T_{06'} - T_{05}]}{T_{06'}} \\
\left. + \frac{\beta \left( T_{10F''} - T_{10F} + \frac{v_{10F''}^2 - v_{10F}^2}{2c_p} \right)}{T_1} \right\} \quad (4.246)
\end{aligned}$$

Then, by utilizing equations (4.235) and (4.234), exergy destruction rate and coefficient of ecological performance become as follows respectively.

$$\dot{E}x_{dest} = \left\{ T_1 \dot{m}_c c_p \left\{ \ln \left[ \left( \frac{T_{10F}}{T_1} \right)^\beta \frac{T_9}{T_1} \left( \frac{T_{04}}{T_9} \right)^\gamma \left( \frac{T_9}{T_{06''}} \right)^{\frac{\alpha(1-\gamma-\theta_1-\theta_2)}{2}} \left( \frac{T_9}{T_{05}} \right)^{\frac{\alpha(1-\gamma-\theta_1-\theta_2)}{2}} \left( \frac{P_1}{P_{10F}} \right)^\beta \left( \frac{P_1}{P_9} \right)^{\frac{k-1}{k}} \left( \frac{P_9}{P_{04}} \right)^\gamma \left( \frac{P_{06''}}{P_9} \right)^{\frac{(k-1)\alpha(1-\gamma-\theta_1-\theta_2)}{2}} \left( \frac{P_{05}}{P_9} \right)^{\frac{(k-1)\alpha(1-\gamma-\theta_1-\theta_2)}{2}} \right] \right. \right. \\ \left. \left. - \frac{(1-\gamma-\theta_1-\theta_2)[(1+\alpha)T_{06'} - T_{05}]}{T_{06'}} \right. \right. \\ \left. \left. + \frac{\beta \left( T_{10F''} - T_{10F} + \frac{v_{10F''}^2 - v_{10F}^2}{2c_p} \right)}{T_1} \right\} \right\} \quad (4.247)$$

and

$$CEP \\ = \{v_1[(\dot{m}_c - \dot{m}_b + \dot{m}_f)v_9 - \dot{m}_c v_1 + \dot{m}_f(v_{10F} - v_1) + A_9(P_9 - P_1) + A_{10F}(P_{10F} - P_1)] \\ + \dot{W}_{aux}\} \\ / \left\{ T_1 \dot{m}_c c_p \left\{ \ln \left[ \left( \frac{T_{10F}}{T_1} \right)^\beta \frac{T_9}{T_1} \left( \frac{T_{04}}{T_9} \right)^\gamma \left( \frac{T_9}{T_{06''}} \right)^{\frac{\alpha(1-\gamma-\theta_1-\theta_2)}{2}} \left( \frac{T_9}{T_{05}} \right)^{\frac{\alpha(1-\gamma-\theta_1-\theta_2)}{2}} \left( \frac{P_1}{P_{10F}} \right)^\beta \left( \frac{P_1}{P_9} \right)^{\frac{k-1}{k}} \left( \frac{P_9}{P_{04}} \right)^\gamma \left( \frac{P_{06''}}{P_9} \right)^{\frac{(k-1)\alpha(1-\gamma-\theta_1-\theta_2)}{2}} \left( \frac{P_{05}}{P_9} \right)^{\frac{(k-1)\alpha(1-\gamma-\theta_1-\theta_2)}{2}} \right] \right. \right. \\ \left. \left. - \frac{(1-\gamma-\theta_1-\theta_2)[(1+\alpha)T_{06'} - T_{05}]}{T_{06'}} + \frac{\beta(T_{10F''} - T_{10F})}{T_1} \right\} \right\} \quad (4.248)$$

When it comes to calculate exergy destruction factor, equation (3.22) has been utilized. As indicated at the beginning of Chapter 4, in assumptions part, potential exergy of air and fuel has been eliminated since there is no elevation difference. Physical exergy of incoming air is considered as zero, and physical exergy of fuel has been assumed as zero because of very small figures considering other terms. Therefore, total exergy input rate is composed of two components; namely, total chemical exergy rate of fuel,  $\dot{E}x_{chem,f}$ , and total kinetic exergy rate of air,  $\dot{E}x_1$ . It has been written as

$$f_{exd} = \frac{\dot{E}x_{dest}}{\dot{E}x_{in}} = \frac{T_1 \dot{S}_{gen}}{\dot{E}x_{chem,f} + \dot{E}x_1} \quad (4.249)$$

where  $\dot{E}x_{dest}$  is total exergy destruction rate as calculated in equation (4.247) and  $\dot{E}x_{in}$  is total exergy input rate. Total chemical exergy rate of fuel has been written as

$$\dot{E}x_{chem,f} = \dot{m}_f ex_{chem,f} \quad (4.250)$$

where  $ex_{chem,f}$  is the specific chemical exergy of the fuel (kerosene). It has been assumed to be 45.8 MJ per kg as utilized by Turgut et al. (2007). Also, total kinetic exergy rate of air has been defined as

$$\begin{aligned}
 & \textit{Total kinetic exergy destruction rate} \\
 & = \textit{Total mass flow rate of incoming air} \\
 & \quad * \frac{(\textit{Velocity of incoming air})^2}{2}
 \end{aligned} \tag{4.251}$$

Then by using Table 4.1, it has been written as

$$\dot{E}x_1 = (\dot{m}_c + \dot{m}_F) \frac{v_1^2}{2} \tag{4.252}$$

or it can be rewritten by using equation (4.1) as

$$\dot{E}x_1 = \dot{m}_c (1 + \beta) \frac{v_1^2}{2} \tag{4.253}$$

Finally, substituting equations (4.250) and (4.253) into equation (4.249), exergy destruction factor becomes

$$f_{exd} = \frac{T_1 \dot{S}_{gen}}{\dot{m}_f ex_{chem,f} + \dot{m}_c (1 + \beta) \frac{v_1^2}{2}} \tag{4.254}$$





## 5. RESULTS AND DISCUSSIONS

In Chapter 4, a twin-spool turbofan engine configuration has been selected and all stations (thermodynamic states) have been determined. All parameters and assumptions have been stated in order to perform a thermodynamic cycle analysis. Inlet and exit conditions of all components have been expressed in terms of known parameters, and all performance indicators have been expressed in terms of these parameters.

In this thesis, main purpose is to investigate the effects of heat leakage on the performance of a twin-spool turbofan engine during the cruise phase of a commercial aircraft. To do this, some reference points of design parameters had to be determined and effect of change in design parameters on performance indicators had to be observed first so that it constructs a base to perform heat leakage analyzes.

Therefore, this chapter starts with the investigation of optimum values of design parameters and corresponding optimal values of performance indicators. This investigation has been performed with the help of 3-D figures which shows relative change of one performance indicator with respect to two independent design parameters each time, while other two design parameters are constant.

After observing optimum levels of design parameters, the analyzes have been narrowed down to 2-D figures, which are actually cross-sections of the above mentioned 3-D figures. In these 2-D figures, one more design parameter has been kept constant and relative change of performance indicators have been observed with respect to remaining single variable design parameter. In this setting, there has been a chance to investigate the effect of heat leakage on the performance indicators, with only one variable design parameter.

Considered performance indicators in these analyzes have been the coefficient of ecological performance  $CEP$ , as indicated in equation (4.248), the overall efficiency  $\eta_o$ , as indicated in equation (4.77), the exergy destruction factor  $f_{exd}$ , as indicated in equation (4.254), the thrust specific fuel consumption  $TSFC$ , as indicated in equation

(4.73), the specific thrust  $F_s$ , as indicated in equation (4.75), and the entropy generation rate  $\dot{S}_{gen}$ , as indicated in equation (4.246) as determined earlier. Design parameters that have been mentioned earlier are the total compressor pressure ratio  $r_{C,Total}$ , as indicated in equation (4.144), the fan pressure ratio  $r_F$ , as indicated in equation (4.116), the bypass air ratio  $\beta$ , as indicated in equation (4.1) and maximum turbine inlet temperature  $T_{max}$  as  $T_{06'}$ .

The effects of heat leakage ratio one  $\varepsilon_{LK1}$ , and heat leakage ratio two  $\varepsilon_{LK2}$ , at three different values, which are 0.00, 0.02 and 0.04, have been investigated on each of six performance indicators by using above mentioned 2-D cross-sections of 3-D analyzes.

## 5.1 Optimal Values of Coupled Design Parameters with 3-D Figures

As mentioned above, design parameters namely  $r_{C,Total}$ ,  $r_F$ ,  $\beta$  and  $T_{max}$  have been coupled and relative variation with respect to performance indicators have been observed.  $r_{C,Total} - \beta$  couple has been selected as the sample couple to illustrate relative variation with all six performance indicators and 3-D figures. These two design parameters have been selected since they represent the characteristics of the twin-spool turbofan engine. For other couples, relative variations of  $CEP$  and  $\eta_o$  have been selected to be illustrated since  $CEP$  represents performance of the engine in terms of ecological concerns by using the second law of thermodynamics (via entropy), while  $\eta_o$  represents the performance of the engine in the first law of thermodynamics point of view (via energy).

### 5.1.1 Determination of optimum values of performance indicators with respect to $r_{C,Total}$ and $\beta$

As mentioned above,  $r_{C,Total} - \beta$  couple has been selected as sample to show relation variation with all six performance indicators in 3-D figures, and it can be seen in Figure 5.1.

In Figure 5.1 (a),  $CEP$  has been calculated by utilizing equation (4.248). It has been seen in Figure 5.1 (a) that  $CEP$  is higher at small  $\beta$  values together with moderate  $r_{C,Total}$  values. For lower  $\beta$  values,  $CEP$  increases very fast with increasing  $r_{C,Total}$

until its maxima, then start to decrease dramatically. At small values of  $r_{C,Total}$ ,  $CEP$  is very low independent of  $\beta$  value. At small values of  $\beta$ ,  $CEP$  reaches higher values and increasing effect of  $r_{C,Total}$  lasts longer, and further increase in  $r_{C,Total}$  does not decrease  $CEP$  as it does at large  $\beta$  values. Maximum  $CEP$  is reached as  $\sim 1.5885$  at  $r_{C,Total} \sim 20.63$  and  $\beta = 1$ .

In Figure 5.1 (b),  $\eta_o$  has been calculated by utilizing equation (4.77). In Figure 5.1 (b) it has been observed that small  $\beta$  values gives lower  $\eta_o$  values. Also, as  $r_{C,Total}$  increases,  $\eta_o$  increases for lower  $\beta$  values. However, at large  $\beta$  values,  $\eta_o$  starts to sharply decrease after some optimum level of  $r_{C,Total}$ , and it goes beyond feasible level. Maxima levels of  $\eta_o$  is reached at moderate levels of  $\beta$  with high levels of  $r_{C,Total}$ ; and high levels of  $\beta$  with moderate levels of  $r_{C,Total}$ . At  $r_{C,Total} \sim 26.1$  and  $\beta \sim 4.8$  maximum level of  $\eta_o$  is reached as  $\sim 0.3132$ .

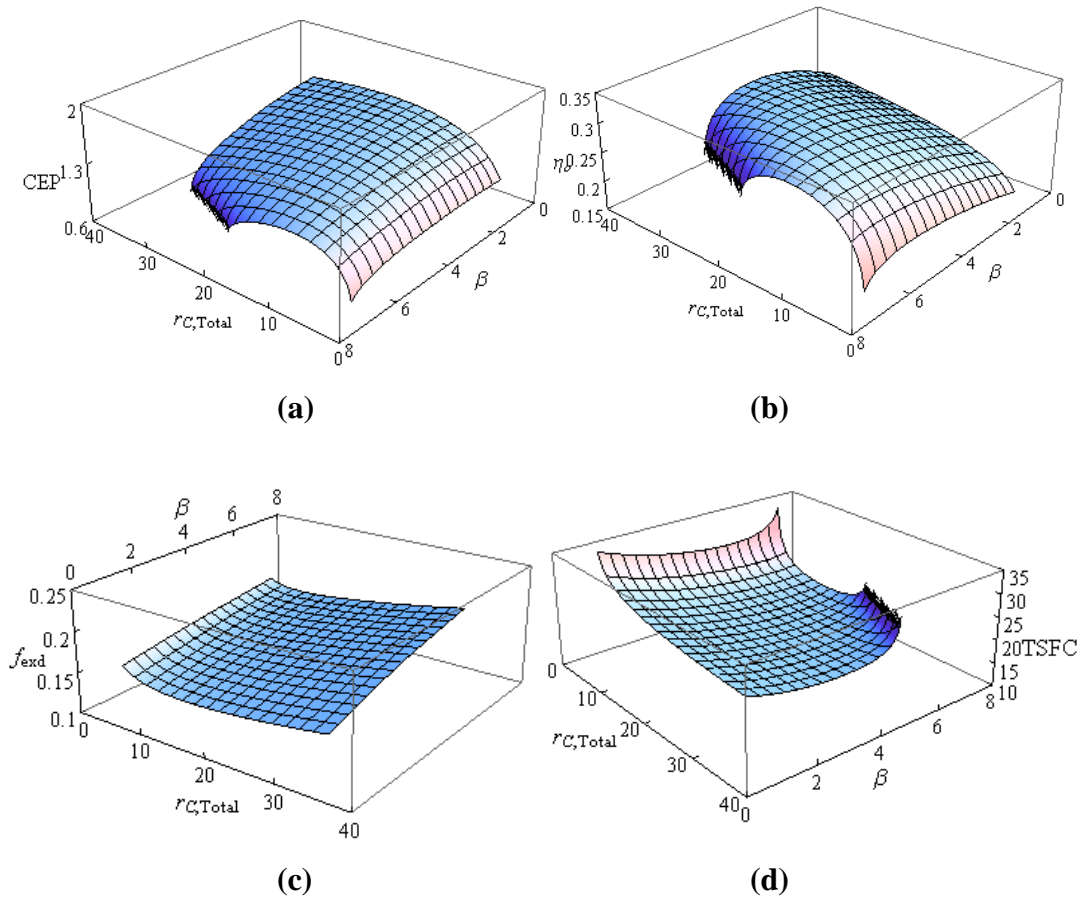


**Figure 5.1 :** Relative change of performance indicators with respect to  $r_{C,Total}$  and  $\beta$  simultaneously.

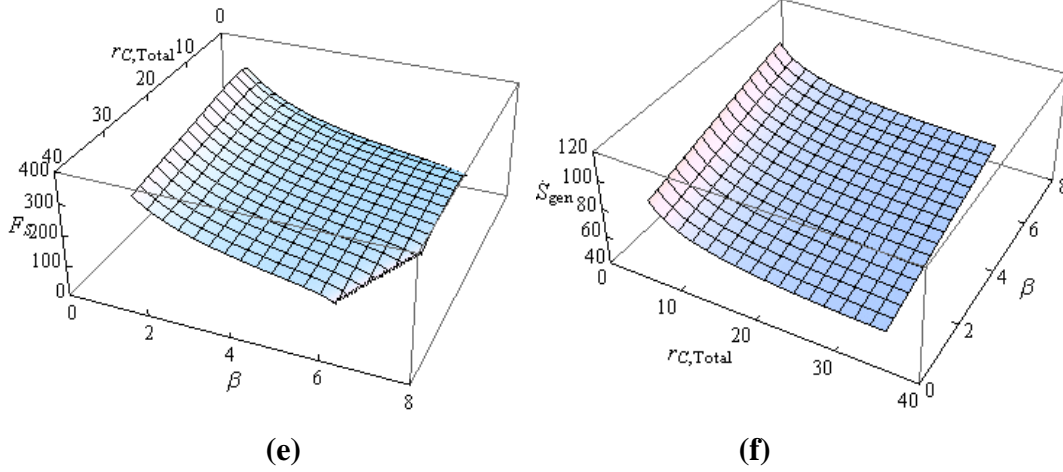


**Figure 5.1 (continued):** Relative change of performance indicators with respect to  $r_{C,Total}$  and  $\beta$  simultaneously.

In Figure 5.1 (c),  $f_{exd}$  has been calculated by utilizing equation (4.254). Figure 5.1 (c) shows that  $f_{exd}$  is at minima levels when  $\beta$  is at minimum (1). As  $\beta$  grows,  $f_{exd}$  increases independent from  $r_{C,Total}$  value. At  $\beta = 1$ , minima  $f_{exd}$  values are observed at small to medium levels of  $r_{C,Total}$ . At very small  $r_{C,Total}$  values,  $f_{exd}$  is still too high, which is not desired. Minimum  $f_{exd}$  value reached is  $\sim 0.13$  at  $r_{C,Total} \sim 12.3$  and  $\beta = 1$ .

In Figure 5.1 (d),  $TSFC$  has been calculated by utilizing equation (4.73). It has been observed in Figure 5.1 (d) that small values of  $r_{C,Total}$  gives worse  $TSFC$  values, since they are too high. Small  $TSFC$  values are observed at larger  $r_{C,Total}$  values with medium-high  $\beta$  values. As seen, at very high  $\beta$  and very high  $r_{C,Total}$  values,  $TSFC$  values goes to infeasible region. However, increasing  $\beta$  with increasing  $r_{C,Total}$  values generally gives small  $TSFC$  values, which is desired, until some optimum levels of  $r_{C,Total}$ . Beyond that optimum level of  $r_{C,Total}$ ,  $TSFC$  starts to an increasing trend. Minimum level of  $TSFC$  is reached as  $\sim 18.65$  at  $r_{C,Total} \sim 25.1$  and  $\beta \sim 4.9$ .

In Figure 5.1 (e),  $F_s$  has been calculated by utilizing equation (4.75). In Figure 5.1 (e) it has been seen that  $F_s$  is at maxima level when  $\beta$  is small, and  $F_s$  gets smaller as  $\beta$  gets larger. Also,  $F_s$  makes a maximum peak with  $r_{C,Total}$  at very small values, but after that peak  $F_s$  starts decreasing with increasing  $r_{C,Total}$ . Therefore, small level of  $r_{C,Total}$  and  $\beta = 1$  provides maxima  $F_s$ . It has been calculated that  $F_s$  reaches  $\sim 339.9 \text{ Ns kg}^{-1}$  at  $r_{C,Total} \sim 5.9$  and  $\beta = 1$ .

In Figure 5.1 (f),  $\dot{S}_{gen}$  has been calculated by utilizing equation (4.246). Figure 5.1 (f) shows that  $\dot{S}_{gen}$  has a very straight attitude with respect to  $r_{C,Total}$  and  $\beta$  together. With increasing  $r_{C,Total}$  and decreasing  $\beta$ ,  $\dot{S}_{gen}$  reaches minima values. On the other hand, as  $r_{C,Total}$  decreases and  $\beta$  increases  $\dot{S}_{gen}$  becomes larger, which means worse scenarios. Therefore, minima  $\dot{S}_{gen}$  values can be found at max.  $r_{C,Total}$  and min.  $\beta$ . Hence  $\dot{S}_{gen}$  reaches minimum level of  $\sim 41.4 \text{ kW K}^{-1}$  at  $r_{C,Total} = 33.5$  (maximum given value) and  $\beta = 1$ .

### 5.1.2 Determination of optimum values of performance indicators with respect to $r_{C,Total}$ and $r_F$

Relative variations of  $CEP$  and  $\eta_o$  with respect to  $r_{C,Total}$  and  $r_F$  in 3-D figures have been shown in Figure 5.2.

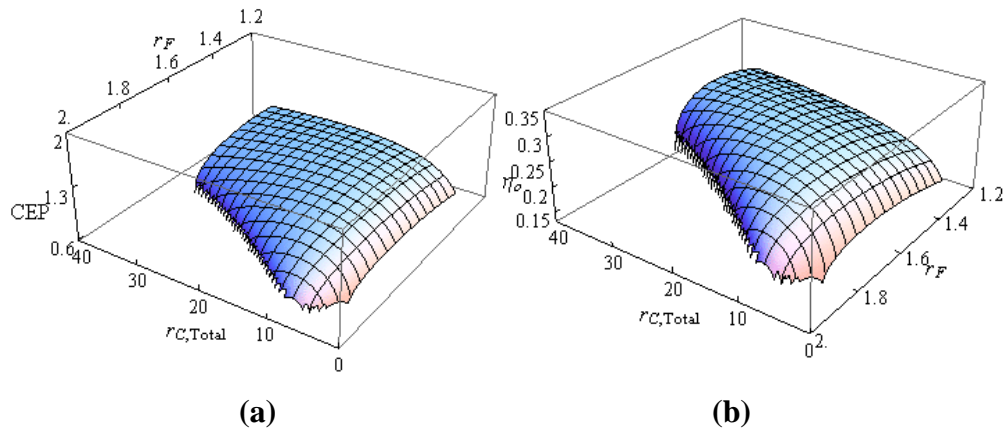


**Figure 5.2 :** Relative change of performance indicators of  $CEP$  and  $\eta_o$  with respect to  $r_{C,Total}$  and  $r_F$  simultaneously.

It can be seen in Figure 5.2 (a) that  $CEP$  increases with increasing  $r_F$  at the beginning, however, it starts to decrease dramatically after some optimum level of  $r_F$ . Also, at small values of  $r_{C,Total}$ ,  $CEP$  increases with increasing  $r_{C,Total}$  very fast, but then after reaching some optimal level of  $r_{C,Total}$ ,  $CEP$  starts to decrease slowly with increasing  $r_{C,Total}$ . Therefore, moderate levels of  $r_F$  with moderate levels of  $r_{C,Total}$  together provides highest  $CEP$  levels. Maximum  $CEP$  level reached is  $\sim 1.36$  at  $r_{C,Total} \sim 16.3$  and  $r_F \sim 1.52$ .

In Figure 5.2 (b) it has been observed that at large levels of  $r_F$ ,  $\eta_o$  increases dramatically with increasing  $r_{C,Total}$ , reaches its local maximum and sharply

decreases with still increasing  $r_{C,Total}$ . At smaller levels of increasing effect of  $r_{C,Total}$  is more stable. Maxima levels of  $\eta_o$  can be observed at moderate  $r_F$  levels together with higher  $r_{C,Total}$  values. Maximum  $\eta_o$  is found  $\sim 0.314$  at  $r_{C,Total} \sim 27.1$  and  $r_F \sim 1.56$ .

### 5.1.3 Determination of optimum values of performance indicators with respect to $r_{C,Total}$ and $T_{max}$

Relative variations of  $CEP$  and  $\eta_o$  with respect to  $r_{C,Total}$  and  $T_{max}$  in 3-D figures have been shown in Figure 5.3.

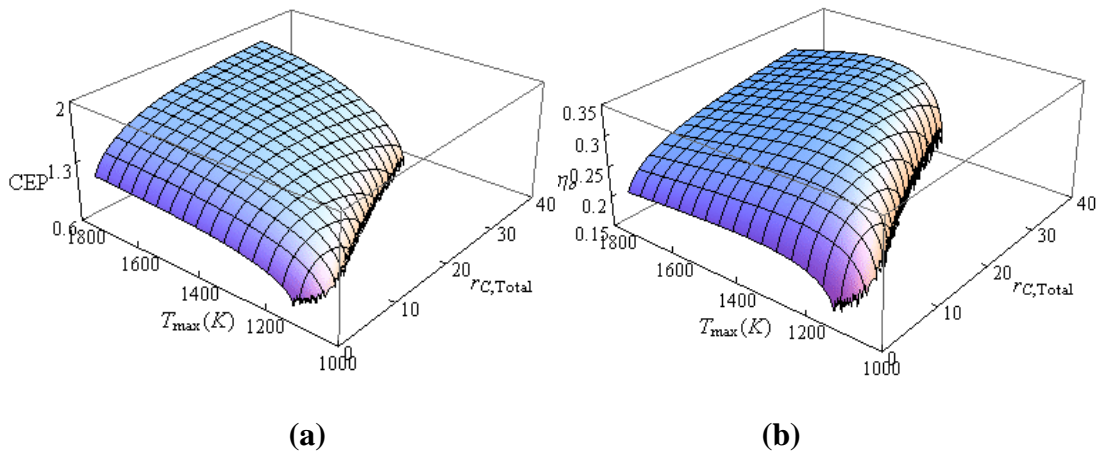


**Figure 5.3 :** Relative change of performance indicators of  $CEP$  and  $\eta_o$  with respect to  $r_{C,Total}$  and  $T_{max}$  simultaneously.

It can be seen in Figure 5.3 (a) that  $CEP$  decreases sharply at small values of  $r_{C,Total}$  and small values of  $T_{max}$ . As  $T_{max}$  and  $r_{C,Total}$  becomes larger together,  $CEP$  reaches larger levels. At maximum level,  $CEP$  is  $\sim 1.77$  at  $r_{C,Total} = 33.5$  (maximum given value) and  $T_{max} = 1800$  K.

In Figure 5.3 (b) it has been observed that at small values of  $T_{max}$ ,  $\eta_o$  increases sharply with increasing  $T_{max}$  and finds its peak. Then it starts to decrease gradually. This sharpness of  $T_{max}$  is more visible at larger  $r_{C,Total}$  values. As  $r_{C,Total}$  gets larger, peak point of  $\eta_o$  becomes higher. Also, at very small values of  $r_{C,Total}$ ,  $\eta_o$  decreases dramatically. Maxima level of  $\eta_o$  can be reached at moderate levels of  $T_{max}$  with maximum level of  $r_{C,Total}$ .  $\eta_o$  reaches its maximum level  $\sim 0.333$  at  $r_{C,Total} = 33.5$  (maximum given value) and  $T_{max} = 1495$  K.

### 5.1.4 Determination of optimum values of performance indicators with respect to $r_F$ and $\beta$

Relative variations of  $CEP$  and  $\eta_o$  with respect to  $r_F$  and  $\beta$  in 3-D figures have been shown in Figure 5.4.

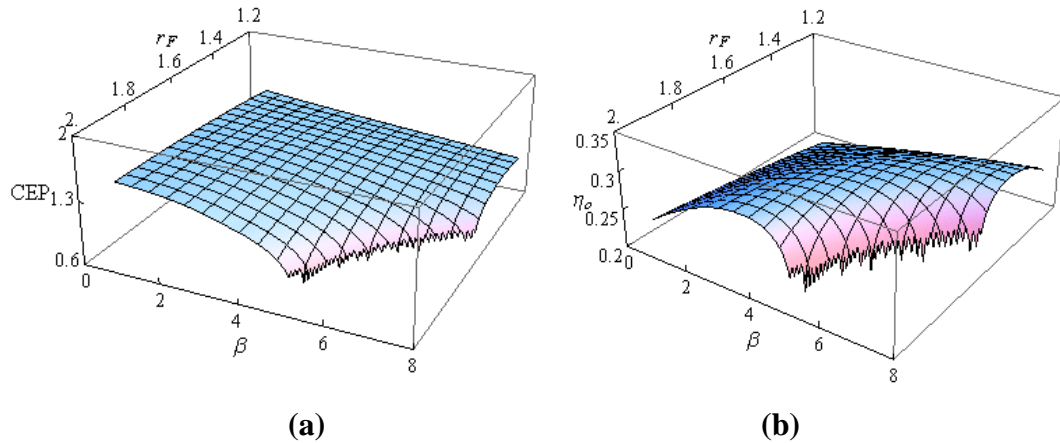


**Figure 5.4 :** Relative change of performance indicators of  $CEP$  and  $\eta_o$  with respect to  $r_F$  and  $\beta$  simultaneously.

It can be seen in Figure 5.4 (a) that  $CEP$  is at maxima level when  $r_F$  is at maximum and  $\beta$  is at minimum. On the other hand,  $CEP$  decreases continuously with increasing  $\beta$  and decreasing  $r_F$  together. Maximum point of  $CEP$  is  $\sim 1.61$  at  $r_F = 2$  and  $\beta = 1$ .

In Figure 5.4 (b) it has been shown that at very large values of  $r_F$ ,  $\beta$  causes a sharp increase and a sharp decrease with a maximum peak point of  $\eta_o$ . However, at small values of  $r_F$ ,  $\beta$  causes a gradual increase in  $\eta_o$ . The same sharp increase-decrease trend around a maximum peak can be observed at very large  $\beta$  values. At moderate  $\beta$  and moderate  $r_F$ ,  $\eta_o$  reaches maxima values.  $\eta_o$  reaches  $\sim 0.308$  at  $r_F \sim 1.69$  and  $\beta \sim 5.6$ .

### 5.1.5 Determination of optimum values of performance indicators with respect to $r_F$ and $T_{max}$

Relative variations of  $CEP$  and  $\eta_o$  with respect to  $r_F$  and  $T_{max}$  in 3-D figures have been shown in Figure 5.5.

It can be seen in Figure 5.5 (a) that  $CEP$  shows a steady trend with increasing  $r_F$  together with increasing  $T_{max}$ . Therefore maxima  $CEP$  is reached at maximum  $r_F$

and maximum  $T_{max}$ . At smaller values of  $T_{max}$ ,  $CEP$  decreases sharply with increase in  $r_F$ . Maximum level of  $CEP$  is  $\sim 1.75$  at  $r_F = 2$  and  $T_{max} = 1800$  K.

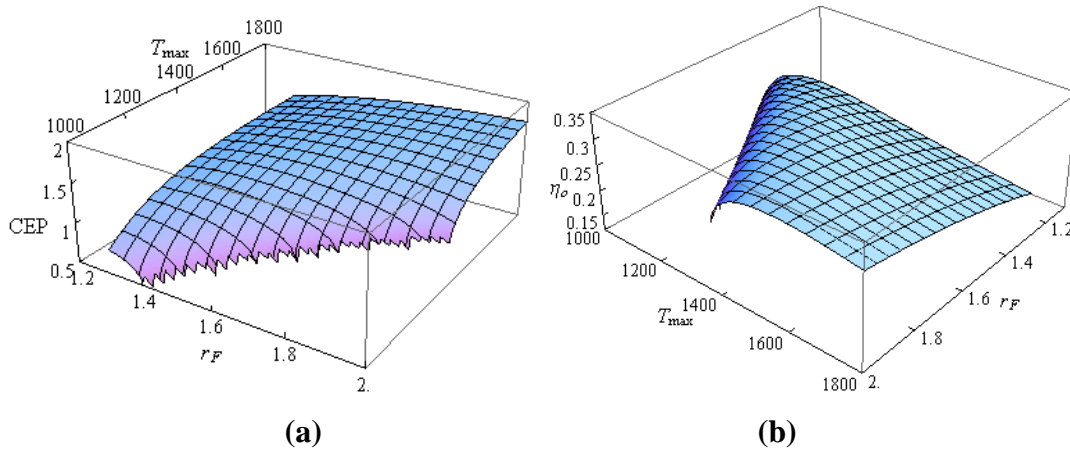


**Figure 5.5 :** Relative change of performance indicators of  $CEP$  and  $\eta_o$  with respect to  $r_F$  and  $T_{max}$  simultaneously.

In Figure 5.5 (b) it has been seen that at smaller  $r_F$  and larger  $T_{max}$  values,  $\eta_o$  becomes very small, and it is undesired. At very small values of  $T_{max}$  and very large values of  $r_F$  together,  $\eta_o$  faces a dramatic drop. Therefore, maxima levels of  $\eta_o$  is reached at maximum  $r_F$  value together with moderate  $T_{max}$  value. Maximum  $\eta_o$  value is  $\sim 0.321$  at  $r_F = 2$  and  $T_{max} = 1565$  K.

### 5.1.6 Determination of optimum values of performance indicators with respect to $\beta$ and $T_{max}$

Relative variations of  $CEP$  and  $\eta_o$  with respect to  $\beta$  and  $T_{max}$  in 3-D figures have been shown in Figure 5.6.

It can be seen in Figure 5.6 (a) that at larger values of  $T_{max}$ ,  $CEP$  reaches larger values for all  $\beta$  levels. At very small  $T_{max}$  and very large  $\beta$  levels,  $CEP$  decreases dramatically.  $CEP$  reaches  $\sim 1.66$  at  $\beta \sim 5.6$  and  $T_{max} = 1800$  as maximum level.

Figure 5.6 (b) shows that increasing  $\beta$  causes sharp drop in  $\eta_o$  at small values of  $T_{max}$ . On the other hand, as  $\beta$  increases,  $\eta_o$  also increases at large  $T_{max}$  levels. Also, maxima levels of  $\eta_o$  is reached at larger  $\beta$  values. Maximum  $CEP$  is  $\sim 0.322$  at  $\beta = 8$  and  $T_{max} = 1520$ .



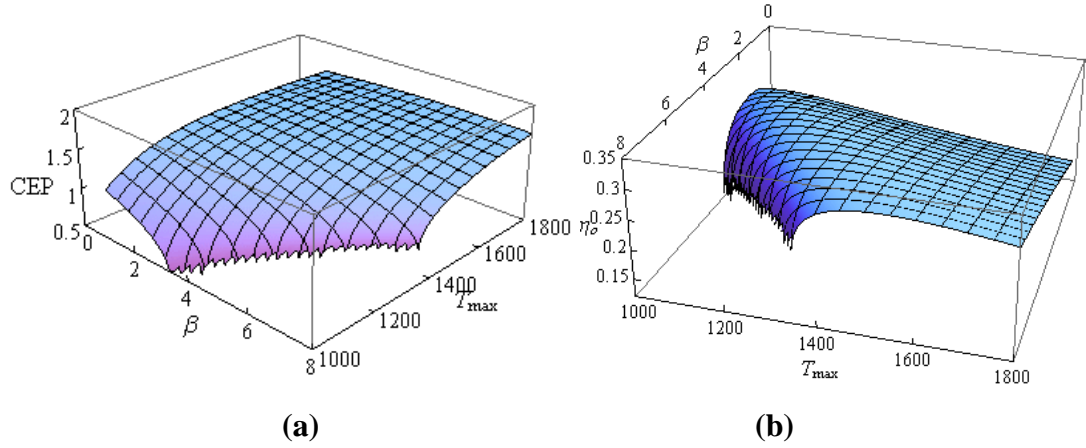


**Figure 5.6 :** Relative change of performance indicators of  $CEP$  and  $\eta_o$  with respect to  $\beta$  and  $T_{max}$  simultaneously.

## 5.2 Effect of Heat Leakage on the Optimal Design Parameters and Performance Indicators

As mentioned earlier, in order to be able to perform heat leakage effect analyzes, firstly optimum levels of design parameters have been calculated. Two of the design parameters have been kept constant and other two have been analyzed each time. Now, in order to inspect effect of heat leakage, one more design parameter has been kept constant and analyzes have been narrowed down to 2-D.

First of all, in order to observe relative importance of two heat leakage types, one of which is from CC to bypass air, and the second one is from bypass air to ambient air ( $\varepsilon_{LK1}$  and  $\varepsilon_{LK2}$  respectively), a comparison between them has been performed.

### 5.2.1 Comparison of the results of two types of heat leakages $\varepsilon_{LK1}$ and $\varepsilon_{LK2}$

First of all, values of  $CEP$ ,  $\eta_o$ ,  $f_{exd}$ ,  $TSFC$ ,  $F_s$  and  $\dot{S}_{gen}$  have been calculated when  $\beta$  has a small value (1.0). These calculations have been performed repeatedly at  $\varepsilon_{LK1}$  equals to 0.00, 0.02 and 0.04 while  $\varepsilon_{LK2}$  is constant at 0.02 for each of the performance indicators. Variations in these performance indicators have been calculated both in terms of their real values and in terms of percentage changes. The same calculations have been performed also for  $\beta$  having a large value (7.0).

Above mentioned effort have been performed again for  $\varepsilon_{LK2}$  having values 0.00, 0.02 and 0.04 while  $\varepsilon_{LK1}$  is constant at 0.02 this time. Results have been illustrated in Table 5.1.

**Table 5.1 :** Comparisons of the variation of performance indicators with  $\varepsilon_{LK1}$  when  $\varepsilon_{LK2}=2\%$  and those with  $\varepsilon_{LK2}$  when  $\varepsilon_{LK1}=2\%$  for small (1) and large (7) values of  $\beta$ .

$\varepsilon_{LK2} = 2\%$	$\beta$	$CEP$	% change	$\eta_o$	% change	$f_{exd}$	% change	$TSFC$	% change	$F_s$	% change	$\dot{S}_{gen}$	% change
$\varepsilon_{LK1} = 0\%$	1.0	1.72	-	0.2405	-	0.12	-	24.35	-	313.3	-	42.5	-
$\varepsilon_{LK1} = 2\%$	1.0	1.58	-8.03%	0.2400	-0.21%	0.13	8.50%	24.40	0.21%	312.6	-0.21%	46.1	8.50%
$\varepsilon_{LK1} = 4\%$	1.0	1.47	-7.16%	0.2394	-0.26%	0.14	7.44%	24.47	0.26%	311.8	-0.26%	49.5	7.44%
$\varepsilon_{LK1} = 0\%$	7.0	1.23	-	0.30	-	0.168	-	19.7	-	96.6	-	73.0	-
$\varepsilon_{LK1} = 2\%$	7.0	1.12	-8.85%	0.28	-4.23%	0.176	5.06%	20.6	4.50%	92.4	-4.31%	76.7	5.07%
$\varepsilon_{LK1} = 4\%$	7.0	1.00	-10.41%	0.27	-6.13%	0.185	4.78%	22.0	6.66%	86.7	-6.24%	80.3	4.78%
$\varepsilon_{LK1} = 2\%$	$\beta$	$CEP$	% change	$\eta_o$	% change	$f_{exd}$	% change	$TSFC$	% change	$F_s$	% change	$\dot{S}_{gen}$	% change
$\varepsilon_{LK2} = 0\%$	1.0	1.60	-	0.2406	-	0.1306	-	24.35	-	313.3	-	45,79	-
$\varepsilon_{LK2} = 2\%$	1.0	1.58	-0.89%	0.2400	-0.22%	0.1315	0.67%	24.40	0.23%	312.6	-0.23%	46,10	0.67%
$\varepsilon_{LK2} = 4\%$	1.0	1.57	-0.87%	0.2395	-0.22%	0.1324	0.65%	24.46	0.23%	311.9	-0.23%	46,40	0.65%
$\varepsilon_{LK2} = 0\%$	7.0	1.16	-	0.286	-	0.172	-	20.4	-	93.6	-	74,9	-
$\varepsilon_{LK2} = 2\%$	7.0	1.12	-3.48%	0.283	-1.20%	0.176	2.36%	20.6	1.24%	92.4	-1.22%	76,7	2.36%
$\varepsilon_{LK2} = 4\%$	7.0	1.08	-3.40%	0.279	-1.22%	0.180	2.25%	20.9	1.26%	91.3	-1.24%	78,4	2.25%

When it comes to investigating and interpreting the resulting numbers, it has been seen that  $CEP$  has the values of 1.72, 1.58 and 1.47 at  $\beta$  equals to 1.0 for  $\varepsilon_{LK1}$  equals to 0.00, 0.02 and 0.04 respectively while  $\varepsilon_{LK2}$  is constant at 0.02. Therefore, percentage changes in  $CEP$  are -8.03% from 0.00  $\varepsilon_{LK1}$  to 0.02  $\varepsilon_{LK1}$  and -7.16% from 0.02  $\varepsilon_{LK1}$  to 0.04  $\varepsilon_{LK1}$ .

The same configuration for constant  $\varepsilon_{LK1}$  at 0.02 and changing  $\varepsilon_{LK2}$  from 0.00 to 0.02 and from 0.02 to 0.04 at  $\beta$  equals to 1.0 result in -0.89% and -0.87% changes in  $CEP$ . This gives a clue on comparison of relative effects of heat leakage one and heat leakage two.

When the comparison is done at  $\beta$  equals to 7.0, it has been observed that increasing effect of  $\varepsilon_{LK1}$  causes change in  $CEP$  as -8.85% and -10.41% while that of  $\varepsilon_{LK2}$  causing -3.48% and -3.40%.

Investigating the other performance indicators, for example  $f_{exd}$  at  $\beta$  equals to 1.0 shows 8.50% and 7.44% changes by increasing  $\varepsilon_{LK1}$  from 0.00 to 0.02 and from 0.02 to 0.04 respectively while  $\varepsilon_{LK2}$  is constant at 0.02. On the other hand, increase in  $\varepsilon_{LK2}$  causes only 0.67% and 0.65% changes in  $f_{exd}$  for the same configuration.

Comparing all the other performance indicators by looking at the same colored cells in Table 5.1 both for  $\beta$  equals to 1.0 and to 7.0, change caused by heat leakage two is relatively smaller than that of heat leakage one. Therefore, this observation guides that effect of heat leakage two (from bypass air to ambient air) is relatively smaller than effect of heat leakage one (from combustion chamber to bypass air through the combustion chamber wall) on the performance of a twin-spool turbofan engine of a commercial aircraft. Hence, this thesis has been focused on investigating the effects of heat leakage one ( $\varepsilon_{LK1}$  and  $\dot{Q}_{LK1}$ ) rather than less significant effects of heat leakage two ( $\varepsilon_{LK2}$  and  $\dot{Q}_{LK2}$ ).

### **5.2.2 Variations of performance indicators with respect to design parameters and $\varepsilon_{LK1}$**

Until now, it has been observed that  $\varepsilon_{LK1}$  is more significant than  $\varepsilon_{LK2}$ . In this part, effects of heat leakage one on performance indicators and optimum levels of design parameters have been investigated one by one.

### 5.2.2.1 Variation with respect to $r_{C,Total}$

Variations of  $CEP$ ,  $\eta_o$ ,  $f_{exd}$ ,  $TSFC$ ,  $F_s$  and  $\dot{S}_{gen}$  with respect to  $r_{C,Total}$  at three different  $\varepsilon_{LK1}$  values have been illustrated in Figure 5.7 (a)-(f). Also, relative variation of  $CEP$  with respect to  $\eta_o$  have been shown for the same range of  $r_{C,Total}$  in Figure 5.7 (g).

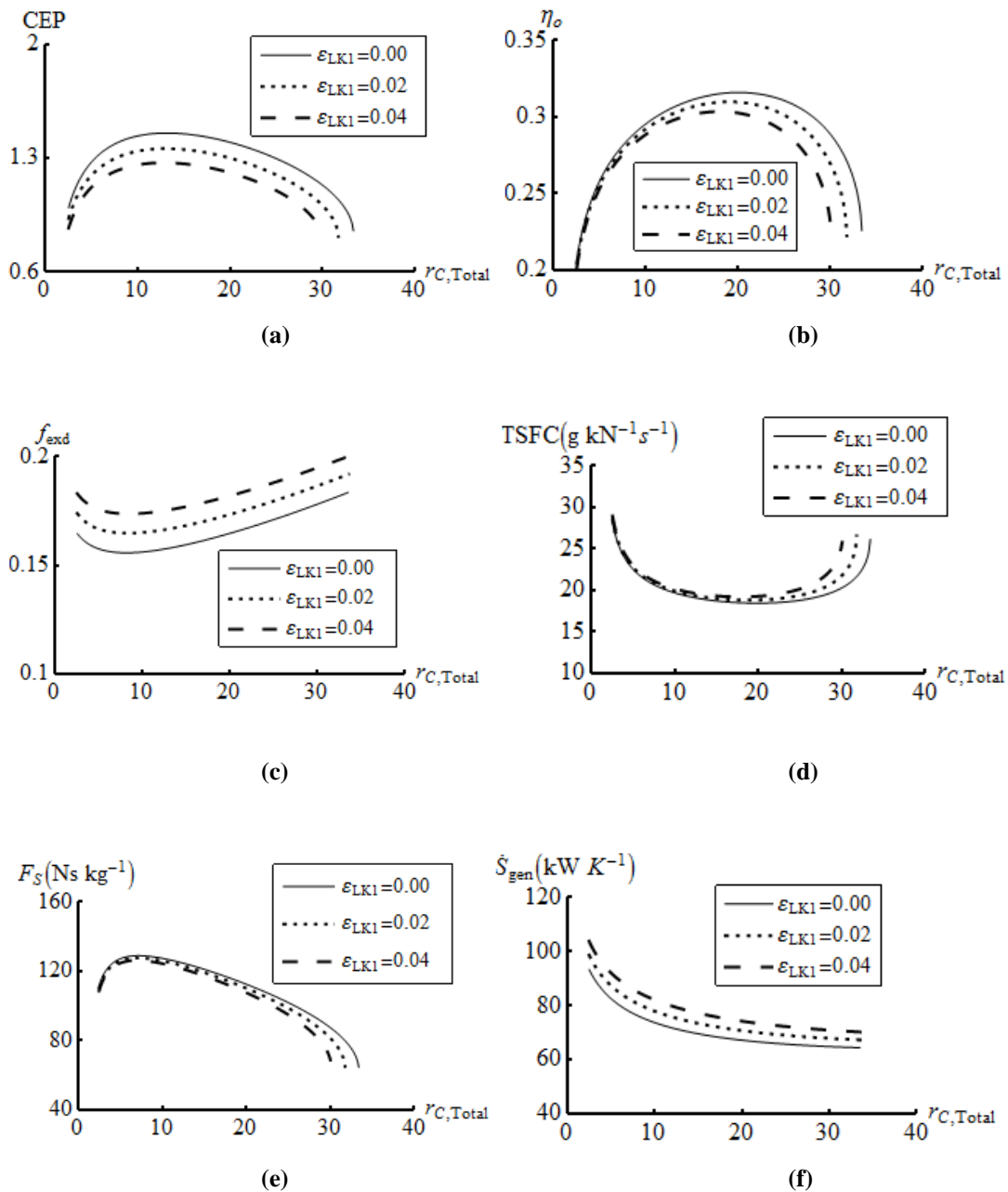
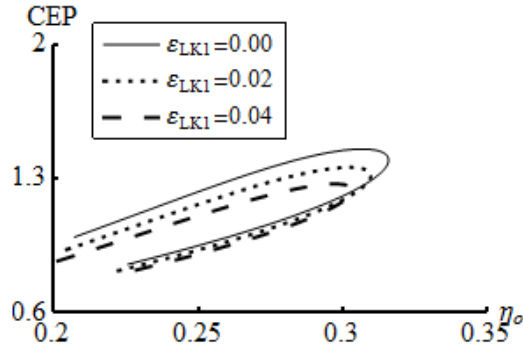


**Figure 5.7 :** Relative change of performance indicators with respect to  $r_{C,Total}$  at three values of  $\varepsilon_{LK1}$ .



(g)

**Figure 5.7 (continued):** Relative change of performance indicators with respect to  $r_{C,Total}$  at three values of  $\epsilon_{LK1}$ .

By looking at Figure 5.7 (a), it has been seen that  $CEP$  reaches certain maximum values for certain  $r_{C,Total}$  values at different values of  $\epsilon_{LK1}$ . For example,  $CEP$  reaches 1.42, 1.33 and 1.24 when  $r_{C,Total}$  values are 13.0, 12.9 and 12.7 at  $\epsilon_{LK1}$  equals to 0%, 2% and 4% respectively. Here, if  $CEP$  is considered to be the objective function, then these  $r_{C,Total}$  values are considered as optimum values. It is clear that maximum value that  $CEP$  can reach decreases with increasing  $\epsilon_{LK1}$ . Also, optimum value of  $r_{C,Total}$  becomes smaller as  $\epsilon_{LK1}$  gets larger.

In Figure 5.7 (b), it has been observed and compiled that optimum  $r_{C,Total}$  values that  $\eta_o$  reaches its maximum at 0%, 2% and 4%  $\epsilon_{LK1}$  are larger than that of  $CEP$ . Numerically,  $\eta_o$  reaches 0.314, 0.308 and 0.301 when  $r_{C,Total}$  values are 20.0, 18.9 and 17.9. This shows that if  $\eta_o$  is considered as the objective function, one should select relatively larger  $r_{C,Total}$  values compared to  $CEP$  in order to have better  $\eta_o$  performance. It is evident that maximum  $\eta_o$  value decreases with increasing  $\epsilon_{LK1}$ . Moreover, optimum  $r_{C,Total}$  values are smaller for the larger  $\epsilon_{LK1}$  values.

It has been seen in Figure 5.7 (c) that  $f_{exd}$  makes a minimum at certain  $r_{C,Total}$  values for 0%, 2% and 4%  $\epsilon_{LK1}$  values. In all of these three  $\epsilon_{LK1}$  values,  $f_{exd}$  reaches its minimum nearly at 10.0  $r_{C,Total}$  value. These minimum points are 0.156, 0.165 and 0.174 respectively. This shows that as  $\epsilon_{LK1}$  value increases, minimum  $f_{exd}$  that can be reached gets larger, so it distorts the  $f_{exd}$  performance. It is evident that when  $f_{exd}$  is set as the objective function, selecting  $r_{C,Total}$  value as 10.0, which is smaller than other two above, gives the best result for all of the three  $\epsilon_{LK1}$  values.

It has been observed in Figure 5.7 (d) that  $TSFC$  has also a minimum value with respect to changing  $r_{C,Total}$  values for each  $\varepsilon_{LK1}$  value. When  $TSFC$  is considered as the objective function, optimum  $r_{C,Total}$  values that gives minimum  $TSFC$  are very close to those of  $\eta_o$ . Numerically, these optimum  $r_{C,Total}$  values are 19.7, 18.7 and 17.7 with respect to 0%, 2% and 4%  $\varepsilon_{LK1}$  values. Corresponding minimum  $TSFC$  values are 18.6, 18.9 and 19.3 g kN<sup>-1</sup> s<sup>-1</sup> respectively. It has been observed from these figures that as  $\varepsilon_{LK1}$  increases, the minimum value that  $TSFC$  can reach increases, so this means a performance distortion. Also, it is clear that optimum  $r_{C,Total}$  values are smaller when  $\varepsilon_{LK1}$  values are larger.

As it has been seen in Figure 5.7 (e) that  $F_s$  reaches a maximum with respect to  $r_{C,Total}$  for each  $\varepsilon_{LK1}$  value. These maximum values are 128.9, 127.6 and 126.2 N s kg<sup>-1</sup> with respect to 0%, 2% and 4%  $\varepsilon_{LK1}$ . Corresponding  $r_{C,Total}$  values are 7.2, 7.1 and 7.0 respectively. This shows that  $\varepsilon_{LK1}$  distorts the maximum point that  $F_s$  can reach, causing smaller maximum points. If  $F_s$  is considered as the objective function, it is evident that  $\varepsilon_{LK1}$  causes optimum  $r_{C,Total}$  values to decrease. It is also clear that  $F_s$  requires smaller  $r_{C,Total}$  values compared to other performance parameters mentioned above.

In Figure 5.7 (f), it has been observed that  $\dot{S}_{gen}$  decreases with the increasing  $r_{C,Total}$ . Therefore, there is no optimum  $r_{C,Total}$  value that makes  $\dot{S}_{gen}$  minimum. However, considering the  $r_{C,Total}$  equals to 29.0 as upper limit in order to have a numerical evaluation, corresponding  $\dot{S}_{gen}$  values are 64.9, 68.0 and 71.1 kW K<sup>-1</sup> with respect to 0%, 2% and 4%  $\varepsilon_{LK1}$  values. It has been clearly observed that  $\dot{S}_{gen}$  level increases with increasing  $\varepsilon_{LK1}$ .

By looking at Figure 5.7 (g), it has been seen that there is a region that  $CEP$  and  $\eta_o$  have larger values. This region provide  $CEP$  values larger than 1.3 and  $\eta_o$  values larger than 0.3 at the upper right corner of Figure 5.7 (g) for 0%  $\varepsilon_{LK1}$ . These values are corresponding to a range of  $r_{C,Total}$  values, roughly between 10.0 ~ 25.0.

### 5.2.2.2 Variation with respect to $r_F$

Figure 5.8 (a)-(f) shows the variation of performance indicators,  $CEP$ ,  $\eta_o$ ,  $f_{exd}$ ,  $TSFC$ ,  $F_s$  and  $\dot{S}_{gen}$  with respect to  $r_F$  at three different  $\varepsilon_{LK1}$  values 0%, 2% and 4%. Also, relative change of  $CEP$  and  $\eta_o$  has been shown in Figure 5.8 (g).

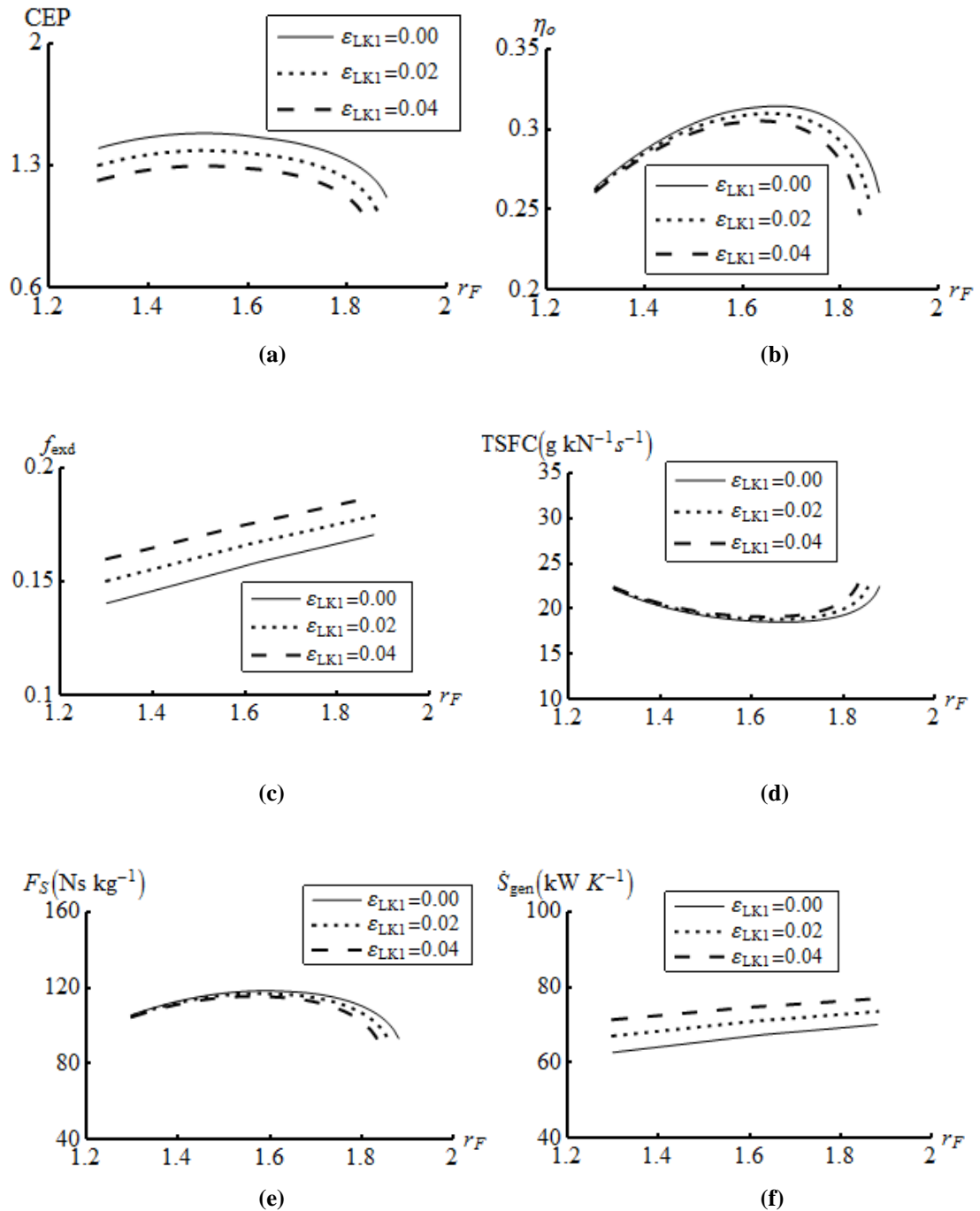
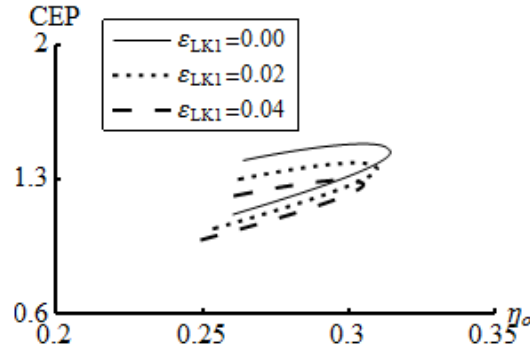


**Figure 5.8** : Relative change of performance indicators with respect to  $r_F$  at three values of  $\varepsilon_{LK1}$ .



(g)

**Figure 5.8 (continued):** Relative change of performance indicators with respect to  $r_F$  at three values of  $\varepsilon_{LK1}$ .

By looking at Figure 5.8 (a), it has been observed that  $CEP$  makes a maximum peak with respect to  $r_F$  at certain values. Numerically,  $CEP$  reaches the maximum values of 1.45, 1.35 and 1.27 when  $r_F$  values are 1.5064, 1.5081 and 1.5069 at 0%, 2% and 4%  $\varepsilon_{LK1}$  values. This means that increase in  $\varepsilon_{LK1}$  have nearly no effect on optimum  $r_F$  value, when  $CEP$  is considered as the objective function. Therefore,  $r_F$  values around 1.50 provide the best  $CEP$  values for different  $\varepsilon_{LK1}$  values. It is evident that increasing  $\varepsilon_{LK1}$  value causes a decrease in maximum  $CEP$  level.

It has been seen in Figure 5.8 (b) that  $\eta_o$  also makes a maximum with respect to  $r_F$  at certain values. However, as observed in Figure 5.8 (b),  $\eta_o$  reaches the maximum point at larger  $r_F$  levels compared to  $CEP$ . Maximum values that  $\eta_o$  has reached are 0.312, 0.308 and 0.303 at 0%, 2% and 4%  $\varepsilon_{LK1}$  values respectively. Corresponding optimum  $r_F$  values if  $\eta_o$  is considered as the objective function are 1.67, 1.65 and 1.64. It is clear that increasing  $\varepsilon_{LK1}$  value distorts the  $\eta_o$  performance, causing a decrease in maximum level reached. Also, as  $\varepsilon_{LK1}$  increases, optimum  $r_F$  value gets smaller.

In Figure 5.8 (c), it has been seen that  $f_{exd}$  decreases as  $r_F$  decreases. Therefore, there is not a certain optimum  $r_F$  value that provides minimum  $f_{exd}$ . As can be observed from Figure 5.8 (c), increasing  $\varepsilon_{LK1}$  decreases the  $f_{exd}$  level. Considering 1.30 as the lower limit for  $r_F$ ,  $f_{exd}$  reaches 0.14, 0.15 and 0.16 as minimum values for this  $r_F$  limit, with respect to 0%, 2% and 4%  $\varepsilon_{LK1}$  values.

It has been observed in Figure 5.8 (d) that  $TSFC$  reaches a minimum relatively larger  $r_F$  values than  $CEP$ , and very close to that of  $\eta_o$ . Minimum values of  $TSFC$  are 18.7, 18.9 and 19.2  $\text{g kN}^{-1} \text{s}^{-1}$  for 0%, 2% and 4%  $\varepsilon_{LK1}$  values respectively. If  $TSFC$



is considered as objective function, optimum  $r_F$  values corresponding to above minimum  $TSFC$  values are 1.67, 1.65 and 1.63. It has been seen that as  $\varepsilon_{LK1}$  gets larger, optimum  $r_F$  values approach to the lower limit. On the other hand,  $TSFC$  reaches larger values with increasing  $\varepsilon_{LK1}$ , which means a distortion in  $TSFC$  performance with increasing heat leakage one.

In Figure 5.8 (e), it has been seen that  $F_s$  reaches a maximum at certain  $r_F$  values for different  $\varepsilon_{LK1}$  levels. The maximum values that  $F_s$  can reach are 118.3, 116.9 and 115.4 N s kg<sup>-1</sup> at 0%, 2% and 4%  $\varepsilon_{LK1}$  values respectively. Corresponding optimum  $r_F$  values are 1.59, 1.57 and 1.56 if  $F_s$  is considered as the objective function. As seen, optimum  $r_F$  values converge to smaller figures when  $\varepsilon_{LK1}$  is increased. Meanwhile, performance of  $F_s$  decreases with increasing heat leakage effect.

It has been observed in Figure 5.8 (f) that  $\dot{S}_{gen}$  continuously increase with increasing  $r_F$  and vice versa. Therefore, there is not an optimum  $r_F$  values that gives the minimum  $\dot{S}_{gen}$  value. However, considering 1.30 as the lower limit for  $r_F$ , it has been compiled that minimum  $\dot{S}_{gen}$  values at that  $r_F$  value are 62.7, 67.1 and 71.4 kW K<sup>-1</sup> with respect to 0%, 2% and 4%  $\varepsilon_{LK1}$ . It is clear that increasing heat leakage ratio increases the  $\dot{S}_{gen}$  level, which means a distortion in performance.

And lastly, by looking at Figure 5.8 (g), there is an optimum region at the upper right corner instead of a point giving the maximum value both for  $CEP$  and for  $\eta_o$ . This region is again above 1.3 for  $CEP$  and above 0.3 for  $\eta_o$ , approximately within 1.5 ~ 1.7 interval for  $r_F$  when  $\varepsilon_{LK1}$  is 0%.

### 5.2.2.3 Variation with respect to $\beta$

In Figure 5.9 (a)-(f), variation of performance indicators,  $CEP$ ,  $\eta_o$ ,  $f_{exd}$ ,  $TSFC$ ,  $F_s$  and  $\dot{S}_{gen}$  with respect to  $\beta$  at three different  $\varepsilon_{LK1}$  values 0%, 2% and 4% have been illustrated. Also, relative variation of  $CEP$  and  $\eta_o$  with respect to changing  $\beta$  has been demonstrated in Figure 5.9 (g).

By looking at Figure 5.9 (a), it has been observed that  $CEP$  decreases with increasing  $\beta$ ; therefore, when  $CEP$  is considered as the objective function, optimum  $\beta$  value should be as small as possible. Considering as a lower limit, if  $\beta$  is selected as 1.0, then corresponding maximum  $CEP$  values are 1.72, 1.58 and 1.47 with

respect to 0%, 2% and 4%  $\varepsilon_{LK1}$  values. It is also clear that increasing  $\varepsilon_{LK1}$  has a negative effect on  $CEP$  values.

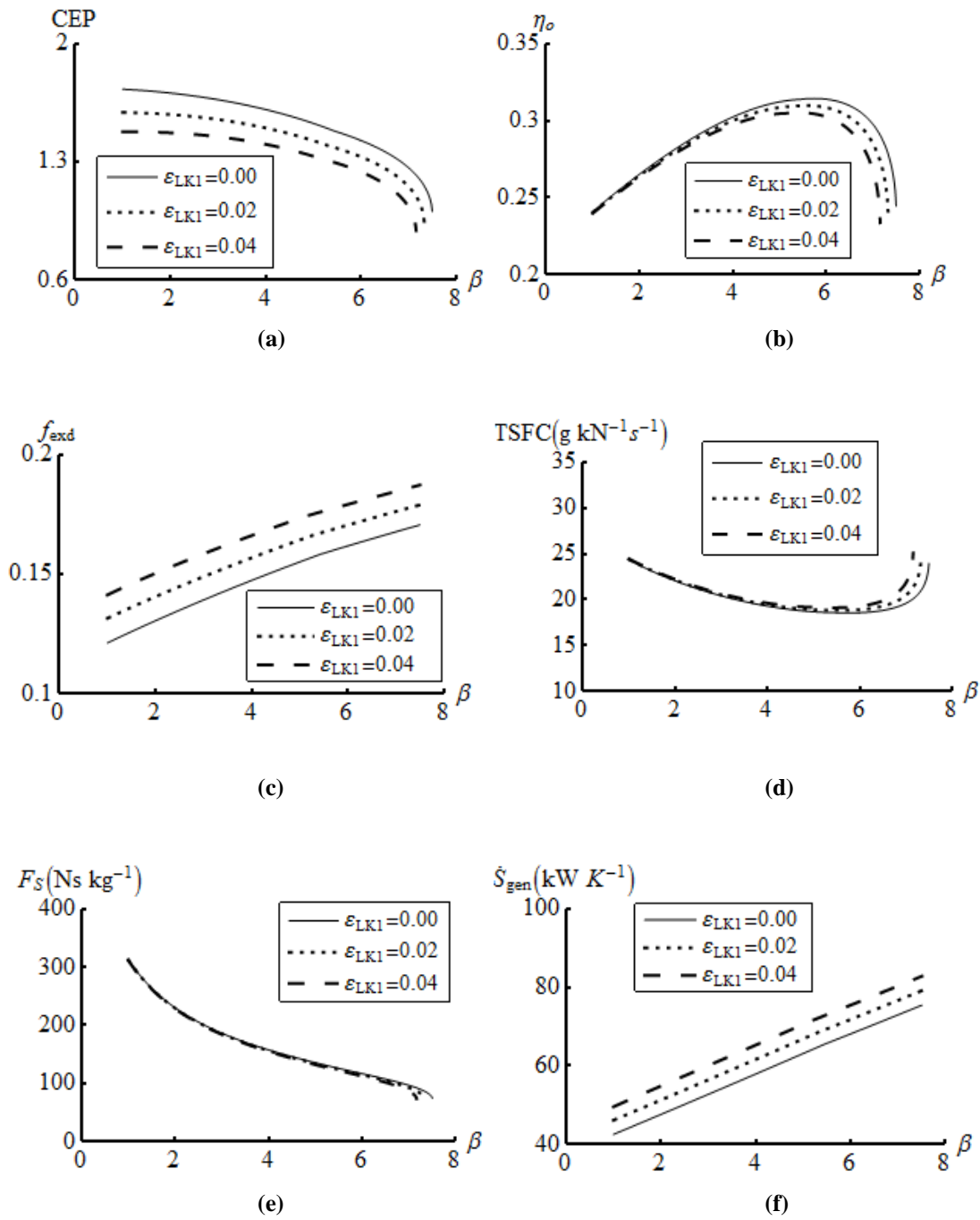


**Figure 5.9 :** Relative change of performance indicators with respect to  $\beta$  at three values of  $\varepsilon_{LK1}$ .

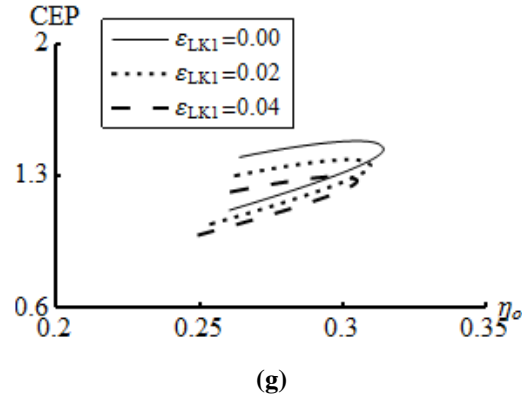


**Figure 5.9 (continued):** Relative change of performance indicators with respect to  $\beta$  at three values of  $\varepsilon_{LK1}$ .

It has been seen in Figure 5.9 (b) that  $\eta_o$  reaches a maximum point for a certain  $\beta$  at each  $\varepsilon_{LK1}$  value. Numerically, the maximum point that are reached by  $\eta_o$  are 0.312, 0.308 and 0.303 and corresponding  $\beta$  values are 5.7, 5.6 and 5.4 at  $\varepsilon_{LK1}$  values 0%, 2% and 4% respectively. It has been observed that as  $\varepsilon_{LK1}$  increases, maximum  $\eta_o$  values decreases, so  $\varepsilon_{LK1}$  has a negative effect on the  $\eta_o$  performance. Also, optimum  $\beta$  values, considering  $\eta_o$  as the objective function, gets smaller when  $\varepsilon_{LK1}$  is increased.

In Figure 5.9 (c), it has been observed that  $f_{exd}$  increases with increasing  $\beta$ . It means that there is not a certain optimum  $\beta$  value that gives the minimum  $f_{exd}$ . As a limiting value, when  $\beta$  is taken as 1.0, corresponding maximum  $f_{exd}$  values at this  $\beta$  value are 0.12, 0.13 and 0.14 with respect to  $\varepsilon_{LK1}$  values 0%, 2% and 4%. It is clear that increasing  $\varepsilon_{LK1}$  increases the minimum  $f_{exd}$  value, so it causes distortion in the  $f_{exd}$  performance.

It has been observed in Figure 5.9 (d) that  $TSFC$  reaches a minimum at a certain  $\beta$  for each  $\varepsilon_{LK1}$  value. If  $TSFC$  is considered as the objective function, optimum  $\beta$  values for minimum  $TSFC$  are 5.7, 5.6 and 5.4 at 0%, 2% and 4%  $\varepsilon_{LK1}$  respectively. Corresponding minimum  $TSFC$  values are 18.7, 18.9 and 19.2  $\text{g kN}^{-1}\text{s}^{-1}$  at these  $\varepsilon_{LK1}$  values. It is clear that increasing  $\varepsilon_{LK1}$  causes optimum  $\beta$  value to become smaller. Also, it has been observed that minimum  $TSFC$  value is increased with increasing  $\varepsilon_{LK1}$ , so  $\varepsilon_{LK1}$  cause a distortion in  $TSFC$  performance.

In Figure 5.9 (e), it has been seen that  $F_s$  does not reach a maximum point for a certain  $\beta$  value. Instead,  $F_s$  decreases with increasing  $\beta$ ; therefore, there is not a certain optimum  $\beta$  value that gives maximum  $F_s$ . Therefore, selecting  $\beta$  equals

to 1.0 as a limiting lower value,  $F_s$  reaches 313.3, 312.6 and 311.8 N s kg<sup>-1</sup> at 0%, 2% and 4%  $\varepsilon_{LK1}$  values respectively. It has been seen that  $\varepsilon_{LK1}$  has a slight decreasing effect on  $F_s$  as observed in Figure 5.9 (e).

In Figure 5.9 (f), it is clear that  $\dot{S}_{gen}$  increases with increasing  $\beta$ . Therefore, there is not a certain  $\beta$  value, giving the minimum  $\dot{S}_{gen}$ . So, taking  $\beta$  equals to 1.0 as a lower limiting value,  $\dot{S}_{gen}$  has the minimum values of 42.5, 46.1 and 49.5 kW K<sup>-1</sup> at 0%, 2% and 4%  $\varepsilon_{LK1}$  values respectively. It has also been observed that increasing  $\varepsilon_{LK1}$  increases the  $\dot{S}_{gen}$  level, so it deteriorates the performance.

Lastly, in Figure 5.9 (g), it has been seen that there is not a certain optimum region in this figure. When  $CEP$  is at maximum above 1.7,  $\eta_o$  is at very low levels below 0.25 for 0%  $\varepsilon_{LK1}$ . Also, when  $\eta_o$  is at its maximum above 0.3,  $CEP$  is at very lower end around 1.4. This is due to the fact that  $CEP$  is very high at small  $\beta$  values; while it is the opposite for  $\eta_o$  because it reaches its maximum at larger  $\beta$  values.

#### 5.2.2.4 Variation with respect to $T_{max}$

Figure 5.10 (a)-(f) shows the variation of performance indicators,  $CEP$ ,  $\eta_o$ ,  $f_{exd}$ ,  $TSFC$ ,  $F_s$  and  $\dot{S}_{gen}$  with respect to  $T_{max}$  at three different  $\varepsilon_{LK1}$  values 0%, 2% and 4%. Also, relative change of  $CEP$  and  $\eta_o$  has been shown in Figure 5.10 (g).

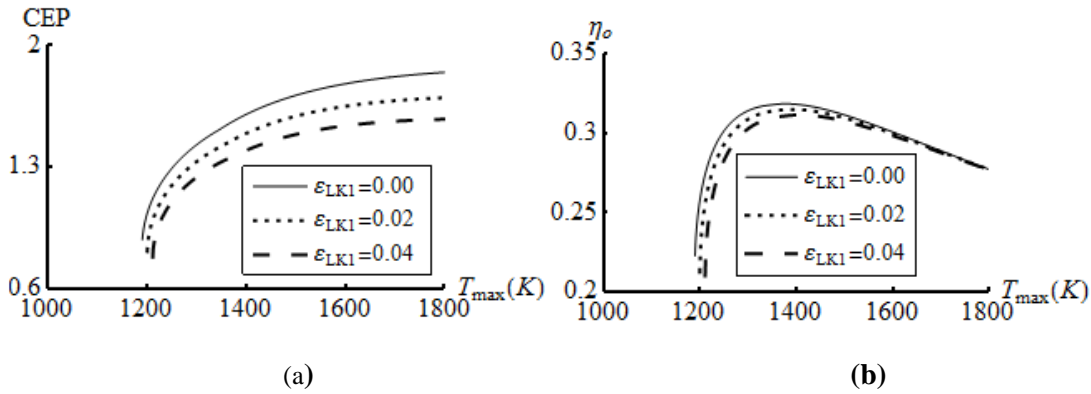


**Figure 5.10 :** Relative change of performance indicators with respect to  $T_{max}$  at three values of  $\varepsilon_{LK1}$ .

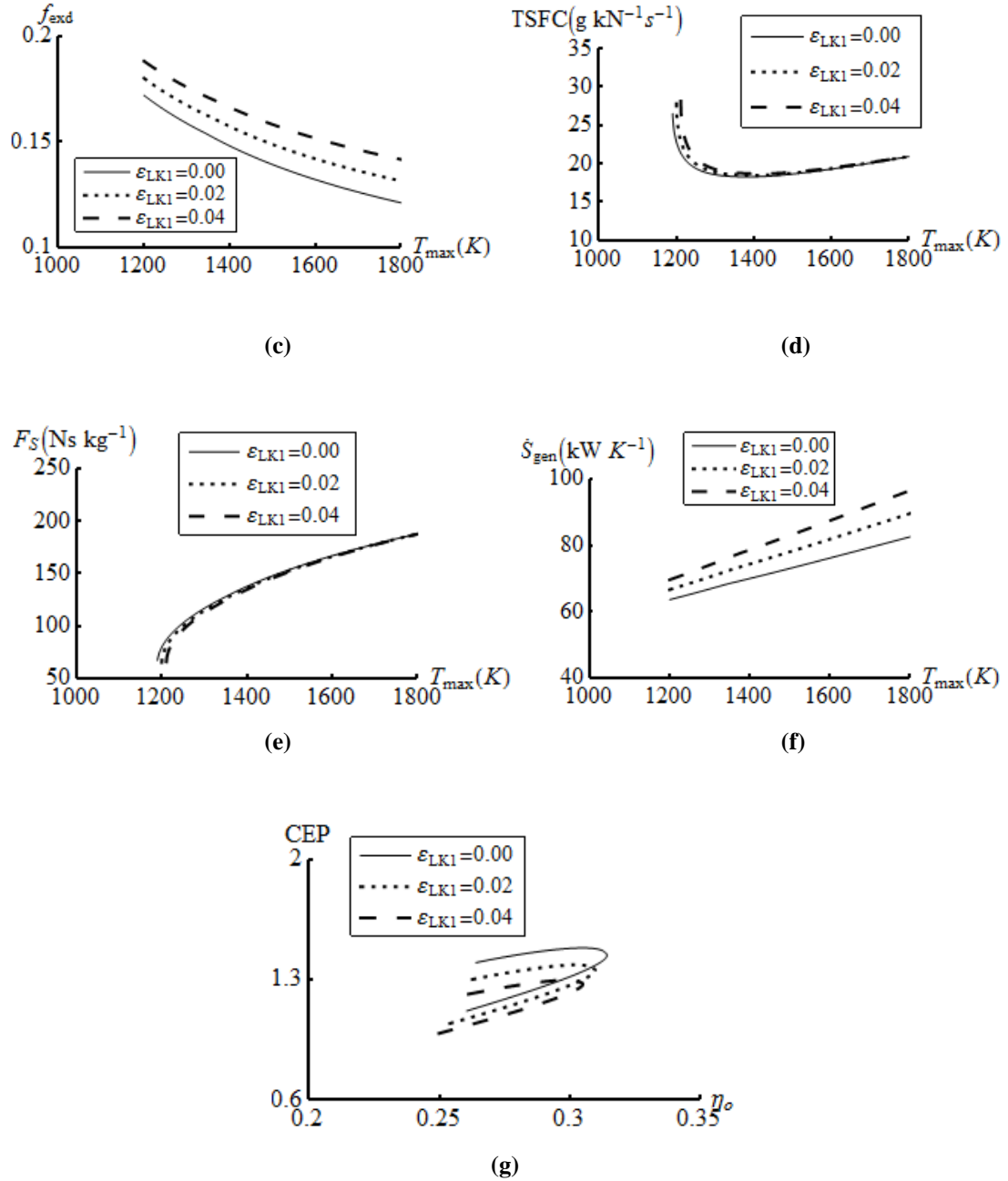


**Figure 5.10 (continued):** Relative change of performance indicators with respect to  $T_{max}$  at three values of  $\epsilon_{LK1}$ .

It has been seen in Figure 5.10 (a) that  $CEP$  increases with increasing  $T_{max}$ . Therefore, there is not a certain optimum  $T_{max}$  giving maximum  $CEP$ . Considering  $T_{max}$  equals to 1800 as an upper limit,  $CEP$  reaches 1.81, 1.66 and 1.54 with respect to 0%, 2% and 4%  $\epsilon_{LK1}$  values at this  $T_{max}$  value. It is clear that increasing  $\epsilon_{LK1}$  has a decreasing effect on  $CEP$  performance.

In Figure 5.10 (b), it has been observed that  $\eta_o$  reaches a maximum point at a certain  $T_{max}$  value for each  $\epsilon_{LK1}$ . Numerically, maximum  $\eta_o$  values are 0.316, 0.313 and

0.310 at 0%, 2% and 4%  $\varepsilon_{LK1}$  values respectively. Corresponding  $T_{max}$  values can be considered as the optimum values, if  $\eta_o$  is considered as the objective function, and these values are 1380, 1394, 1409 respectively. As seen, these optimum  $T_{max}$  values are closer to smaller end of the  $T_{max}$  scale. It is clear that  $\varepsilon_{LK1}$  has a negative effect on  $\eta_o$  since increase in  $\varepsilon_{LK1}$  causes decrease in  $\eta_o$  level. Also, increasing  $\varepsilon_{LK1}$  shifts the optimum  $T_{max}$  to larger values.

It has been seen in Figure 5.10 (c) that as  $T_{max}$  increases,  $f_{exd}$  decreases. Therefore, there is not a certain optimum  $T_{max}$  value that minimizes  $f_{exd}$ . Considering  $T_{max}$  equals to 1800 K as a limiting upper bound, minimum value of  $f_{exd}$  reaches 0.12, 0.13 and 0.14 with respect to 0%, 2% and 4%  $\varepsilon_{LK1}$  values. It has also been observed that increasing  $\varepsilon_{LK1}$  increases the  $f_{exd}$  level, so it causes a decline in performance.

In Figure 5.10 (d), it has been observed that  $TSFC$  reaches a minimum point at a certain  $T_{max}$  value for each  $\varepsilon_{LK1}$ . If  $TSFC$  is considered as the objective function, optimum  $T_{max}$  values are 1385, 1399 and 1414 K at 0%, 2% and 4%  $\varepsilon_{LK1}$  values respectively. Corresponding minimum  $TSFC$  values are 18.4, 18.6 and 18.8 g kN<sup>-1</sup>s<sup>-1</sup> respectively. It has been seen that optimum  $T_{max}$  values become larger when  $\varepsilon_{LK1}$  is increased. Also, it is clear that  $\varepsilon_{LK1}$  has a negative effect on  $TSFC$  performance, since it increases the  $TSFC$  level.

In Figure 5.10 (e), it has been seen that  $F_s$  increases with increasing  $T_{max}$ ; therefore, there is not a certain optimum  $T_{max}$  value maximizing the  $F_s$ . Considering  $T_{max}$  equals to 1800 K as the upper limit, maximum  $F_s$  values are 187.7, 187.6 and 187.4 N s kg<sup>-1</sup> with respect to 0%, 2% and 4%  $\varepsilon_{LK1}$  values. It is clear that  $\varepsilon_{LK1}$  causes a distortion in  $F_s$  but slightly.

It has been observed in Figure 5.10 (f) that  $\dot{S}_{gen}$  increases with increasing  $T_{max}$ . Therefore, if  $\dot{S}_{gen}$  wanted to be minimized, small values of  $T_{max}$  should be selected. As a lower limit, 1250 K has been selected for  $T_{max}$  and corresponding minimum  $\dot{S}_{gen}$  values have been calculated as 66.5, 69.8 and 73.2 kW K<sup>-1</sup> with respect to 0%, 2% and 4%  $\varepsilon_{LK1}$  values. It is also clear that increasing  $\varepsilon_{LK1}$  causes an increase in  $\dot{S}_{gen}$  so a decline in performance.

In Figure 5.10 (g), it has been observed again that  $T_{max}$  shows different characteristics for  $CEP$  and  $\eta_o$ . Since  $CEP$  is maximum at larger  $T_{max}$  values but  $\eta_o$  is maximum at relatively smaller  $T_{max}$  values, there is not an optimum region in Figure 5.10 (g) for having maximum of  $CEP$  and  $\eta_o$  together. As  $CEP$  increases with increasing  $T_{max}$ ,  $\eta_o$  value starts to decline after its maximum peak point.

### 5.2.3 Optimum values of performance indicators with respect to design parameters

All of the above mentioned optimum values of  $r_{C,Total}$ ,  $r_F$ ,  $\beta$  and  $T_{max}$  with corresponding maximum values of  $CEP$ ,  $\eta_o$ ,  $F_s$  and minimum values of  $f_{exd}$ ,  $TSFC$  and  $\dot{S}_{gen}$  have been summarized and illustrated together in Table 5.2. These calculation have been presented at three levels of  $\varepsilon_{LK1}$ , 0%, 2% and 4%. In all of the calculations,  $\varepsilon_{LK2}$  has been kept constant at 2%.

The yellow highlighted values in Table 5.2 represent the active constraints which do not make a peak minimum or maximum. Instead, values of  $CEP$ ,  $\eta_o$ ,  $F_s$ ,  $f_{exd}$ ,  $TSFC$  and  $\dot{S}_{gen}$  have been calculated at a limiting maximum or minimum point of  $r_{C,Total}$ ,  $r_F$ ,  $\beta$  and  $T_{max}$  as stated above in the comments of Figures 5.7 - 5.10.

### 5.2.4 Relative change of performance indicators at different levels of design parameters with respect to change in $\varepsilon_{LK1}$

Relative % changes of  $CEP$ ,  $\eta_o$ ,  $f_{exd}$ ,  $TSFC$ ,  $F_s$  and  $\dot{S}_{gen}$  when  $\varepsilon_{LK1}$  is shifted from 0% to 2%, and from 2% to 4% have been calculated for three levels of  $r_{C,Total}$ ,  $r_F$ ,  $\beta$  and  $T_{max}$ , which are small, optimum and large. The purpose here is to determine relative % change of each performance indicator when heat leakage ratio one is increased to 2% and 4% in order to observe characteristic of effect of heat leakage ratio one on the performance indicators. This observation has been done for small values, optimum values and large values of design parameters ( $r_{C,Total}$ ,  $r_F$ ,  $\beta$  and  $T_{max}$ ) in order to observe this effect for different ranges of design parameters. In other words, considering  $\varepsilon_{LK1}$  may have different relative % effect on the values of performance indicators, investigation of this effect have been performed at different design parameter levels.

**Table 5.2 :** The optimum values of design parameters and corresponding maximum values of  $CEP$ ,  $\eta_o$  and  $F_s$  and minimum values of  $f_{exd}$ ,  $TSFC$  and  $\dot{S}_{gen}$  at  $\varepsilon_{LK1} = 0\%$ ,  $2\%$  and  $4\%$  when  $\varepsilon_{LK2} = 2\%$ .

$\varepsilon_{LK1}$ (%)	$r_{C,Total,opt}$	$CEP_{max}$	$r_{C,Total,opt}$	$\eta_{o,max}$	$r_{C,Total,opt}$	$f_{exd,min}$	$r_{C,Total,opt}$	$TSFC_{min}$	$r_{C,Total,opt}$	$F_{s,max}$	$r_{C,Total,act}$	$\dot{S}_{gen,min}$
0	13.0	1.42	20.0	0.314	10.0	0.156	19.7	18.6	7.2	128.9	29	64.9
2	12.9	1.33	18.9	0.308	10.0	0.165	18.7	18.9	7.1	127.6	29	68.0
4	12.7	1.24	17.9	0.301	10.0	0.174	17.7	19.3	7.0	126.2	29	71.1
$\varepsilon_{LK1}$ (%)	$r_{F,opt}$	$CEP_{max}$	$r_{F,opt}$	$\eta_{o,max}$	$r_{F,act}$	$f_{exd,min}$	$r_{F,opt}$	$TSFC_{min}$	$r_{F,opt}$	$F_{s,max}$	$r_{F,act}$	$\dot{S}_{gen,min}$
0	1.5064	1.45	1.67	0.312	1.30	0.14	1.67	18.7	1.59	118.3	1.30	62.7
2	1.5081	1.35	1.65	0.308	1.30	0.15	1.65	18.9	1.57	116.9	1.30	67.1
4	1.5069	1.27	1.64	0.303	1.30	0.16	1.63	19.2	1.56	115.4	1.30	71.4
$\varepsilon_{LK1}$ (%)	$\beta_{act}$	$CEP_{max}$	$\beta_{opt}$	$\eta_{o,max}$	$\beta_{act}$	$f_{exd,min}$	$\beta_{opt}$	$TSFC_{min}$	$\beta_{act}$	$F_{s,max}$	$\beta_{act}$	$\dot{S}_{gen,min}$
0	1.0	1.72	5.7	0.312	1.0	0.12	5.7	18.7	1.0	313.3	1.0	42.5
2	1.0	1.58	5.6	0.308	1.0	0.13	5.6	18.9	1.0	312.6	1.0	46.1
4	1.0	1.47	5.4	0.303	1.0	0.14	5.4	19.2	1.0	311.8	1.0	49.5
$\varepsilon_{LK1}$ (%)	$T_{max,act}$	$CEP_{max}$	$T_{max,opt}$	$\eta_{o,max}$	$T_{max,act}$	$f_{exd,min}$	$T_{max,opt}$	$TSFC_{min}$	$T_{max,act}$	$F_{s,max}$	$T_{max,act}$	$\dot{S}_{gen,min}$
0	1800	1.81	1380	0.316	1800	0.12	1385	18.4	1800	187.7	1250	66.5
2	1800	1.66	1394	0.313	1800	0.13	1399	18.6	1800	187.6	1250	69.8
4	1800	1.54	1409	0.310	1800	0.14	1414	18.8	1800	187.4	1250	73.2



### 5.2.4.1 Relative % change of performance indicators at small, optimum and large $r_{C,Total}$ values

Relative % change of  $CEP$ ,  $\eta_o$ ,  $f_{exd}$ ,  $TSFC$ ,  $F_s$  and  $\dot{S}_{gen}$  corresponding to 2% increase (from 0% to 2%) and another additional 2% increase (from 2% to 4%) in  $\epsilon_{LK1}$  at small, optimum and large values of  $r_{C,Total}$  have been calculated and presented in Figure 5.11. The selected small and large level of  $r_{C,Total}$  are 5.0 and 29.0 in order to cover all values seen in Figure 5.7 (a)-(f) at 0%, 2% and 4%  $\epsilon_{LK1}$ .

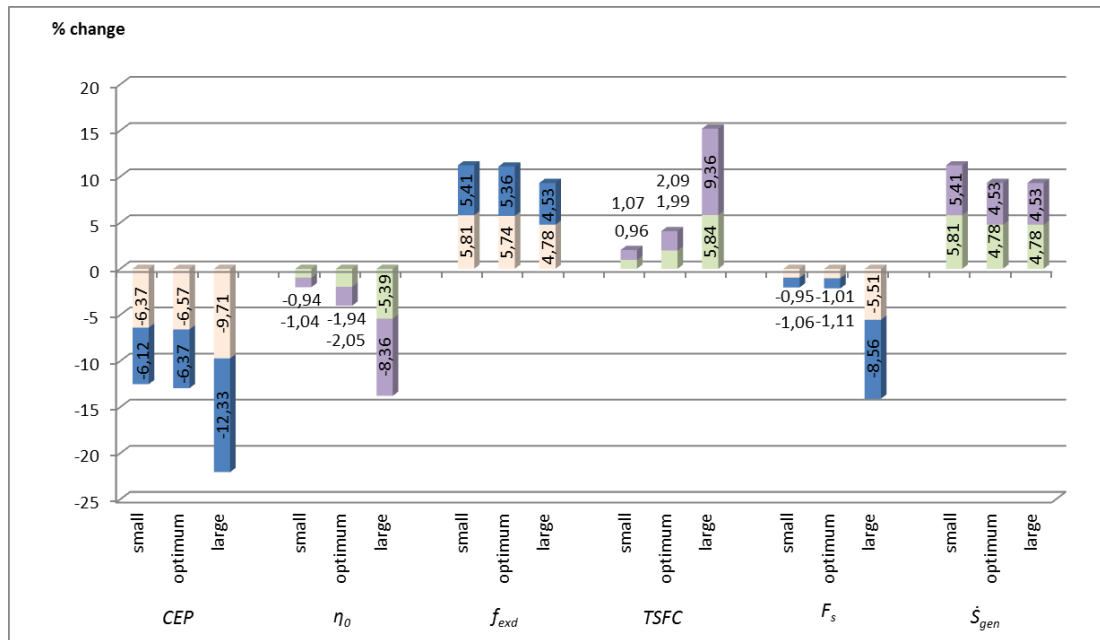


**Figure 5.11 :** Relative % change of performance indicators at small, optimum and large levels of  $r_{C,Total}$ .

By looking at Figure 5.11 and Figure 5.7 (a), it has been observed that effect of  $\epsilon_{LK1}$  on  $CEP$  is significant at all levels of  $r_{C,Total}$ . For the small  $r_{C,Total}$  value (5.0), increasing  $\epsilon_{LK1}$  by 2% causes 6.37% decrease in  $CEP$ , and additional 2% increase in  $\epsilon_{LK1}$  causes 6.12% decrease in  $CEP$ . At optimum level of  $r_{C,Total}$ , there is 6.57% and additional 6.37% decline in  $CEP$ , which means slightly more effective than small level of  $r_{C,Total}$ . At large  $r_{C,Total}$  (29.0), 2% increase in  $\epsilon_{LK1}$  causes 9.71% decrease and another additional 2% causes 12.33% decrease in  $CEP$ . Therefore, it is clear that  $\epsilon_{LK1}$  causes more distortion on  $CEP$  at larger levels of  $r_{C,Total}$  compared to small and optimum levels, yet  $\epsilon_{LK1}$  has significantly effective on  $CEP$  at all levels.

In Figure 5.11 and Figure 5.7 (b), it is clearly observable that effect of  $\epsilon_{LK1}$  on  $\eta_o$  is significantly larger at larger  $r_{C,Total}$  levels. As seen in Figure 5.7 (b), lines of 0%, 2%

and 4%  $\varepsilon_{LK1}$  separates from each other more significantly as  $r_{C,Total}$  gets larger. In Figure 5.11, it has been represented numerically. Comparing to 0.94% and 1.04% decline in  $\eta_o$  at small value of  $r_{C,Total}$ , and 1.94% and 2.05% decline in  $\eta_o$  at optimum level of  $r_{C,Total}$ ; 5.39% and 8.36% decline in  $\eta_o$  at large value of  $r_{C,Total}$  is far more significant. These values are valid for first 2% increase and further 2% increase in  $\varepsilon_{LK1}$  respectively. Therefore, it is evident that  $\varepsilon_{LK1}$  is significantly more effective on  $\eta_o$  at larger  $r_{C,Total}$  values, of course in a negative way.

It has been observed by looking at Figure 5.11 and Figure 5.7 (c) that effect of  $\varepsilon_{LK1}$  on  $f_{exd}$  is significant at all levels of  $r_{C,Total}$ . In Figure 5.11, it has been seen that 2% increase in  $\varepsilon_{LK1}$  causes 5.81% increase in  $f_{exd}$  and another 2% causes 5.41% increase at small level of  $r_{C,Total}$ . Slightly less significant, increase in  $\varepsilon_{LK1}$  causes 5.74% and 5.36% increase in  $f_{exd}$ . And lastly, at large level of  $r_{C,Total}$ ,  $\varepsilon_{LK1}$  causes 4.78% and 4.53% increase in  $f_{exd}$ . Therefore, it is clear that negative effect of  $\varepsilon_{LK1}$  on  $f_{exd}$  is more significant at smaller levels of  $r_{C,Total}$  compared to larger levels, recognizing that it is significant for all levels.

In Figure 5.7 (d), it has been seen that effect of  $\varepsilon_{LK1}$  on  $TSFC$  is clearly observable by the divergence of the lines at larger  $r_{C,Total}$  values. In Figure 5.11, it has been shown that at small level of  $r_{C,Total}$ ,  $TSFC$  is increased by 0.96% and 1.07% with the increase of  $\varepsilon_{LK1}$  by 2% and another 2% respectively. Also, it has been seen that at optimum level of  $r_{C,Total}$ , this effect is 1.99% and 2.09% respectively. As seen, it is more significant than the effect at small level of  $r_{C,Total}$ . And lastly, at larger  $r_{C,Total}$  level,  $\varepsilon_{LK1}$  causes 5.84% and 9.36% increase in  $TSFC$  for 2% and additional 2% increase respectively. Therefore, it is evident that  $\varepsilon_{LK1}$  is more effective on  $TSFC$  at larger levels of  $r_{C,Total}$ .

Figure 5.7 (e) shows the similar pattern with Figure 5.7 (d) that is divergence of lines caused by heat leakage ( $\varepsilon_{LK1}$ ) in Figure 5.7 (e) becomes more obvious at larger levels of  $r_{C,Total}$ . At small level of  $r_{C,Total}$ ,  $F_s$  is decreased by 0.95% and 1.06% and at optimum level of  $r_{C,Total}$ , this distortion effect is 1.01% and 1.11% for 2% and another additional 2% increase in  $\varepsilon_{LK1}$ . However, at larger level of  $r_{C,Total}$  this effect becomes very significant and numerically 5.51% and 8.56% decrease in  $F_s$  have been

observed. Therefore, it has been clearly observed that effect of  $\varepsilon_{LK1}$  is more significant on  $F_s$  at larger values of  $r_{C,Total}$ .

By looking at Figure 5.11 and Figure 5.7 (f), it has been seen that effect of  $\varepsilon_{LK1}$  on  $\dot{S}_{gen}$  is significant at all levels of  $r_{C,Total}$ . With respect to 2% increase and another additional 2% increase in  $\varepsilon_{LK1}$ ,  $\dot{S}_{gen}$  is increased 5.81% and 5.41% at small level of  $r_{C,Total}$ , 4.78% and 4.53% at optimum level of  $r_{C,Total}$  and lastly 4.78% and 4.53% at larger level of  $r_{C,Total}$ . It has been concluded that effect of  $\varepsilon_{LK1}$  on  $\dot{S}_{gen}$  is comparably more significant at smaller  $r_{C,Total}$  values, acknowledging the fact that it is significant at all  $r_{C,Total}$  levels.

Analyzing Figure 5.7 (a)-(f) and Figure 5.11, two important additional observation have been made. Firstly, effect of  $\varepsilon_{LK1}$  on performance indicators is not linear. That is first 2% increase in  $\varepsilon_{LK1}$  causes certain % distortion in performance indicators, and additional 2% increase in  $\varepsilon_{LK1}$  causes another % distortion, sometimes being less sometimes being more than the first 2% but not equal. Secondly, it has been observed that effect of  $\varepsilon_{LK1}$  is significant on  $CEP$ ,  $f_{exd}$  and  $\dot{S}_{gen}$  at all levels of  $r_{C,Total}$ , that is more independent from  $r_{C,Total}$  level.

#### **5.2.4.2 Relative % change of performance indicators at small, optimum and large $r_F$ values**

Relative % change of  $CEP$ ,  $\eta_o$ ,  $f_{exd}$ ,  $TSFC$ ,  $F_s$  and  $\dot{S}_{gen}$  corresponding to 2% increase (from 0% to 2%) and another additional 2% increase (from 2% to 4%) in  $\varepsilon_{LK1}$  at small, optimum and large values of  $r_F$  have been calculated and presented in Figure 5.12. The selected small and large level of  $r_F$  are 1.30 and 1.80 in order to cover all values seen in Figure 5.8 (a)-(f) at 0%, 2% and 4%  $\varepsilon_{LK1}$ .

By looking at Figure 5.12 and Figure 5.8 (a), it has been observed that effect of  $\varepsilon_{LK1}$  on  $CEP$  is significant at all levels of  $r_F$ . At small level of  $r_F$  (1.30),  $CEP$  is decreased by 7.01% and 6.58% with respect to 2% and additional 2% increase in  $\varepsilon_{LK1}$ . At optimum level, this decreasing effect is 6.66% and 6.37% being slightly less significant than small level. Lastly, at large level of  $r_F$  (1.80), 2% increase in  $\varepsilon_{LK1}$  causes 9.71% decrease in  $CEP$  and additional 2% increase in  $\varepsilon_{LK1}$  causes additional 12.33% decrease in  $CEP$ . It is clear that negative effect of  $\varepsilon_{LK1}$  on  $CEP$  is significant at all levels of  $r_F$ , but it is slightly more significant at large  $r_F$  level.

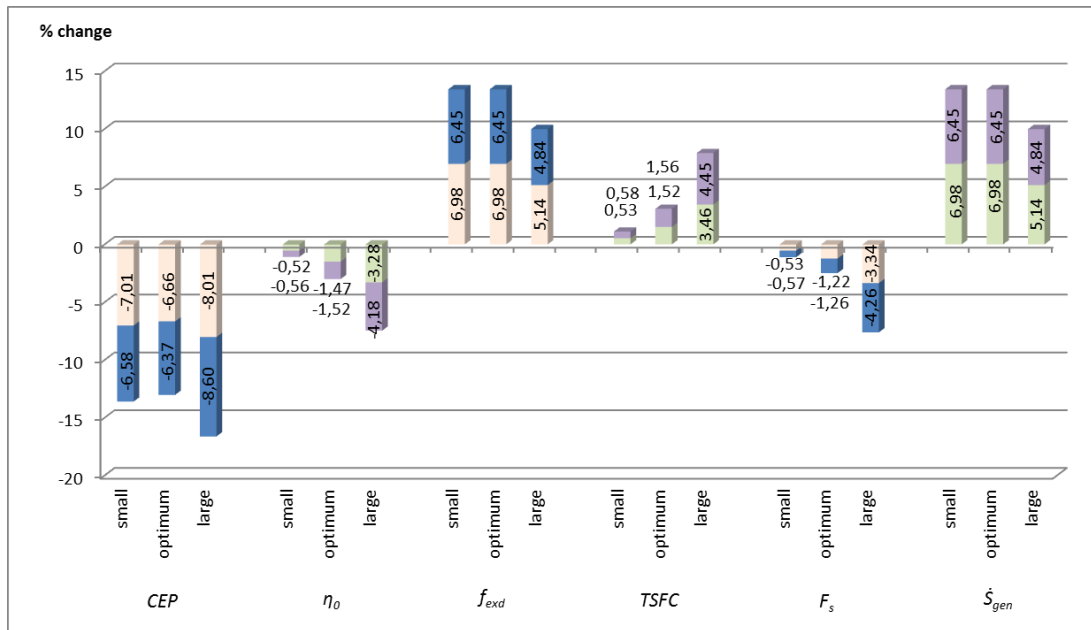


**Figure 5.12 :** Relative % change of performance indicators at small, optimum and large levels of  $r_F$ .

In Figure 5.12 and Figure 5.8 (b) it has been observed that as  $r_F$  increases, relative effect of  $\varepsilon_{LK1}$  on  $\eta_0$  becomes larger. In Figure 5.8 (b), this effect is observable when looked at the right side of the figure as the lines of different  $\varepsilon_{LK1}$  levels diverge more clearly. At small level of  $r_F$ , 2% increase in  $\varepsilon_{LK1}$  causes 0.52% decrease in  $\eta_0$  and additional 2% causes 0.56% decrease. At optimum level, this decreasing effect is 1.47% and 1.52% which is more significant than small level of  $r_F$ . And more significantly, 2% increase in  $\varepsilon_{LK1}$  causes 3.28% decrease in  $\eta_0$  and additional 2% causes 4.18% additional decrease. As realized, decreasing effect of  $\varepsilon_{LK1}$  on  $\eta_0$  is less significant at smaller  $r_F$  levels, while it becomes more significant at larger  $r_F$  levels.

It has been observed in Figure 5.12 and Figure 5.8 (c) that effect of  $\varepsilon_{LK1}$  on  $f_{exd}$  is significant at all levels of  $r_F$ . Numerically, at small level of  $r_F$ , 2% increase in  $\varepsilon_{LK1}$  causes 6.98% increase in  $f_{exd}$  and additional 2% increase in  $\varepsilon_{LK1}$  causes an additional 6.45% increase in  $f_{exd}$ . Since  $f_{exd}$  does not make a minimum peak at some certain  $r_F$  (active constraint) as seen in Table 5.2, small level of  $r_F$  had been considered as a lower limit that maximize  $f_{exd}$ . Therefore, at optimum level, the effect is the same as small level due to the fact that optimum level and small level of  $r_F$  are the same (1.30) for  $f_{exd}$ . Lastly, at large level of  $r_F$ , consecutive two 2% increases in  $\varepsilon_{LK1}$  causes 5.14% and 4.84% increase in  $f_{exd}$  which is less significant than lower levels of  $r_F$ . It has been observed that effect of  $\varepsilon_{LK1}$  on  $f_{exd}$  is

comparatively more significant at lower levels of  $r_F$ ; although, it is significant at all levels.

By looking at Figure 5.8 (d), it has been seen that effect of  $\varepsilon_{LK1}$  shows similar pattern to Figure 5.8 (b), that is effect of  $\varepsilon_{LK1}$  on  $TSFC$  becomes more significant as  $r_F$  becomes larger. This effect is again observable in Figure 5.8 (d) with diverging lines at right side (larger  $r_F$  levels). At small level of  $r_F$ ,  $TSFC$  is increased by 0.53% with 2% increase in  $\varepsilon_{LK1}$  and additional 2% causes additional 0.58% increase in  $TSFC$ . At optimum level, being slightly more significant,  $TSFC$  is increased by 1.52% and 1.56% with two consecutive 2% increases in  $\varepsilon_{LK1}$  at optimum level of  $r_F$ . Then, at larger  $r_F$  level, this effect is 3.46% and 4.45% which is clearly more significant than smaller levels.

In Figure 5.8 (e), there is a similar pattern with Figure 5.8 (b) and Figure 5.8 (d). As  $r_F$  becomes larger, effect of  $\varepsilon_{LK1}$  on  $F_s$  becomes more significant. Numerically, at small level of  $r_F$ ,  $F_s$  decreases by 0.53% and 0.57% with 2% and additional 2% increase in  $\varepsilon_{LK1}$ , while these figures are 1.22% and 1.26% at optimum  $r_F$  level. More significantly,  $\varepsilon_{LK1}$  causes 3.34% and 4.26% decrease in  $F_s$  with two consecutive 2% increases in  $\varepsilon_{LK1}$ . Therefore, it is evident that negative effect of  $\varepsilon_{LK1}$  on  $F_s$  is more significant at larger  $r_F$  values.

And lastly, it has been seen in Figure 5.8 (f) that  $\varepsilon_{LK1}$  is significantly effective on  $\dot{S}_{gen}$ . In Figure 5.12, it has been observed that at small level of  $r_F$ ,  $\dot{S}_{gen}$  increases by 6.98% and by 6.45% with 2% and additional 2% increase in  $\varepsilon_{LK1}$ . The same numbers are also valid for optimum  $r_F$  level, since  $r_F$  is an active constraint for  $\dot{S}_{gen}$  and the minimum  $\dot{S}_{gen}$  is reachable at minimum  $r_F$  as discussed earlier and demonstrated in Table 5.2 above. At large level of  $r_F$ , these figures become 5.14% and 4.84% respectively, which are clearly more significant compared to lower levels of  $r_F$ . However, it is still a fact that effect of  $\varepsilon_{LK1}$  on  $\dot{S}_{gen}$  is significant for all levels of  $r_F$ .

Again analyzing Figure 5.8 (a)-(f) and Figure 5.12, two additional observations have been made. Firstly, effect of  $\varepsilon_{LK1}$  on performance indicators is again not linear. Secondly,  $CEP$ ,  $f_{exd}$  and  $\dot{S}_{gen}$  have been effected by  $\varepsilon_{LK1}$  more significantly at all levels of  $r_F$ , that is again effect of heat leakage on these three performance indicators are more independent of  $r_F$  level.

### 5.2.4.3 Relative % change of performance indicators at small, optimum and large $\beta$ values

Relative % change of  $CEP$ ,  $\eta_o$ ,  $f_{exd}$ ,  $TSFC$ ,  $F_s$  and  $\dot{S}_{gen}$  corresponding to 2% increase (from 0% to 2%) and another additional 2% increase (from 2% to 4%) in  $\varepsilon_{LK1}$  at small, optimum and large values of  $\beta$  have been calculated and presented in Figure 5.13. The selected small and large level of  $\beta$  are 1.0 and 7.0 in order to cover all values seen in Figure 5.9 (a)-(f) at 0%, 2% and 4%  $\varepsilon_{LK1}$ .

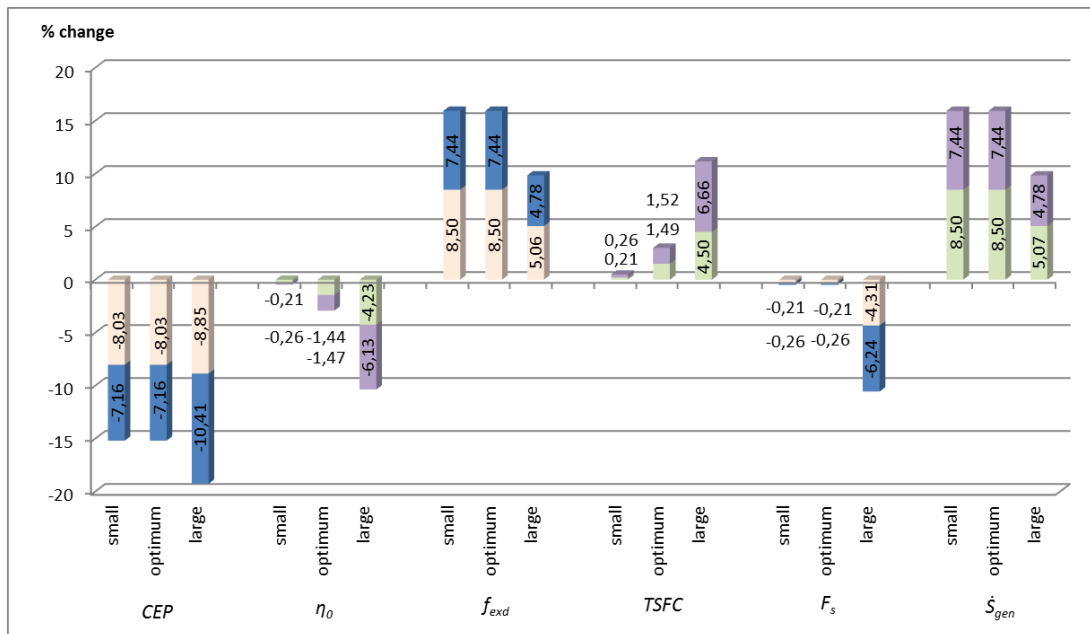


**Figure 5.13 :** Relative % change of performance indicators at small, optimum and large levels of  $\beta$ .

It has been observed by looking at Figure 5.9 (a) that effect of  $\varepsilon_{LK1}$  on  $CEP$  is significant at all levels of  $\beta$ . As observed in Figure 5.13, at small level of  $\beta$  (1.0), 2% increase in  $\varepsilon_{LK1}$  causes 8.03% decrease in  $CEP$ , and another 2% increase in  $\varepsilon_{LK1}$  causes additional 7.16% decrease in  $CEP$ . Since  $CEP$  does not make a maximum at a certain  $\beta$  value (active constraint) as seen in Figure 5.13 and the maximum value that  $CEP$  reaches is realized at minimum  $\beta$  as seen in Figure 5.9 (a), optimum  $\beta$  level is equal to the small  $\beta$  level (1.0). Therefore, effect of 2% and additional 2%  $\varepsilon_{LK1}$  is the same; 8.03% and 7.16%. And lastly, at large level of  $\beta$  (7.0),  $CEP$  is decreased by 8.85% and additional 10.41% due to 2% and additional 2% increase in heat leakage ( $\varepsilon_{LK1}$ ). As seen, this effect at large  $\beta$  level is more significant compared to that of small level (and optimum level) of  $\beta$ , considering that effect of  $\varepsilon_{LK1}$  on  $CEP$  is significant at all levels of  $\beta$ .

By looking at Figure 5.9 (b) and Figure 5.13, it has been seen that effect of  $\varepsilon_{LK1}$  becomes more significant as  $\beta$  gets larger. It has been observed that at small level of  $\beta$ , 2% increase in  $\varepsilon_{LK1}$  causes 0.21% decrease in  $\eta_o$ . Also, another 2% increase causes additional 0.26% decrease. At optimum level of  $\beta$ , successive 2% increases cause 1.44% and 1.47% decreases in  $\eta_o$ , which is a larger effect than small  $\beta$  level. At larger level of  $\beta$ , these effects becomes 4.23% and 6.13% decrease in  $\eta_o$ , which is significantly larger than small and optimum level  $\beta$  value. It is clear that as  $\beta$  increases, effect of heat leakage ( $\varepsilon_{LK1}$ ) on  $\eta_o$  becomes more significant.

It has been observed in Figure 5.9 (c) and Figure 5.13 that effect of  $\varepsilon_{LK1}$  on  $f_{exd}$  is significant for all levels of  $\beta$ . As seen in Figure 5.9 (c),  $f_{exd}$  does not have a minimum peak with respect to  $\beta$ , so the minimum  $\beta$  is active constraint for  $f_{exd}$ , and minimum and optimum  $\beta$  values are the same (1.0). At that minimum level of  $\beta$ , 2% increase in  $\varepsilon_{LK1}$  causes 8.50% increase in  $f_{exd}$  and additional 2% increase in  $\varepsilon_{LK1}$  causes 7.44% additional increase in  $f_{exd}$ . At large level of  $\beta$ , this effect becomes 5.06% and 4.78%, which is less significant than small level of  $\beta$ . Therefore, it has been observed that effect of  $\varepsilon_{LK1}$  on  $f_{exd}$  is more significant at small level of  $\beta$ ; although, it is significant at all levels.

In Figure 5.9 (d) and Figure 5.13, it has been seen that effect of  $\varepsilon_{LK1}$  on  $TSFC$  increases with increasing  $\beta$ , due to diverging lines at larger  $\beta$  values. Numerically, at small  $\beta$  value, 2% increase in  $\varepsilon_{LK1}$  causes 0.21% and additional 2% causes 0.26% increase in  $TSFC$ . At optimum level of  $\beta$ ,  $TSFC$  is increased by 1.49% and 1.52% by first 2% and second 2% increase in  $\varepsilon_{LK1}$ . And lastly, this effect becomes 4.50% and 6.66% at large  $\beta$  value. Therefore, it has been observed that  $TSFC$  has been affected by  $\varepsilon_{LK1}$  more significantly at large  $\beta$  level compared to small  $\beta$  level.

By looking at Figure 5.9 (e) and Figure 5.13, it has been seen that effect of  $\varepsilon_{LK1}$  is less significant except at the large edge of  $\beta$ . Since  $F_s$  does not make a peak with respect to  $\beta$ , and decreases with increasing  $\beta$ , optimum point giving the maximum  $F_s$  for  $\beta$  is the small limit, (1.0). Therefore, optimum and small  $\beta$  is the same. When it comes to investigating the effect of  $\varepsilon_{LK1}$ , at small level of  $\beta$ , 2% increase in  $\varepsilon_{LK1}$  causes 0.21% decrease in  $F_s$  and another 2% causes 0.26% decrease. At larger level, this effect becomes 4.31% and 6.24% respectively. This numbers and Figure 5.9 (e)

shows that effect of  $\varepsilon_{LK1}$  is nearly insignificant on  $F_s$  except very high level of  $\beta$  such as (7.0).

It has been observed in Figure 5.9 (f) that effect of  $\varepsilon_{LK1}$  on  $\dot{S}_{gen}$  is significant at all levels of  $\beta$ . In Figure 5.13, it has been seen that at small level of  $\beta$ ,  $\dot{S}_{gen}$  has been increased by 8.50% and 7.44% due to 2% and additional 2% increase in  $\varepsilon_{LK1}$ . Optimum level of  $\beta$  is the same as small level of  $\beta$ , since  $\dot{S}_{gen}$  does not make a peak with respect to  $\beta$ , and it becomes larger as  $\beta$  is selected larger. Therefore, in order to have smaller  $\dot{S}_{gen}$  values,  $\beta$  has been selected as small as possible, which is (1.0). Hence, effect of  $\varepsilon_{LK1}$  on  $\dot{S}_{gen}$  is the same; numerically, 8.50% and 7.44%. At large level of  $\beta$ , this effect becomes 5.07% and 4.78% increase in  $\dot{S}_{gen}$  due to 2% and another 2% increase in  $\varepsilon_{LK1}$ . Therefore, it has been observed that  $\varepsilon_{LK1}$  is more effective on  $\dot{S}_{gen}$  at small levels of  $\beta$  compared to large level of  $\beta$ , pointing that it is significantly effective at all levels of  $\beta$ .

Analyzing Figure 5.9 (a)-(f) and Figure 5.13, two additional observations have been stated. First, the effect of  $\varepsilon_{LK1}$  on performance indicators is not linear. Second,  $CEP$ ,  $f_{exd}$  and  $\dot{S}_{gen}$  have been effected by  $\varepsilon_{LK1}$  more significantly at all levels of  $\beta$ , that is again effect of heat leakage on these three performance indicators are more independent of  $\beta$  level. On the other hand, effect of  $\varepsilon_{LK1}$  on  $\eta_o$ ,  $TSFC$  and  $F_s$  is more dependent on  $\beta$  level, since it changes the significance of effect of  $\varepsilon_{LK1}$ .

#### **5.2.4.4 Relative % change of performance indicators at small, optimum and large $T_{max}$ values**

Relative % change of  $CEP$ ,  $\eta_o$ ,  $f_{exd}$ ,  $TSFC$ ,  $F_s$  and  $\dot{S}_{gen}$  corresponding to 2% increase (from 0% to 2%) and another additional 2% increase (from 2% to 4%) in  $\varepsilon_{LK1}$  at small, optimum and large values of  $T_{max}$  have been calculated and presented in Figure 5.14. The selected small and large level of  $T_{max}$  are 1250 K and 1800 K in order to cover all values seen in Figure 5.10 (a)-(f) at 0%, 2% and 4%  $\varepsilon_{LK1}$ .

As seen in Figure 5.10 (a) and Figure 5.14, effect of  $\varepsilon_{LK1}$  on  $CEP$  is significant at all levels of  $T_{max}$ . At small level of  $T_{max}$  (1250 K), 2% increase in  $\varepsilon_{LK1}$  causes 7.54% decrease in  $CEP$  and additional 2% of  $\varepsilon_{LK1}$  causes 7.85% decrease in  $CEP$ . As  $CEP$  increases with increasing  $T_{max}$ , there is not a maximum peak. Instead,  $T_{max}$  equals



to 1800 K has been selected as the point that  $CEP$  reaches the maximum value for this interval of  $T_{max}$  (active constraint). Therefore, optimum  $T_{max}$  for  $CEP$  is equal to maximum  $T_{max}$ , 1800 K. At large (and optimum) level of  $T_{max}$ ,  $CEP$  is decreased by 7.89% and 7.24% consecutively due to 2% and additional 2% increase in  $\epsilon_{LK1}$ .

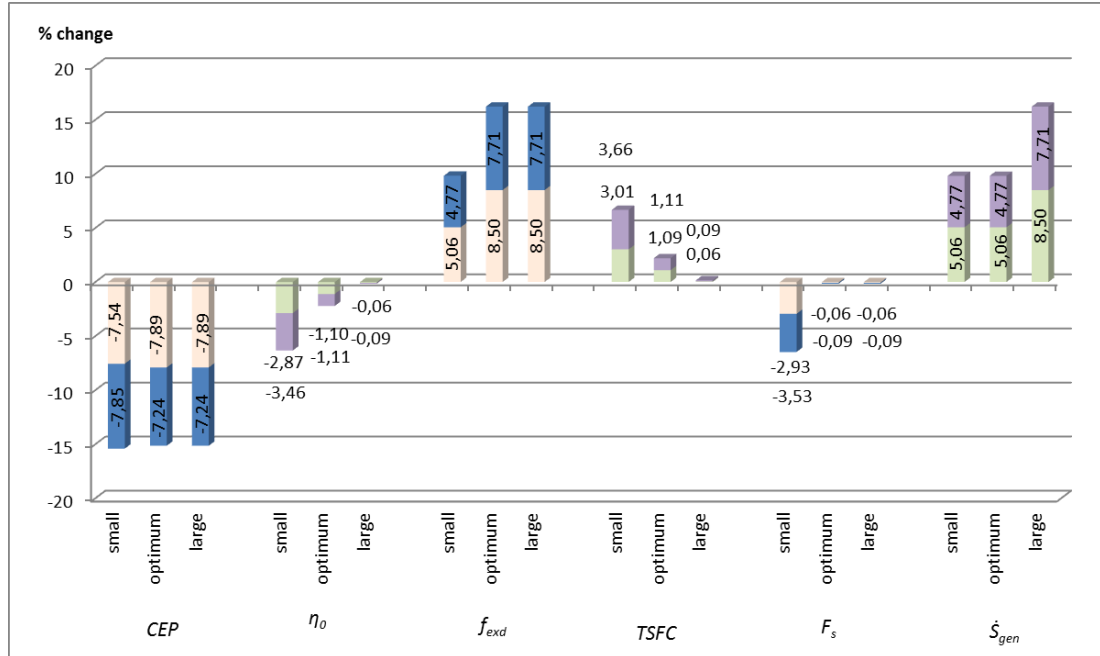


**Figure 5.14 :** Relative % change of performance indicators at small, optimum and large levels of  $T_{max}$ .

In Figure 5.10 (b) and Figure 5.14, it has been observed that  $\eta_0$  is effected by  $\epsilon_{LK1}$  more significantly at small values of  $T_{max}$  compared to large values of it. At small  $T_{max}$ , 2% increase in  $\epsilon_{LK1}$  causes 2.87% decrease in  $\eta_0$  and another 2% increase in  $\epsilon_{LK1}$  causes 3.46% decrease in  $\eta_0$ . At optimum level of  $T_{max}$ ,  $\eta_0$  has been decreased by 1.10% and 1.11% due to 2% and another 2% increase in  $\epsilon_{LK1}$  respectively. Also, at large level of  $T_{max}$ , this effect becomes only 0.06% and 0.09%. Therefore, it is evident that  $\eta_0$  is effected by  $\epsilon_{LK1}$  significantly when  $T_{max}$  is small; however, this effect becomes insignificant as  $T_{max}$  becomes larger.

By looking at Figure 5.10 (c) and Figure 5.14, it has been observed that effect of  $\epsilon_{LK1}$  on  $f_{exd}$  is significant for all levels of  $T_{max}$ . At small level of  $T_{max}$ , 2% increase in  $\epsilon_{LK1}$  causes 5.06% increase in  $f_{exd}$ . An additional 2% increase in  $\epsilon_{LK1}$  causes additional 4.77% increase in  $f_{exd}$ . Since  $f_{exd}$  does not make a peak minimum with respect to  $T_{max}$ , and it becomes smaller as  $T_{max}$  gets larger, the optimum  $T_{max}$  has been selected as the maximum value (1800 K) in order to have minimum  $f_{exd}$  at

that range (active constraint). At maximum level of  $T_{max}$ , effect of  $\varepsilon_{LK1}$  becomes 8.50% and 7.71% increase in  $f_{exd}$  due to 2% and additional 2% increase in  $\varepsilon_{LK1}$ . Therefore, it has been seen that as  $T_{max}$  becomes larger, effect of  $\varepsilon_{LK1}$  on  $f_{exd}$  becomes more significant.

It has been seen in Figure 5.10 (d) and Figure 5.14 that effect of  $\varepsilon_{LK1}$  on  $TSFC$  is significant at small values of  $T_{max}$  and this effect becomes insignificant with increasing  $T_{max}$  value. Numerically, at small level of  $T_{max}$  2% increase in  $\varepsilon_{LK1}$  causes 3.01% increase in  $TSFC$  and additional 2% increase in  $\varepsilon_{LK1}$  causes additional 3.66% increase in  $TSFC$ . At optimum level of  $T_{max}$ , two consecutive 2% increases in  $\varepsilon_{LK1}$  causes 1.09% and 1.11% increase in  $TSFC$ . And lastly, at large values of  $T_{max}$ , this effect becomes 0.06% and 0.09%. Therefore, it has been concluded that negative effect of  $\varepsilon_{LK1}$  on  $TSFC$  is more significant at small levels of  $T_{max}$ , while it is comparably insignificant at larger levels of  $T_{max}$ .

In Figure 5.10 (e) and Figure 5.14, effect of  $\varepsilon_{LK1}$  on  $F_s$  with respect to  $T_{max}$  has been observed. At small level of  $T_{max}$ , increasing the  $\varepsilon_{LK1}$  by 2% causes 2.93% decrease in  $F_s$ . Additional 2% increase in  $\varepsilon_{LK1}$  causes 3.53% decrease in  $F_s$ . Since  $F_s$  does not make a maximum peak with respect to  $T_{max}$ , and  $F_s$  value increases with increasing  $T_{max}$ , in order to have maximum  $F_s$  value, maximum  $T_{max}$  value has been selected as optimum value (active constraint). Therefore, maximum level of  $T_{max}$  and optimum  $T_{max}$  value is the same. At that maximum level of  $T_{max}$ ,  $F_s$  decreases by 0.06% and 0.09% with respect to two consecutive 2% increases of  $\varepsilon_{LK1}$ . Therefore, it has been seen that at small values of  $T_{max}$ ,  $\varepsilon_{LK1}$  effect on  $F_s$  is more significant compared to that of large level of  $T_{max}$ .

Lastly in Figure 5.10 (f) and Figure 5.14, it has been seen that  $\dot{S}_{gen}$  has been effected due to heat leakage,  $\varepsilon_{LK1}$ , significantly. This effect is significant at all levels of  $T_{max}$  as seen in Figure 5.10 (f). In Figure 5.14, it has been observed that at small level of  $T_{max}$ ,  $\dot{S}_{gen}$  increases by 5.06% and 4.77% due to 2% and additional 2% increase in  $\varepsilon_{LK1}$ . Optimum  $T_{max}$  level is equal to the minimum  $T_{max}$  level since  $\dot{S}_{gen}$  does not make a minimum with respect to  $T_{max}$ , and it increases with increasing  $T_{max}$ . Therefore, minimum  $\dot{S}_{gen}$  at that range of  $T_{max}$  can be found at minimum  $T_{max}$ . At large level of  $T_{max}$ , effect of 2% increase in  $\varepsilon_{LK1}$  on  $\dot{S}_{gen}$  is 8.50% increase, and additional 2% increase causes 7.71% increase respectively. Therefore, it is evident

that effect of  $\varepsilon_{LK1}$  on  $\dot{S}_{gen}$  is significant at all levels of  $T_{max}$ ; however, it is more significant at larger levels of  $T_{max}$ .

Analyzing Figure 5.10 (a)-(f) and Figure 5.14, two additional observations have been made. First, the effect of  $\varepsilon_{LK1}$  on performance indicators is not linear. Second,  $CEP$ ,  $f_{exd}$  and  $\dot{S}_{gen}$  have been effected by  $\varepsilon_{LK1}$  more significantly at all levels of  $T_{max}$ , that is again effect of heat leakage on these three performance indicators are more independent of  $T_{max}$  level. On the other hand, effect of  $\varepsilon_{LK1}$  on  $\eta_o$ ,  $TSFC$  and  $F_s$  is more dependent on  $T_{max}$  level, since it changes the significance of effect of  $\varepsilon_{LK1}$ .



## 6. CONCLUSIONS AND RECOMMENDATIONS

In this thesis, the main purpose is to investigate the effects of heat leakage on the optimal performance of a twin-spool turbofan engine during the cruise phase of a commercial aircraft. There have been considered six different performance indicators, namely the coefficient of ecological performance  $CEP$ , the overall efficiency  $\eta_o$ , the exergy destruction factor  $f_{exd}$ , the thrust specific fuel consumption  $TSFC$ , the specific thrust  $F_s$ , and the entropy generation rate  $\dot{S}_{gen}$ . The effects of heat leakage ratio one  $\varepsilon_{LK1}$ , and heat leakage ratio two  $\varepsilon_{LK2}$ , at three different values namely 0.00, 0.02 and 0.04, on these six performance indicators have been investigated when design parameters have been considered as variable on different ranges. These design parameters are the total compressor pressure ratio  $r_{C,Total}$ , the fan pressure ratio  $r_F$ , the bypass air ratio  $\beta$ , and maximum turbine inlet temperature  $T_{max}$ .

Firstly, operating conditions of aircraft and parameters of the engine have been set, and related equations have been derived starting from the entrance until the exit of the engine. Secondly, optimal operating areas have been determined for each design parameter considering six performance indicators. And lastly, effect of heat leakage on the optimal performance of the engine in term of both design parameters and performance indicators have been investigated.

### 6.1 Conclusions of the Thesis

Conclusions of the thesis have been summarized as follows

- Considering two primary performance indicators namely  $CEP$  and  $\eta_o$ , very small values of  $r_{C,Total}$ ,  $r_F$  and  $T_{max}$  are not suitable areas to consider in design phase, since in these areas performance indicators shows sharp performance drops.
- Effect of one design parameter on any performance indicator is highly dependent on the values of other design parameters. Shape of the curve

changes for a performance indicator with respect to a design parameter when values of other design parameters are changed.

- Effect of heat leakage from combustion chamber to by-pass air through the CC wall ( $\varepsilon_{LK1}$ ) on the performance of a twin-spool turbofan engine is considerably more significant than the effect of heat leakage from by-pass air to environment ( $\varepsilon_{LK2}$ ).
- Effect of heat leakage one ( $\varepsilon_{LK1}$ ) is significant on  $CEP$ ,  $f_{exd}$  and  $\dot{S}_{gen}$  at all levels of design parameters including optimum levels.
- Effect of heat leakage one ( $\varepsilon_{LK1}$ ) is more significant on  $CEP$ ,  $f_{exd}$  and  $\dot{S}_{gen}$  at small and optimum values of  $r_{C,Total}$ ,  $r_F$  and  $\beta$ ; and at large and optimum values of  $T_{max}$  compared to effect on  $\eta_o$ ,  $TSFC$  and  $F_s$ .
- On the other hand, this effect is significant on  $\eta_o$ ,  $TSFC$  and  $F_s$  at large values of  $r_{C,Total}$ ,  $r_F$  and  $\beta$ ; and at small values of  $T_{max}$ .
- The different characteristic of effect of heat leakage one on  $CEP$ ,  $f_{exd}$  and  $\dot{S}_{gen}$  compared to effect on  $\eta_o$ ,  $TSFC$  and  $F_s$  is mainly due to the fact that the heat loss from the combustion chamber during the combustion is high-quality, and the process is highly irreversible. Large temperature difference between the combustion chamber and by-pass air causes an increase in entropy generation rate during this heat loss and exergy destruction rate also increases significantly. Therefore, the performance indicators which are derived by the 2<sup>nd</sup> Law of Thermodynamics ( $CEP$ ,  $f_{exd}$  and  $\dot{S}_{gen}$ ) are affected more significantly than the other performance indicators which are derived by the 1<sup>st</sup> Law of Thermodynamics ( $\eta_o$ ,  $TSFC$  and  $F_s$ ) by this heat loss even the loss amount is very small.
- Optimum values of design parameters are dependent on the amount of heat leakage, which means that as heat leakage amount changes, optimum values of design parameters and corresponding values of performance indicators also change.
- The effect of heat leakage on the performance indicators is not linear with respect to relative % change in performance indicators for different levels of heat leakage.

## 6.2 Recommendations for Future Studies

In this thesis, thermodynamic analysis for a twin-spool turbofan engine has been conducted in terms of energy and exergy. Effects of heat leakage on the optimal performance of these engines have been investigated. The selected configuration was front-fan, no-afterburner and no-mixed-exhaust type twin-spool turbofan engine with kerosene as a fuel.

For the future studies, a configuration with an afterburner can be selected to perform thermodynamic analysis. Due to a second combustion process after turbine exit, the mass flow rates, entropy generation rate and so exergy destruction rate, temperature of the flow at different stages, optimum design parameters and corresponding performance indicators would change. Also, effect of heat leakage would be analyzed both from first combustion and from second combustion, and it would make the analysis different from this thesis to be considered as a future study. In addition, examinations of rear-fan, mixed exhaust and triple-spool configurations would enrich the study.

Apart from the conventional transportation from one place to another in the world, space transportation has become a topic of interest for researchers. Recognizing the high investment values of conventional vehicles and engines for space transportation, researches have been focused on new solutions with reviews of current technologies (Hempsell, 2010). Turbojet, turbofan, turboramjet, scramjet, LACE (liquid air cycle engine) and SABRE (Synergetic air-breathing and rocket engine) have been investigated for new opportunities (Webber et al, 2007; Jivraj et al, 2007; Varvill and Bond, 2003; Cecere et al, 2014) .

Moreover, instead of flight speeds of conventional commercial aircrafts, which is around 0.8 – 0.9 Mach, some researchers have focused on higher speeds. Transportation in supersonic (1.2 – 5.0 Mach) and hypersonic (5.0 – 10.0 Mach) speeds have become a new interest area for many researchers. Transporting between any two places of the world in 4 – 5 hours with acceptable noise levels has become one of the main drivers of these researches (Jivraj et al, 2007).

For high level of speeds, researches have been focused on hydrogen instead of current fossil fuels both in terms of environmental effect and in terms of convenience

of thermophysical and thermochemical properties of hydrogen for thermodynamic cycles of such high-speed flights.

Derived from the SABRE engine, the Scimitar engine has been proposed for hypersonic speeds. This engine is an air-breathing engine utilizing hydrogen both as fuel and as pre-cooler of incoming air. It can operate both in subsonic speeds and in hypersonic speeds, and utilizes air, hydrogen and helium gases in its thermodynamic cycle (Jivraj et al, 2007).

Considering new fuel utilization other than conventional fossil fuels, hypersonic speeds of travel instead of conventional subsonic speeds of travel and complex thermodynamic cycle with introduction of hydrogen and helium instead of conventional aero-type engines (turbojet, turbofan etc.), the Scimitar engine is an opportunity for future studies. Analyzing its thermodynamic cycle, performing optimization of design parameters and assessing the energy and exergy performances is considered as a valuable contribution to the literature.



## REFERENCES

- Altuntas, O., Karakoc, T.H. and Hepbasli, A.** (2012). Exergetic, exergoeconomic and sustainability assessments of piston-prop aircraft engines. *Journal of Thermal Science and Technology*, 32 (2), 133-143.
- Aydin, H., Turan, O., Midilli, A. and Karakoc, T.H.** (2012). Energetic and exergo-economic analysis of a turboprop engine: A case study for CT7-9C. *International Journal of Exergy*, 11 (1), 69-88.
- Aydin, H., Turan, Ö., Karakoç, T.H. and Midilli, A.** (2013a). Exergo-sustainability indicators of a turboprop aircraft for the phases of a flight. *Energy*, 58, 550-560.
- Aydin, H., Turan, O., Midilli, A. and Karakoc, T.H.** (2013b). Energetic and exergetic performance assessment of a turboprop engine at various loads. *International Journal of Exergy*, 13 (4), 553-564.
- Aydin, H., Turan, O., Karakoc, T.H. and Midilli, A.** (2014a). Sustainability assessment of PW6000 turbofan engine: an exergetic approach. *International Journal of Exergy*, 14 (3), 388-412.
- Aydin, H., Turan, O., Midilli, A. and Karakoc, T.H.** (2014b). Exergetic performance of a low bypass turbofan engine at takeoff condition. In Dincer, I., Midilli, A., Kucuk, H. (Eds.), *Progress in Exergy, Energy and the Environment* (Vol.1, pp.293-303). Cham : Springer International Publishing.
- Balli, O., Aras, H., Aras, N. and Hepbasli, A.** (2008). Exergetic and exergoeconomic analysis of an Aircraft Jet Engine (AJE). *International Journal of Exergy*, 5 (5-6), 567-581.
- Balli, O. and Hepbasli, A.** (2013). Energetic and exergetic analyses of T56 turboprop engine. *Energy Conversion and Management*, 53 (1), 106-120.
- Balli, O. and Hepbasli, A.** (2014). Exergoeconomic, sustainability and environmental damage cost analyses of T56 turboprop engine. *Energy Conversion and Management*, 64 (1), 582-600.
- Baskharone, E.A.** (2006). *Principles of Turbomachinery in Air-Breathing Engines*. New York: Cambridge University Press.
- Bejan, A. and Siems, D.L.** (2001) The need for exergy analysis and thermodynamic optimization in aircraft development. *Exergy*, 1 (1), 14-24.
- Bejan, A., Tsatsaronis, G. and Moran, M.** (1996). *Thermal Design and Optimization*. New York: Wiley.

- Cecere, D., Giacomazzi, E. and Ingenito, A.** (2014). A review on hydrogen industrial aerospace applications. *International Journal of Hydrogen Energy*, 39 (20), 10731-10747.
- Chen, L., Zhang, W. and Sun F.** (2007). Power, efficiency, entropy generation rate and ecological optimization for a class of generalized irreversible universal heat engine cycles. *Applied Energy*, 84 (5), 512-525.
- Clarke, J.M., Horlock, J.H.** (1975). Availability and propulsion. *Journal of Mechanical Engineering Science*, 17 (4), 223-232.
- Cohen, H., Rogers, G.F.C. and Saravanamuttoo, H.I.H.** (1996). *Gas Turbine Theory*, 4th ed. Essex: Longman Group Limited.
- Colakoglu, M., Tanbay, T., Durmayaz, A. and Sogut, O.S.** (2014). Effect of Heat Leakage on the Performance of a Twin-Spool Turbofan Engine. In Canan Kandilli, (Ed.), *7<sup>th</sup> IEESE. Proceedings of the 7<sup>th</sup> International Ege Energy Symposium & Exhibition*, (pp. 477-500). Turkey : Usak University Green Economy Research and Application Centre, June 18-20.
- Colakoglu, M., Tanbay, T., Durmayaz, A. and Sogut, O.S.** (in press). Effect of heat leakage on the performance of a twin-spool turbofan engine. *International Journal of Exergy*.
- Connelly L, Koshland CP.** (2001a). Exergy and industrial ecology. Part 1: An exergy-based definition of consumption and a thermodynamic interpretation of ecosystem evolution. *Exergy, An International Journal*, 1 (3), 146-165.
- Connelly L, Koshland CP.** (2001b). Exergy and industrial ecology. Part 2: A non-dimensional analysis of means to reduce resource depletion. *Exergy, An International Journal*, 1 (4), 234-255.
- Çengel, Y.A. and Boles, M.A.** (2005). *Thermodynamics: An Engineering Approach*, 5<sup>th</sup> ed. New York: McGraw-Hill.
- Dagaut, P. and Cathonnet M.** (2006). The ignition, oxidation and combustion of kerosene: A review of experimental and kinetic modeling. *Progress in Energy and Combustion Science*, 32 (1), 48-92.
- Dincer, I. and Rosen, M.A.** (1998). Worldwide perspective on energy, environment and sustainable development. *International Journal of Energy Research*, 22 (15), 1305-1321.
- Dincer, I. and Rosen, M.A.** (2005). Thermodynamic aspects of renewables and sustainable development. *Renewable and Sustainable Energy Reviews*, 9 (2), 169-189.
- Dincer, I. and Rosen, M.A.** (2007). *Exergy: Energy, Environment and Sustainable Development*. Oxford: Elsevier.
- Durmayaz, A., Sogut, O. S., Sahin, B. and Yavuz, H.** (2004). Optimization of thermal systems based on finite-time thermodynamics and thermoeconomics. *Progress in Energy and Combustion Science*, 30 (2), 175-217.

- Ehyaci, M.A., Anjiridezfuli, A. and Rosen M.A.** (2013). Exergetic analysis of an aircraft turbojet engine with an afterburner. *Thermal Science*, 17 (4), 1181-1194.
- El-Sayed, A.F.** (2008). *Aircraft Propulsion and Gas Turbine Engines*. Florida: CRC Press.
- Etele, J. and Rosen M.A.** (2001). Sensitivity of exergy efficiencies of aerospace engines to reference environmental selection. *International Journal of Exergy*, 1 (2), 91-99.
- Hempsell, M.** (2010). A phased approach to orbital public access. *Acta Astronautica*, 66 (12) 1639-1644.
- Hepbasli, A.** (2008). A key review on exergetic analysis and assessment of renewable energy resources for a sustainable future. *Renewable and Sustainable Energy Reviews*, 12 (3), 593-661.
- Hill, P.G. and Peterson, C.R.** (1992). *Mechanics and Thermodynamics of Propulsion*, 2<sup>nd</sup> ed. Massachusetts: Addison Wesley Publishing Company.
- Hünecke, K.** (2003). *Jet Engines: Fundamentals of Theory, Design and Operation*, 6<sup>th</sup> ed. Iowa: Motorbooks International Publishers and Wholesalers.
- Jivraj, F., Varvill, R., Bond, A. and Paniagua, G.** (2007). The Scimitar precooled Mach 5 engine, The 2<sup>nd</sup> European Conference for Aerospace Sciences, Brussels, Belgium : 1 – 6 July.
- Kotas, T.J.** (1995). *The Exergy Method of Thermal Plant Analysis*. Florida: Krieger Publishing Company.
- Langston, L.S.** (2011). Turbine fuel efficiency: Fitting a pitch. *American Society of Mechanical Engineers*. Retrieved: November 22, 2015, from <https://www.asme.org/engineering-topics/articles/turbines/turbine-fuel-efficiency-fitting-a-pitch>
- Mattingly, J.D.** (2006). *Elements of Propulsion: Gas Turbines and Rockets*, 2nd ed. Virginia: American Institute of Aeronautics and Astronautics.
- Mattingly, J.D., Heiser, W.H. and Pratt D.T.** (2002). *Aircraft Engine Design*, 2nd ed. Virginia: American Institute of Aeronautics and Astronautics.
- Midilli, A. and Dincer, I.** (2009). Development of some exergetic parameters for PEM fuel cells for measuring environmental impact and sustainability. *International Journal of Hydrogen Energy*, 34 (9), 3858-3872.
- Midilli, A. and Dincer, I.** (2010). Effects of some micro-level exergetic parameters of a PEMFC on the environment and sustainability. *International Journal of Global Warming*, 2 (1), 65-80.
- Midilli, A., Kucuk, H., Dincer, I.** (2011). Exergetic sustainability evaluation of a recirculating aquaculture system, *Global Conference on Global Warming 2011*, Lisbon, Portugal : July 11-14.
- Mollaoglu, G., Durmayaz, A., Sogut, O.S. and Aydin, M.** (2009). Performance optimization of a gas-cooled-reactor nuclear power plant with finite-rate heat transfer, *The 4<sup>th</sup> International Exergy, Energy and Environment Symposium*, Sharjah, UAE : April 18-23.

- Najjar, Y.S.H. and Al-Sharif, S.F.** (2006). Thermodynamic optimization of the turbofan cycle. *Aircraft Engineering and Aerospace Technology*, 78 (6), 467-480.
- Oates, G.C.** (1998). *Aerothermodynamics of Gas Turbine and Rocket Propulsion*, 3rd ed. Virginia: American Institute of Aeronautics and Astronautics.
- Rolls-Royce.** (1996). *The jet engine*, 5<sup>th</sup> ed. Derby: The Technical Publications Department, Rolls-Royce plc.
- Rosen, M. A.** (2002). Assessing energy technologies and environmental impacts with the principles of thermodynamics. *Applied Energy*, 72 (1), 427-441.
- Rosen, M. A. and Etele, J.** (2004). Aerospace systems and exergy analysis: applications and methodology development needs. *International Journal of Exergy*, 1 (4), 411-425.
- Szargut, J.** (2005). *Exergy Method Technical Ecological Applications*. Southampton: WIT Press.
- Szargut, J., Morris, D.R. and Steward, F.R.** (1988). *Exergy Analysis of Thermal, Chemical, and Metallurgical Processes*. New York: Hemisphere Publishing Co.
- Szargut, J., Ziebig, A. and Stanek, W.** (2002). Depletion of the non-renewable natural exergy resources as a measure of the ecological cost. *Energy Conversion and Management*, 43 (9), 1149-1163.
- Tai, V.C., See, P.C. and Mares, C.** (2014). Optimisation of energy and exergy of turbofan engines using genetic algorithms. *International Journal of Sustainable Aviation*, 1 (1), 25-42.
- Tanbay, T., Durmayaz, A. and Sogut, O.S.** (2013). Turbojet motorunun sonlu zaman termodinamiği ile ekolojik optimizasyonu, *19.Ulusal Isı Bilimi ve Tekniği Kongresi*, Samsun, Turkey : September 9-12.
- Tanbay, T., Durmayaz, A. and Sogut, O.S.** (2015). Exergy-based ecological optimization of a turbofan engine. *International Journal of Exergy*, 16 (3), 358-381.
- Tona, C., Raviolo, P.A., Pellegrini, L.F. and Oliveira Jr., S.** (2010). Exergy and thermoeconomic analysis of a turbofan engine during a typical commercial flight. *Energy*, 35 (2), 952-959.
- Turan, O.** (2012). Effect of reference altitudes for a turbofan engine with the aid of specific-exergy based method. *International Journal of Exergy*, 11 (2), 252-270.
- Turan, O., Aydin, H., Karakoc, T.H. and Midilli, A.** (2014a). First law approach of a low bypass turbofan engine. *Journal of Automation and Control Engineering*, 2 (1), 62-66.
- Turan, O., Aydin, H., Karakoc, T.H. and Midilli, A.** (2014b). Some exergetic measures of a JT8D turbofan engine. *Journal of Automation and Control Engineering*, 2 (2), 110-114.
- Turan, O., Karakoc, H. and Sogut, M.Z.** (2013). Exergetic definition of sustainability for small turbojet engines, *12<sup>th</sup> International Conference*

on Sustainable Energy Technologies, Hong Kong, China : August 26-29.

- Turan, O. and Karakoc, T.H.** (2010). Effects of fuel consumption of commercial turbofans on global warming. In Dincer, I., Midilli, A., Hepbasli, A. and Karakoc, T.H. (Eds.), *Global Warming: Engineering Solutions* (Vol. 1, pp.241–253). New York : Springer.
- Turan, Ö., Orhan, İ. and Karakoç, T.H.** (2008). On-design analysis of high bypass turbofan engines. *Journal of Aeronautics and Space Technologies*, 3 (3), pp.1–8.
- Turgut, E.T., Karakoc T.H. and Hepbasli A.** (2007). Exergetic analysis of an aircraft turbofan engine. *International Journal of Energy Research*, 31 (14), 1383–1397.
- Turgut, E.T., Karakoc T.H. and Hepbasli A.** (2009a). Exergoeconomic analysis of an aircraft turbofan engine. *International Journal of Exergy*, 6 (3), 277–294.
- Turgut, E.T., Karakoc T.H., Hepbasli A. and Rosen, M.A.** (2009b). Exergy analysis of a turbofan aircraft engine. *International Journal of Exergy*, 6 (2), 181–199.
- Ust, Y., Sogut, O.S., Sahin, B. and Durmayaz, A.** (2006). Ecological Coefficient of Performance (ECOP) optimization for an irreversible Brayton heat engine with variable-temperature thermal reservoirs. *Journal of Energy Institute*, 79 (1), 47-52.
- Van Gool, W.** (1997). Energy policy: fairy tales and factualities. In Soares, O.D.D, Martins da Cruz, A., Costa Pereira, G., Soares, I.M.R.T. and Reis, A.J.P.S. (Eds.), *Innovation and Technology-Strategies and Policies*, (Vol. 1, pp.93-105). Dordrecht : Kluwer Academic Publishers.
- Varvill, R. and Bond, A.** (2003). A comparison of propulsion concepts for SSTO reusable launches. *Journal of the British Interplanetary Society*, 56 (3), 108-117.
- Wang, J., Chen, L., Ge, Y. and Sun, F.** (2014). Ecological performance analysis of an endoreversible modified Brayton cycle. *International Journal of Sustainable Energy*, 33 (3), 619-634.
- Wang, W., Chen, L. and Sun, F.** (2011). Ecological optimisation of an irreversible ICR gas turbine cycle. *International Journal of Exergy*, 9 (1), 6-79.
- Webber, H., Bond, A., and Hemsell, M.** (2007). The sensitivity of precooled air-breathing engine performance to heat exchanger design parameters. *Journal of the British Interplanetary Society*, 60, 188-196.
- Xia, D., Chen, L., Sun, F. and Wu, C.** (2006). Universal ecological performance for endoreversible heat engine cycles. *International Journal of Ambient Energy*, 27 (1), 15-20.
- Xiang, J.Y., Cali, M., Santarelli, M.** (2004). Calculation for physical and chemical exergy of flows in systems elaborating mixed-phase flows and a case study in an IRSOFC plant. *International Journal of Energy Research*, 28 (2), 101-115.

**Yildirim, E., Altuntas, O., Karakoc, T.H. and Mahir, N.** (2013). Energy and exergy analysis of piston-prop helicopters, *8<sup>th</sup> International Green Energy Conference*, Kyiv, Ukraine : June 17-19.

**Zhang, W., Chen, L., Sun F. and Wu, C.** (2007). Exergy-based ecological optimal performance for a universal endoreversible thermodynamic cycle. *International Journal of Ambient Energy*, 28 (1), 51-56.

**Url-1** <[http://www.pw.utc.com/JT8D\\_Engine](http://www.pw.utc.com/JT8D_Engine)>, date retrieved 29.08.2015.

## **APPENDICES**

**APPENDIX A:** Calculation of  $\varphi$  for kerosene and formulation of  $\varphi$  for solid fuels

**APPENDIX B:** Derivation of isentropic efficiency of compressor shown in equation (4.117)





## APPENDIX A

In equation (2.25) and (2.26) ratio of specific chemical exergy to lower heating value of the fuel,  $\varphi$ , has been introduced and written explicitly. For kerosene, considering the chemical formula of  $C_{12}H_{23}$ , mass fractions of  $H$ ,  $C$ ,  $O$  and  $S$  has been calculated for each element by

*Mass fraction of an element*

$$= \frac{\text{Total mass of the element in fuel molecule}}{\text{Total mass of the fuel molecule}} \quad (\text{A.1})$$

Atomic mass of  $H$ ,  $C$ ,  $O$  and  $S$  are 1.00794, 12.0107, 15.9994 and 32.066 respectively in amu. Therefore mass fractions are calculated as

$$H = \frac{23 * 1.00794}{(12 * 12.0107) + (23 * 1.00794)} = 0.13856003 \quad (\text{A.2a})$$

$$C = \frac{12 * 12.0107}{(12 * 12.0107) + (23 * 1.00794)} = 0.86143997 \quad (\text{A.2b})$$

$$O = \frac{0 * 15.9994}{(12 * 12.0107) + (23 * 1.00794)} = 0 \quad (\text{A.2c})$$

$$S = \frac{0 * 32.066}{(12 * 12.0107) + (23 * 1.00794)} = 0 \quad (\text{A.2d})$$

Therefore by using equation (2.26),  $\varphi$  becomes

$$\varphi = \left[ 1.0401 + 0.1728 \frac{0.13856003}{0.86143997} + 0 \right] = 1.067894 \quad (\text{A.3})$$

Then by using equation (2.25), specific chemical exergy of kerosene becomes

$$e_{chem} = \varphi Q_{LHV} = 1.067894 * 43.15 = 46.0796261 \quad (\text{A.4})$$

in units of MJ per kg. The value that is taken from the literature to utilize in the thesis has been 45.8 MJ per kg. Therefore the difference between the value calculated in equation (A.4) and the value taken from the literature is

$$Deviation = 1 - \frac{45.8}{46.0796261} = 0,00606 \cong 0.6\% \quad (A.5)$$

which is insignificant and ignorable.

For solid fuels, equation (2.25) is also valid; however,  $\varphi$  formulation differs from that of liquid fuels (Szargut et al,1988; Kotas, 1995). For solid fuels consisting of  $H, C, O$  and  $N$ ; and having mass ratio of oxygen to carbon less than 0.667,  $\varphi$  has been presented in equation (A.6).

$$\varphi_{dry} = 1.0437 + 0.1882 \frac{H}{C} + 0.0610 \frac{O}{C} + 0.0404 \frac{N}{C} \quad (A.6)$$

It has been noted that equation (A.6) is not valid for wood. For solid fuels having oxygen to carbon ration between 2.67 and 0.667,  $\varphi$  has been presented in equation (A.7), which is also valid for wood.

$$\varphi_{dry} = \frac{1.0438 + 0.1882 \frac{H}{C} - 0.2509 \left(1 + 0.7256 \frac{H}{C}\right) + 0.0383 \frac{N}{C}}{1 - 0.3035 \frac{O}{C}} \quad (A.7)$$

For solid fuels,  $\varphi$  value can be calculated by using equation (A.6) or equation (A.7) and then by using equation (2.25), specific chemical exergy can be calculated.

## APPENDIX B

Isentropic efficiency formulation of a compressor in terms of stage isentropic efficiency, stage pressure ratio and compressor pressure ratio has been presented in equation (4.117).

For any  $j^{\text{th}}$  stage in compressor, equation (4.123) has been rewritten as

$$\eta_{sj} = \frac{(r_{sj})^{(k-1)/k} - 1}{\frac{T_j}{T_{j-1}} - 1} \quad (\text{B.1})$$

where  $r_{sj}$  is pressure ratio of  $j^{\text{th}}$  stage to  $j-1^{\text{th}}$  stage. Rewriting equation (B.1)

$$\frac{T_j}{T_{j-1}} = 1 + \left(\frac{1}{\eta_{sj}}\right) [(r_{sj})^{(k-1)/k} - 1] \quad (\text{B.2})$$

Then, by extending it from stage 1 to stage N

$$\frac{T_N}{T_0} = \prod_{j=1}^N \left\{ 1 + \left(\frac{1}{\eta_{sj}}\right) [(r_{sj})^{(k-1)/k} - 1] \right\} \quad (\text{B.3})$$

Also for the whole compressor, pressure ratio has been defined as

$$\frac{P_N}{P_0} = \prod_{j=1}^N \left\{ \left(\frac{P_{sj}}{P_{sj-1}}\right) \right\} \quad (\text{B.4})$$

where

$$\frac{P_N}{P_0} = r_C \quad (\text{B.5})$$

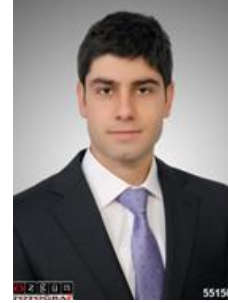
Also, as written in equation (4.123), isentropic efficiency of the whole compressor has been written as

$$\eta_C = \frac{(r_C)^{(k-1)/k} - 1}{\frac{T_N}{T_0} - 1} \quad (\text{B.6})$$

Then, by substituting equation (B.3) into equation (B.6), equation (4.117) in Chapter 4 has been obtained as the isentropic efficiency of the compressor as a function of

compressor pressure ratio, isentropic efficiency of each stage and pressure ratio of each stage.

## CURRICULUM VITAE



**Name-Surname** : Mert Çolakoglu  
**Place and Date of Birth** : Iskenderun /Turkey – 28/09/1989  
**E-mail** : mertcolakoglu@gmail.com

### EDUCATION:

- **B.Sc.** : 2011, METU, Faculty of Engineering, Industrial Engineering

### PROFESSIONAL EXPERINCE AND REWARDS:

- Best Paper Award was presented to Colakoglu, M., Tanbay, T., Durmayaz, A. and Sogut, O.S. for the paper Colakoglu et al. (2014) in the 7<sup>th</sup> International Ege Energy Symposium & Exhibition, Uşak, Turkey, June 18-20 among nearly 140 papers.

### PUBLICATIONS, PRESENTATIONS AND PATENTS ON THE THESIS:

- Colakoglu, M., Tanbay, T., Durmayaz, A. and Sogut, O.S. (2014). Effect of Heat Leakage on the Performance of a Twin-Spool Turbofan Engine. In Canan Kandilli, (Ed.), *7<sup>th</sup> IESE. Proceedings of the 7<sup>th</sup> International Ege Energy Symposium & Exhibition*, (pp. 477-500). Turkey : Usak University Green Economy Research and Application Centre, June 18-20.
- Colakoglu, M., Tanbay, T., Durmayaz, A. and Sogut, O.S. (in press). Effect of heat leakage on the performance of a twin-spool turbofan engine. *Int. J. Exergy*.